NOAA Grant NA90RAH00077
National Oceanic and Atmospheric Administration

NSF Grant ATM-9015485
National Science Foundation

An Observational and Theoretical Study of Squall Line Evolution

by
Erik Rasmussen

Department of Atmospheric Science
Colorado State University
Fort Collins, Colorado

Steven A. Rutledge, P.I.

Colorado State University

Department of Atmospheric Science

Paper No. 500

AN OBSERVATIONAL AND THEORETICAL STUDY OF SQUALL LINE EVOLUTION

by

Erik Rasmussen

Department of Atmospheric Science

Colorado State University

Fort Collins, CO 80523

Research Supported by

National Oceanic and Atmospheric Administration

under Grant NA90RAH00077

National Science Foundation

under Grant ATM-9015485

May 29, 1992

Atmospheric Science Paper No. 500

ABSTRACT OF DISSERTATION

AN OBSERVATIONAL AND THEORETICAL STUDY OF SQUALL LINE EVOLUTION

This study documents a class of squall lines that appears to be approximately two-dimensional, has a solid leading edge echo during a portion of its life cycle, and has line-normal flow characterized by a continuous zone of negative horizontal vorticity that slopes upward from the leading edge to the rear of the storm. Structure and evolution are established using Doppler radar observations of a number of storms at unprecedented temporal resolution.

It is shown that squall lines of this type evolve through identifiable stages of reflectivity structure. This evolution appears to be strongly related to changes that occur in the kinematic structure. As a typical system evolves, the rearward-sloping zone of horizontal vorticity, which is predominantly associated with vertical shear, develops on the scale of the system, presumably driven by the horizontal buoyancy gradients across the system. The vorticity that is generated allows further generation to take place by causing the superposition of a saturated, precipitating anvil cloud aloft over potentially cooler air below in the trailing region. The rearward-sloping vorticity zone gradually tilts toward the horizontal. The rate at which this zone tilts seems to be the primary difference between the systems studied. To a first approximation, the inflow streamlines parallel the sloping vorticity zone, so as it approaches a horizontal slope, vertical motion becomes smaller.

Eventually, convective-scale ascent ceases, giving the impression that the gust front has surged out ahead of the precipitation.

To gain understanding of the dynamics of this class of squall lines, this study explores the role of horizontal vorticity, and the means through which the environment influences the rate of tilting and hence the time scale of evolution. The observed generation of vorticity in six systems is discussed and compared to earlier theories for squall line longevity. Motivated by these observations, a new theory is developed which attempts to explain squall line evolution, and the possibility of steadiness, as a function of an environment that has both upper and lower shear regions. Predictions based on the theory are compared to the new observations, as well as other observed and numerically simulated squall lines.

Erik Nels Rasmussen
Atmospheric Science Department
Colorado State University
Fort Collins, CO 80523
Spring 1992

ACKNOWLEDGEMENTS

I wish to thank my advisor, Dr. Steven Rutledge, for his support, encouragement, and helpful discussions. I gratefully acknowledge the support provided by the National Severe Storms Laboratory, particularly Drs. Robert Maddox and Charles Doswell III, who encouraged me to pursue this degree.

The patient support of Lisa Rasmussen, and the friendship of her family have been invaluable. I also wish to thank my parents for many years of encouragement.

Finally, the support and friendship of Mike Smith and Dan Bowman at WeatherData, Inc., without which the pursuit this degree would have been much more difficult, are acknowledged with much gratitude.

TABLE OF CONTENTS

Chapter 1

Introduction

Squall lines can be defined as any non-frontal line or band of convective activity, and the convective activity need not be continuous along the leading edge (Hane, 1986). This study will examine a subset of this class of convection in which the line is solid, quasi-two-dimensional, and the system contains stratiform trailing precipitation sometime during its life cycle. Further refinements of this definition will be made which mainly involve the kinematic structure of the systems.

Numerous earlier studies have focused on the kinematic and reflectivity structure of this type of precipitation system, presenting "snapshots" which generally document a "mature" phase. Many findings of the more recent studies are summarized in Rutledge (1991). Synthesis of the observational studies has led to a conceptual model of the structure of a mature squall line (Houze *et al.*, 1989) illustrated in Fig. 1. Of particular relevance here is the existence of mesoscale quasi-horizontal flow branches in the trailing region of the storm.

As depicted in Fig. 1, a rear inflow branch slopes downward toward the front of the system, and is located beneath a front-to-rear branch that slopes upward toward the rear. The strength of the storm-relative rear inflow has been shown to vary from one system to another (Smull and Houze, 1987a). Although this variation may be partly the result of the reference frame chosen for the analyses, Smull and Houze showed that storms with strong

rear inflow also had stronger front-to-rear (FTR) flow aloft. They also showed that relative rear-to-front (RTF) flow was in some cases the result of dynamical processes internal to the squall lines, and not the result of environmental momentum being conserved as air entered the rear of the system.

Although in previously published cases, the FTR and RTF branches vary in relative strength from one system to another, careful inspection shows that there is almost always a sloping band of negative horizontal vorticity in these systems which is largely the result of vertical shear between the flow branches. In some storms, the vorticity zone does not extend across the entire system, but appears only in the trailing region. In the type of squall line investigated herein, the vorticity zone extends across the entire system.

Horizontal vorticity is defined as

$$\eta = \frac{\partial u}{\partial z} - \frac{\partial w}{\partial x} \tag{1}$$

in a right-handed cartesian system with x normal to the squall line in the direction of motion, and z vertical. In this study, discussion of the "vorticity zone" refers to the region of negative horizontal vorticity which typically extends from near the surface at the leading edge to middle or upper levels at the rear of the system. In the conceptual model shown in Fig. 1, it is found between the sloping RTF and FTR branches.

Examination of several previously published cases provides examples of the nature of the vorticity zone. The 2-3 August 1981 CCOPE (Cooperative Convective Precipitation Experiment) squall line (Schmidt and Cotton, 1989) contained a relatively weak rear inflow jet (Fig. 2). However, it featured a sloping region of large values of negative horizontal vorticity. This region, situated just above the relative rear inflow zone, began near the surface at the

leading edge, and sloped upward toward the rear of the storm. Similarly, a squall line observed on 23 June 1981 during the COPT 81 (*Convection Profonde Tropicale*) experiment in tropical West Africa (Roux, 1988) also featured the sloping zone of vorticity (Fig. 3). In this case, it appears to be the result of strong shear just below the upper FTR flow. An example of a system with comparatively stronger relative rear inflow is the 10-11 June 1985 PRE-STORM (Preliminary Regional Experiment for Stormscale Operational and Research Meteorology) squall line (Rutledge *et al.*, 1988), which will be examined in further detail in this study.

In many published squall line cases, evidence can be clearly seen in the velocity distribution of the sloping zone of negative vorticity (see, for example Chong *et al.*, 1987; Chalon, *et al.*, 1988). In addition, field observations made by the author of many squall lines in tropical northern Australia indicate that this feature is common to most, if not all, of the squall lines that occur there. The existence of negative vorticity in the interior part of the squall line is a common feature of this class of squall lines, whereas the relative strengths of the individual flow branches is not consistent from storm to storm.

Some published cases do not show evidence of a well-defined *continuous* rearward-sloping zone of negative horizontal vorticity. The Oklahoma squall line of 22 May 1976 has been documented using Doppler radar analyses (Smull and Houze, 1985; Smull and Houze, 1987b) and sounding network analyses (Ogura and Liou, 1980). Fig. 4 shows the along-line averaged reflectivity and line-normal horizontal velocity relative to the leading edge of this storm (from Smull and Houze, 1985). Fig. 5 shows the larger-scale view of the same storm based on sounding analyses by Ogura and Liou (1980). In this particular squall line, a region of negative vorticity was

present near the leading edge (x = 0 in Fig. 5) in the lowest two kilometers, and another region sloped upward from about 800 hPa to 400 hPa in the trailing region. However, this storm did not appear to have a well-defined, *continuous* rearward-sloping zone of negative vorticity. The Oklahoma squall line of 19 May 1977 (Kessinger *et al.*, 1987) is similar to the 22 May 1976 squall line and also did not fit the vorticity structure of the conceptual model described herein.

In the cases cited above, relatively little documentation was provided on the evolution of the squall lines. One of the few studies that was able to address evolution was that of Leary and Houze (1979). Using reflectivity data from the GATE (GARP Atlantic Tropical Experiment), they associated the following stages with observed reflectivity patterns:

- *formative stage*: line of isolated cells;
- *intensifying stage*: breaks fill in between cells and reflectivity increases;
- *mature stage*: mesoscale precipitation features are present;
- *dissipating stage*: leading edge convection dissipates

The squall lines examined in this study generally followed similar patterns in reflectivity evolution as those described by Leary and Houze. Since there is no clear reason to depart from their terminology, these names for the various stages will be used herein. However, the echo character and evolution described in this study will differ significantly from those of Leary and Houze.

This study will show evidence that certain characteristics of the squall line, seen in both the reflectivity and kinematic structure, determine the stage of evolution. It will be shown that squall lines undergo common patterns of evolution. In addition, this dissertation will describe the interdependency

between the evolution of the reflectivity structure and the evolution of the vorticity structure of squall lines.

Over 250 Doppler volume scans have been analyzed in the course of this research, documenting numerous squall lines. For many of these cases, data were analyzed at time intervals of about ten minutes, providing information about squall line structure and evolution in unprecedented detail. Ten cases were selected for detailed study based primarily on data coverage (spatial and temporal) and the desire to span a large variety of ambient CAPE (Convective Available Potential Energy) and environmental wind shear conditions.

Recently, several theories have been advanced to explain the structure and motion of squall lines and the potential for steady, long-lived systems. Verification of these theories has awaited detailed observational and modelling work. The validity of these theories is examined herein from the perspective of the observations. Motivated by the theoretical approaches of the earlier studies, a new theory is advanced to crudely account for variations in the environmental vertical shear structure, and to explain evolution without making a steadiness assumption.

Based on the results of numerical simulations, the potential for steadiness in a squall line was examined by Rotunno *et al.* (1988, hereafter referred to as RKW). RKW studied storm longevity by examining the degree of balance (or imbalance) between vorticity transports associated with the low-level shear in the pre-storm environment, and the generation of vorticity

due to the convectively-generated cold pool. The vorticity equation appropriate to this two-dimensional, inviscid, Boussinesq problem is

$$\frac{\partial \eta}{\partial t} + \nabla \cdot \eta \mathbf{V} = -g \frac{\partial B}{\partial x} \tag{2}$$

where η is given by (1) and

$$B = 1 - \frac{\theta_v}{\overline{\theta_v}} + q_c \quad . \tag{3}$$

Total buoyancy is represented by B, with q_c being the total condensate mixing ratio, and θ_v is the virtual potential temperature.

Several assumptions were made by RKW to permit the integration of this vorticity equation. First, it was assumed that an ideal condition in a long-lived, intense squall line was a vertically-issuing, symmetric updraft above the propagating cold pool. Furthermore, it was assumed that vorticity is only transported across the forward boundary of the integration volume, and not the rear boundary. By assuming a steady flow, RKW demonstrated that a balance between the cold-pool generation of vorticity and the transport of the low-level ambient vorticity associated with the vertical shear of the horizontal wind in the pre-storm environment is required for steady, intense systems. RKW focussed on the dynamics of the lowest few kilometers, and did not address the effects of buoyancy gradients or transport in the regions above.

In simulations of a West Africa squall line case from the COPT 81 experiment, Lafore and Moncrieff (1989, hereafter referred to as LM) recognized that vorticity generation occurs on the scale of the squall line, including the trailing stratiform region. In terms of the horizontal extent detected by radar, this can be as broad as 100 km or more (refer to Fig. 1). They argued that vorticity is generated by horizontal gradients of buoyancy that

result from thermodynamic and microphysical processes throughout the storm, not just in the vicinity of the leading edge of the cold pool. This argument is clearly supported by the observations of vorticity evolution presented herein. However, LM did not address the issue of how the system-scale vorticity structure and generation impacts the rate of evolution or potential for steadiness.

In comments following publication of LM, Rotunno *et al.* (1990) indicate that the theory of RKW only addressed the conditions necessary for producing vigorous, uninhibited ascent at the gust front of a squall line. They suggested that an intense, long-lived system would be more likely when such ascent occurs. In reply, Lafore and Moncrieff (1990) reiterated that although the process described by RKW is a necessary condition for an intense, long-lived system, other factors impact "both the leading edge convection and the global dynamics." Further, Lafore and Moncrieff (1990) stressed that the upstream environment, in which low-level shear is measured, is itself modified by squall lines.

Seitter and Kuo (1983) also argued that vorticity generation is a storm-scale process, and showed the role of gravity in generating buoyancy gradients through the decoupling of the buoyant updraft air and the negatively buoyant precipitation-laden air. Emanuel (1986) used linear theory to expand on this concept and demonstrate the likely modes of propagation and orientation of squall-line like disturbances.

It is very convenient to use vorticity arguments to describe storm dynamics. Clearly, the buoyancy and momentum distributions lead to the generation of pressure perturbations which also could be used to describe the evolution of the flow. Many observational studies have focussed on the role of these pressure perturbations. For example, Lemone (1983) documented the

role of lowered pressure beneath the sloping cloudy region, warmed by condensation heating, to explain various observed accelerations. The roles of the surface mesoscale pressure perturbations have also been explored (e.g. Johnson and Hamilton, 1988). Modelling studies have long indicated the importance of perturbation high pressure near the summits of updrafts in leading to adverse vertical accelerations as well as summit divergent flow (e.g. Schlesinger, 1975). It is important to note that the accelerations that must occur to alter the distribution of horizontal vorticity are partially the result of these pressure perturbations. Any or all of the following pressure features may be associated with increasing negative vorticity in the interior of the squall line: high pressure aloft near the leading edge, low pressure along the underside of a *sloping* region of relatively warm air, and high pressure near the surface in the area behind the convective line. However, in order to understand the evolution of squall lines, horizontal vorticity arguments are often simpler and do not require discussion of the actual distribution of pressure in the storm.

Following the vorticity viewpoint and utilizing Doppler radar observations, this study will further explore the role of buoyancy gradients and vorticity transport in controlling squall line evolution. Motivated by the observational findings, a theory is presented for squall line evolution that includes consideration of environmental shear in two layers (a "lower" and "upper" layer in contrast to the single layer in RKW) and the storm-generated vorticity structure.

Chapter 2

Observational data and methods

The focus of this study is the evolution of the two-dimensional, line-normal structure of squall lines. Such a focus is best suited to cases in which the variation in flow along the convective line is small compared to that across the line. From a dynamical viewpoint, one condition for two-dimensionality is that the regions containing buoyancy anomalies of a given sign be much longer than they are wide. These conditions generally exclude those periods of squall line life cycles with structures typified by mesoscale vortex motion, and squall lines composed of individual storms separated by echo-weak regions, while still allowing for some cellular structure to the leading edge convection. The possibility of along-line flow is not excluded, even if it is strong.

All of the squall lines analyzed in this research were chosen because of their apparently high degree of two-dimensionality in order facilitate interpretation of their dynamics from theoretical perspectives. The dynamics of squall lines that satisfy two-dimensionality can be readily assessed using single Doppler radar data, provided that data samples can be obtained normal to the leading edge of the system. Of great importance is the availability of data with sufficient temporal resolution to document changes in the squall line structure. The needed temporal resolution depends somewhat on the rate of evolution, but most of the cases selected for this study had volume scan data at intervals of ten to fifteen minutes.

a. Data and cases studied

Radar data used in this research were obtained in two experiments: the Down-Under Doppler and Electricity Experiment ("DUNDEE", Rutledge *et al.*, 1992) in tropical northern Australia, and the 1985 PRE-STORM experiment (Cunning, 1986) in Kansas and Oklahoma. The radars from these experiments used in this study were the MIT (Massachusetts Institute of Technology) and NOAA/TOGA (National Oceanic and Atmospheric Administration/Tropical Oceans and Global Atmosphere) radars in the DUNDEE cases, and the NCAR (National Center for Atmospheric Research) CP-4 radar in the PRE-STORM case. All of these radars are 5 cm wavelength Doppler radars. Further details concerning these radars can be found in the references cited immediately above.

Table 1 summarizes the cases studied. Various data sets had certain limitations, such as inadequate temporal resolution, failure to scan at high elevation angles, etc. So although all ten cases were useful in determining

Table 1: List of cases analyzed.

Case	Number of volume scans analyzed	Experiment
10-11 June 1985	25	PRE-STORM
26 November 1988	21	DUNDEE
26 January 1989	20	DUNDEE
18 November 1989	23	DUNDEE
5 December 1989	19	DUNDEE
24 January 1990	9	DUNDEE
7 February 1990, first storm	14	DUNDEE
7 February 1990, second storm	18	DUNDEE
7 February 1990, third storm	9	DUNDEE
14 February 1990	29	DUNDEE

the general features of structure and evolution described in this study, only seven were suitable for the detailed analyses required to evaluate vorticity budget integrals.

b. Analysis methods

The first step in the data analysis involved editing the raw radar data to remove non-meteorological echoes and unfold the radial velocity data. It was assumed that the target velocity vectors were composed of purely horizontal flow plus the hydrometeor fallspeed, so that

$$v_h = \frac{v_r}{\cos\alpha} - v_t \tan\alpha \qquad (4)$$

where v_h is the horizontal velocity component, v_r is the radial (measured) component, α is the elevation angle, and v_t is an estimated terminal velocity. The terminal velocity was estimated using a power law relation with different values for coefficientand exponent above and below the melting level. The general conclusions reached herein are based largely on velocities observed at elevation angles low enough that the $\cos\alpha$ and v_t sensitivities were unimportant.

In order to examine the evolution of the 2-D flow on the scale of the squall line, reflectivity and horizontal velocity data were averaged in slabs that extended across the squall line approximately orthogonal to the leading edge. The slabs were usually 20 km wide, and the orientation and width was held constant for the duration of the storm, even if the squall line orientation shifted somewhat as the system propagated. Each radar data point that fell

within the slab was assigned to the nearest grid point, with the grid resolution being 1000 m in the horizontal, line-normal direction, and 500 m in the vertical.

The purpose of the slab-averaging technique was to filter the features in the along-line direction, while retaining all features with broad line-normal extent. Using only single Doppler radar data, it was not possible to obtain legitimate 2-D averages over wider sections of the squall line. The good degree of temporal continuity in the slab-averaged data suggests that the technique is a reasonably good method for filtering the convective scale along-line variations. In order to ensure that the horizontal velocity computed in the manner described above was representative of the component in the line-normal direction, only data that fell within 12.5° azimuth of the slab center-line were used. This requirement implied that at ranges very close to the radar, smaller-scale features were being retained since a smaller along-line sample is utilized. Because of this, quantities such as vertical velocity are interpreted with great caution when diagnosed near the radar, because they may be representative of an individual convective cell instead of an average over the slab width. Finally, if more than one-third of all possible radar data points that mapped to a single slab data point had data, the data were averaged for that point. If too few radar data estimates were available, the slab-average value was not obtained for that grid point.

After computing slab averages, an additional smoothing step was performed on the horizontal velocities using a Gaussian filter. This filter retained approximately 75% of the amplitude of features with 4 kilometer wavelengths, increasing toward 100% at longer wavelengths and filtering more strongly at shorter wavelengths. For regions below the radar horizon of 1.5 km depth or less, horizontal velocity estimates were filled using

objectively analyzed estimates of du/dz, applying the same Gaussian weighting function to the nearby estimates of du/dz above the radar horizon. This technique was tested by assuring that the resulting vorticity fields had good spatial continuity from data-rich to data-poor regions, and that as the storms propagated into regions with different radar horizons, vorticity fields near the ground showed good temporal continuity. The primary purpose of filling velocities below the radar horizon was to obtain estimates of horizontal divergence in that region for use in computing vertical velocity. The sub-horizon velocity estimates do not have a significant impact on the findings presented herein.

The vertical velocity was diagnosed using downward integration of the anelastic continuity equation, with the boundary condition being w=0 at the radar echo top. A density profile appropriate for the particular geographical region was used. Residual velocity at the bottom of each column was used to compute the amount of divergence required over the column depth to satisfy a lower boundary condition of w=0. This divergence was then applied, and the integration performed again, resulting in satisfying boundary conditions of w=0 at both the echo top and ground. It was found that this technique produced vertical velocity fields that were more uniform in time and space, and more "realistic looking", than those produced with simple top-down integration. Using centered finite differences, horizontal vorticity (Eq. 1) was then computed from horizontal and vertical velocity data.

Chapter 3

Observations

A large number of slab-average fields have been examined in detail (temporal resolution of 10-15 min) for ten squall line cases. These fields include reflectivity, horizontal and vertical velocity, horizontal vorticity, divergence, and vertical and horizontal shear. In this section, each stage of evolution will be described in detail. These descriptions form a conceptual model of squall line evolution that is based on thorough analysis of all ten squall line cases, and represents a synthesis of those features that appear to be common to all of the cases. In addition to the ten cases, numerous other storms have been observed by the author that fit the general model presented here. Based on the case study analysis, four distinct stages of evolution are recognizable. Retaining the nomenclature of Leary and Houze (1979), these are called the formative, intensifying, mature, and dissipating stages. Since not every storm was observed in all four stages (because of limitations in radar coverage), those cases best representing each stage will be used for illustration in this section. A special nomenclature will be used to name the cases consisting of the date and a suffix (F,M,S) to indicate whether the storm was fast-evolving, moderately evolving, or slow-evolving when subjectively compared to the other cases in this study. For example, the case designated 7feb90M is a squall line that occurred on 7 February 1990, and was moderate in speed of evolution compared to the other cases.

The data will be described in terms of storm-relative flow, with the translation speed being that of the leading edge of the squall line during the mature stage. This seems to be the most common way to represent squall line flow. However, two caveats are necessary. First, squall line motion is not generally steady in the systems examined. Rather, the systems tend to accelerate during the intensifying stage. Second, propagation speed is not uniform for all parts of the convective system. The leading edge propagates the most quickly, with features further rearward propagating more slowly, and the trailing anvil edge moving the slowest. This variance in propagation speed is obviously required if the system is to expand rearward with time. It is for these reasons that the squall lines discussed herein will be described mainly in terms of vorticity, which is invariant for any choice of translation speed.

All of the slab-average vertical cross sections shown in this dissertation are oriented so that the system is propagating from left to right. The leading edge convection is placed near the right edge of the figures. The horizontal distance is in km along the path of propagation (positive x), with the radar situated near x=115 km. The orientation of the slabs is depicted in the figures showing the horizontal distribution of reflectivity.

Defining the four stages of evolution is done mainly to facilitate discussion. The evolution is really a continuum of changes in the kinematic and reflectivity structure, broadly characterized by gradual tilt, the flow branches and reduction in updraft strength and echo intensity. Further discussion and illustration of the four stages can be found in Chapter 5 and Fig. 45.

a. Formative stage

In the formative stage, the squall lines consist of cells with gaps between, which are generally oriented in a line (Fig. 6). Presumably, the cells are initiated along a convergence zone that is linear in structure, although no effort was made to identify the mechanisms of initiation for the squall lines in this study. In the vertical cross sections (Fig. 7) the slab-averaged reflectivity pattern shows small cells compared to later times, with an erect orientation. As this stage progresses, the cells gradually fill in the along-line direction.

When the lines consist of scattered to broken cells, the slab-average velocity structure (Fig. 8) is difficult to interpret. In most cases, however, the horizontal velocity field is relatively unperturbed in the formative stage (compared to later stages) indicating that the atmosphere, on a scale larger than the convective cells, is not yet strongly effected by their heat and momentum sources. In both of the cases shown (5dec89F and 10jun85M), the velocity distributions shown have strong similarities to the ambient storm-relative flow, especially away from the convective regions.

b. Intensifying stage

The transition from formative to intensifying stages occurs when the convective line first becomes solid. Any characterization of an echo pattern as solid is admittedly subjective. However, nothing is gained by attempting to establish arbitrary rules for reflectivity levels and coverage. Despite the subjectivity involved, the changes in character of the leading edge echo are quite apparent in the analysis process, with marked changes occurring in a

matter of minutes (i.e. from one volume scan to the next). Comparison of the horizontal reflectivity distributions of the formative stage (Fig. 6) and the intensifying stage (Fig. 9) shows the change in echo character.

The slab-averaged reflectivity (Fig. 10) shows that the cells have grown in horizontal and vertical extent. There is a slight rearward tilt to the leading edge convective cores (especially 26nov88S, 5dec89F, and 10jun85M; panels b-d), and there is also a small area of trailing echo in some of the cases. This trailing echo may be the remnants of earlier convective cells that have moved rearward relative to the leading edge.

By the end of the intensifying stage, the leading edge convective cells reach their greatest vertical extent and largest updraft speeds. Examples of the evolution of updraft speeds, based on the 2-D calculation of vertical velocity, are shown in Fig. 11. For each slab, vertical velocities were averaged in regions 2 km deep and 5 km in line-normal extent. The vertical velocities obtained with this averaging method are shown in Fig. 11. Neglecting the higher frequency variations, broad peaks in vertical velocity of about 5-6 ms^{-1} occur toward the end of the intensifying stage. The peak updraft velocity then falls off rapidly during the mature stage. This pattern is repeated among all of the cases, and thus it is suggested that the peak vertical velocity is the clearest indicator of the transition from intensifying to mature stages.

The observations above indicate that the intensifying stage should be defined as the period beginning when the line becomes solid, and ending at the time of maximum vertical echo extent and updraft intensity in the leading edge. This definition of the intensifying stage differs from that of Leary and Houze which allows gaps between cells. However, the data presented herein suggest that changes in the flow structure occur much more rapidly after the line becomes solid. This is almost certainly associated with

the presence of a developing buoyancy perturbation that is now much longer than it is wide. In particular, divergence near the summit of the leading edge induces relative FTR flow to the rear of the summit. During the intensifying stage, RTF accelerations occur in the lower and middle levels to the immediate rear of the leading edge. The vertical shear induced by both of these flow changes combine to drive the horizontal vorticity in the interior region to larger negative values. This change in vorticity is consistent with horizontal buoyancy gradients associated with greater buoyancy at the front of the system than at the rear. Thus, the transition from the formative stage to the intensifying stage is also marked by a change in the trend of the average vorticity in the interior region toward more rapidly lowering values.

These changes are illustrated by the four slab averages shown in Fig. 12. During the formative stage of 10jun85M, a vertically-oriented band of negative vorticity was present (near x=64 in Fig. 8) due to the horizontal shear between the up- and downdrafts. By 2357 UTC (Fig. 12a), the flow resembles a deep jump updraft (Thorpe et al., 1982). The vorticity zone tilts rearward with height, and is now the consequence of shear between the jump updraft and the relatively stagnant flow below. Divergence has increased strongly near the summit of the leading edge, giving rise to a rearward extension of the vorticity zone behind the jump updraft (from x=40 to x=60 km, at about 9 km elevation).

Although the structure is more complicated than that of 10jun85M, similar changes can be seen in the slab average for 5dec89F (Fig. 12b). The vorticity zone is just beginning to develop at 0750 UTC, with its generation being the result of rearward accelerations above about 7 km, and forward accelerations below. In 26nov88S (Fig. 12c), the vorticity zone extends from the surface at x=32 km to elevations of about 8 km at a distance 25 km from

the leading edge. A similar slope can be seen in the vorticity pattern of 14feb90M (Fig. 12d).

Another interesting transition found in the majority of the cases is seen in the propagation speed of the leading edge convection, shown in Fig. 13. During the formative and intensifying stages, the speed is relatively small and less than the mean flow through the depth of the convection. It is perhaps representative of some combination of "steering flow" and low-level momentum. However, at about the time of the transition between the intensifying and mature stages, the squall line suddenly accelerates to a speed more representative of a density current propagation speed (Charba, 1974). The reasons for these changes in propagation speed are not clear, but it is possible that the acceleration in the speed of the system may be associated with the development of a low-level cold pool that propagates in a similar fashion to a density current and forces ascent along its leading edge.

c. Mature Stage

The transition from the intensifying to the mature stage is more subtle than the transition between the earlier stages. During the intensifying stage, convective vigor increases as measured by peak updraft velocities, for example. During the mature stage, the *vorticity zone and attendant draft structure gradually tilt toward the horizontal,* leading to a gradual decrease in the updraft strength. Based on updraft speed alone, it could be argued that there is not a "mature" stage, since the leading edge updrafts begin dissipating after the intensifying stage. However, mesoscale ascent and vorticity generation continue, leading to a marked increase in the horizontal extent of the system. Thus, although leading edge vigor may wane slowly during the mature stage,

the system continues to grow and produce precipitation over larger areas, in agreement with the findings of McAnelly and Cotton (1989).

During the mature stage, inflow is initially lifted near the leading edge of the cold pool, but then continues to ascend for some distance behind the leading edge. As tilting progresses, the streamlines become more horizontal after passing over the gust front. The mature stage ends when these streamlines become oriented so horizontally that the leading edge character changes from a solid line of convection to patchy, weak, and shallow convective cells atop the cold pool or weak stratiform ascent. This is a difficult transition to detect, but is dynamically important since the heating generated by convective ascent at the leading edge of the system changes from a solid, relatively deep and strong heat source to a shallow, weak source which may be discontinuous along the line. At the same time, heating forced by mesoscale ascent becomes more widespread in the trailing region.

Negative vorticity continues to be generated through the mature stage. This generation is the result of buoyancy gradients between the solid leading edge (positive buoyancy anomaly) and a negative buoyancy anomaly toward the rear of the system. The increasing FTR relative flow aloft increases the transport of hydrometeors from the leading region into the trailing region aloft, causing the echo and precipitation area to expand rearward. Increasing RTF relative flow beneath this expanding anvil cloud, or often simply the expansion of the anvil over relatively stagnant lower-level air, can lead to cooling from evaporation and sublimation. Cooling owing to melting also occurs as ice hydrometeors fall through the melting level. Observations of the location and slope of the vorticity zone in the squall lines in this study indicate that the negative buoyancy anomaly is better characterized as a

sloping region, presumably following the underside of the anvil cloud in the trailing region, rather than a "cold pool" at the ground.

Thus the mesoscale flow structure is characterized by negative vorticity, with relative rearward-directed flow above weaker flow in the same direction, or relative forward-directed flow. As the vorticity increases, the relative flows increase, and ice is transported to ever greater distances to the rear of the leading edge. This in turn causes the continual spreading of the negative buoyancy anomaly further toward the rear aloft. As long as these buoyancy anomalies persist, the negative vorticity can increase. One effect of this feedback process is that the overall system increases in horizontal scale. This is because the generation of vorticity in the storm is manifested as increasingly-sheared horizontal flow, which allows the precipitation-generating anvil cloud to move rearward relative to the leading edge source region.

The general structure of all of these squall lines is one of a jump updraft (Thorpe *et al.* 1982), with the overturning updraft branch occasionally observed. The inflowing air turns upward in the jump updraft and then turns rearward at higher elevations, with storm-relative streamlines parallel to the vorticity zone (to a first approximation), as shown in Fig. 14. The more erect portion of the jump updraft comprises the convective-scale ascent, and since the streamlines are approximately parallel to the vorticity zone, the slight slope of the trailing portion indicates mesoscale ascent. As time progresses during the mature stage, the vorticity zone becomes less sloped, tending toward a more horizontal orientation. Thus the ascent becomes weaker and spread over a wider band. This agrees with the observation that leading edge echoes become broader and weaker with time. The dynamics and implications of this tilting process are discussed in detail in Chapter 4.

Data from cases 10jun85M, 14feb90M, 26nov88S, and 26jan89S are used to illustrate various aspects of the mature stage. The low-level, horizontal distribution of reflectivity is shown in Fig. 15. Several marked changes are apparent when this stage is compared to the intensifying stage (Fig. 9). First, the leading edge convection remains relatively intense in the low levels, but the convective cores have widened rearward. Because of the more horizontal orientation of the streamlines described above, the leading edge ascent, and thus precipitation generation, is now spread over a wider zone. Three storms featured transition zones (all but 14feb90M). In all cases, stratiform precipitation had become quite widespread in the mature stage. This is a consequence of the strong storm-generated shear and the mechanism of upscale-growth described above. Clearly, this increase in horizontal scale is the major difference between the intensifying and mature stage.

The slab-average vertical reflectivity structure is shown in Fig. 16. It can be seen, especially in the vertical extent of the 20 dBZ contour, that the leading edge convection in the mature stage is shallower than in the intensifying stage (cf. Fig. 10). Also shown is the major increase in horizontal line-normal extent of the precipitation region. Although these depictions are not designed to highlight the bright band, this feature can be clearly seen in the 10jun85M system rearward of x=125 km.

Strong similarities between systems can be seen in the velocity and vorticity depictions of the mature stage (Fig. 17). All of the systems, including the four illustrated here, featured jump updrafts. The shear on the underside of the jump updraft is associated with the sloping zone of negative vorticity already discussed. Rearward of the jump updraft, the vorticity zone is associated with a region of shear between the upper FTR flow, and the weaker flow below. The strength of the RTF in the four cases illustrated varied from

near zero (26nov88S, Fig. 17a) to about 8 ms^{-1} (10jun85M, Fig. 17c). In general, positive horizontal vorticity can be found in the upper part of the leading edge region, but vorticity of either sign is found in the lower part of the trailing region.

In all of the cases, including the four shown in Fig. 17, the vorticity zone and the streamlines slope slightly upward toward the rear in the trailing region, with the flow generally parallel to the vorticity zone. This implies that weak ascent is occurring in the trailing region during the mature stage. In the case of 10jun85M (Fig. 17c), the slope is very slight, but the flow along the streamlines is relatively large. Thus significant ascent was occurring despite the very shallow slope. The typical vertical velocity in the upper portion of the trailing region was 0.15 to 0.5 ms^{-1}, with a typical mesoscale downdraft velocity of -0.4 to -0.6 ms^{-1} centered at about 3 km elevation. These values are in good agreement with the EVAD-derived vertical velocities found in this storm by Rutledge et al. (1988).

d. Dissipating stage

Eventually, deep ascent near the leading edge can no longer be maintained. Depending on the reference frame chosen for squall line propagation, this event is manifested as the gust front surging ahead of the system, or the precipitation-producing inflow being swept rearward over the cold pool. This transition can be very rapid, with horizontal reflectivity depictions showing a sharp change from fairly continuous large reflectivity along the leading edge, to a more "scalloped" pattern with weaker, discrete cells. Slab-average analyses show that these weaker cells are also much shallower than the earlier convection. In some systems the convection

comes to consist of weak, patchy cells atop the propagating cold pool, with little or no convection immediately above the surface gust front. In other systems, the precipitation pattern at this stage resembles one of stratiform ascent near the leading edge.

The transition to weak, shallow stratiform ascent or patchy shallow convection at the leading edge marks the change from mature to dissipating stages. The dissipating stage is usually the longest-duration stage. In fact, in most of the cases examined in this study, the dissipating stage persisted until the squall lines moved out of the observational domains. With the demise of the continuous along-line heat source, the buoyancy gradients weaken, and negative vorticity generation weakens or ceases in the storm interior. Thus the transition from the mature to dissipating stage often occurs near the time of the peak magnitudes of horizontal vorticity, but during the dissipating stage the negative horizontal vorticity in the interior becomes smaller in magnitude.

The dissipating stage is characterized by the nearly-horizontal orientation of the zone of maximum negative vorticity. If RTF exists, the vorticity distribution implies that it also is nearly horizontal. In fact, during the dissipating stage, a horizontal RTF flow is usually observed that penetrates through the stratiform precipitation region, and often through the leading edge. Since the flow is approximately parallel to the vorticity surfaces, the horizontal orientation indicates a cessation of organized ascent on the scale of the squall line.

The total precipitation rate over the area of the storm is not immediately reduced in the dissipating stage. In fact, the stratiform precipitation may reach its greatest extent during this stage in agreement with the observations of McAnelly and Cotton (1989). The term "dissipating", as

used here, refers to the vigor and organization of the leading edge convection, not the entire storm. The mesoscale precipitation area can persist as long as upward motion and hydrometeor generation persist on that scale (generally requiring finite slope to the mesoscale flow), and for a period afterward that is determined by the time taken for hydrometeors to fall from upper levels.

Horizontal reflectivity patterns in the dissipating stage are illustrated in Fig. 18. As described above, the nature of the leading edge convection has changed markedly since the mature stage ended. Precipitation is generally less intense, and echoes are patchy compared to the solid echoes earlier. Examination of the vertical reflectivity distributions for these cases (Fig. 19) reveals that the leading edge echoes are much shallower than in earlier stages. In 26nov88S and 26jan89S (Figs. 19a,b), the ascent is more stratiform, with a very broad, rather weak leading edge region. In 14feb90M and 5dec89F Figs. 19c,d), there are patchy shallow cells near the leading edge of the cold pool (near x=100 km in Fig. 19c and near x=173 km in Fig. 19d).

The trailing regions reveal a variety of patterns. In general, trailing echoes seem to be most intense where earlier convection was the most vigorous, allowing for translation of the hydrometeors deposited in upper levels. The more slowly evolving systems seem to have more uniform trailing precipitation areas. These systems maintain greater updraft slopes over longer periods, implying that for a typical updraft strength, ice is deposited over large upper regions. Shorter-lived systems have deep convection over relatively short time periods, and thus deposit ice in the upper levels over smaller areas, and have less likelihood of in situ production of ice due to mesoscale ascent. In terms of precipitation processes in the trailing region, it is important to note that the slab-average vertical velocity fields in all ten cases show organized small-scale ascent and descent

with magnitudes on the order of 1 ms^{-1} and line-normal horizontal wavelengths of about 5-15 km. Whether or not these features are real or an artifact of noise and the data processing remains to be determined.

The respective patterns of vorticity and velocity in the dissipating stage are shown in Fig. 20. In 26nov88S (Fig. 20a) there is a small, weak updraft at the leading edge of the cold pool near x=170 km. The streamlines and vorticity zone then rise only slightly to the rear, supporting the broad weak leading edge echo. A similar pattern is shown for 26jan89S (Fig. 20b), with the weak leading edge updraft near x=130 km. The slab average shown for 14feb90M (Fig. 20c) is from very early in the dissipating stage, at which time there is still slight slope to the vorticity zone; after this time it quickly becomes quasi-horizontal. In the case of 5dec89F (Fig. 20d), the vorticity zone is elevated near z=5 km and is nearly horizontal.

e. The sloping vorticity zone

A few additional details need to be presented concerning the nature of the sloping zone of negative horizontal vorticity. As described previously, the tilt of the zone of negative vorticity is consistently observed to become more horizontal with time, and there appears to be a strong link between the slope of the vorticity zone and the nature of mesoscale vertical motion in the trailing region. To a first approximation, the vorticity is uniform in broad, sloped regions, and the streamlines are parallel to the vorticity surfaces. This is especially true away from the ground and the tropopause. Since the streamlines slope upward toward the rear of the storm, then everywhere that the flow is front-to-rear (FTR) relative to the ground, there is upward motion. Likewise, everywhere the flow is rear-to-front (RTF), there is downward

motion. This pattern of downward motion in the RTF flow and ascent in the FTR flow has been previously documented by Rutledge *et al.* (1988) for the 10-11 June 1985 PRE-STORM squall line. In examining the squall lines discussed in the previous section, it is found that this pattern of ascent and descent is common to most squall lines that feature rearward-sloping vorticity zones, and is, in the simplest sense, a consequence of the tilt of the parallel flow branches.

In this study, emphasis is placed on the vorticity distribution and storm evolution, not the presence or absence of FTR or RTF flow. To further examine the role of the vorticity zone and the mesoscale vertical motion, it is of interest to compare the distributions of vorticity and horizontal divergence. As a first approximation, assume that there is a region of the storm in which the vorticity surfaces and streamlines are parallel (i.e. the vorticity is the result of shear only), and the windspeed is constant along each streamline. If the streamlines and vorticity surfaces are oriented at some angle θ from the horizontal (in general, $\pi/2 < \theta < \pi$ if θ is measured from the +x axis), then

$$\eta = -\frac{1}{\sin\theta\cos\theta}\frac{\partial u}{\partial x} \tag{5}$$

and thus *horizontal* divergence can be expressed as a function of vorticity:

$$\frac{\partial u}{\partial x} = -\eta \sin\theta\cos\theta \tag{6}$$

The function $\sin\theta\cos\theta$ is negative whenever the slope is upward toward rear, and largest when the slope is upward toward the rear at a 45 degree angle. Therefore, for sheared parallel flow with constant speed along each

streamline, horizontal convergence will occur most strongly where vorticity is the most negative. In all of the squall lines examined in the previous section, the sloping zone of negative vorticity was approximately collocated with a region of horizontal convergence. This implies that the flow in squall lines (at least those examined in this research) is fairly well represented by the simplifications made above. More importantly, the presence of horizontal convergence in the region of negative vorticity implies a tendency for larger vertical velocity above the vorticity zone, and smaller or negative vertical velocity below.

Mesoscale vertical motion in the trailing region can thus be viewed from two perspectives. In one, it is merely a consequence of the tilted structure of the streamlines. In the other, sheared parallel flow is shown to have maximum horizontal convergence associated with maximum negative vorticity. From either viewpoint, it is clear that the mesoscale ascent in the upper part of the trailing region, and the mesoscale descent below, is associated with the tilt of the mesoscale flow branches themselves. The trailing region is not characterized by convergence between two horizontal streams, leading to ascent somewhere in the midst of the region. Rather, it is more adequately characterized by tilted, sheared flow, or FTR and RTF streams slipping past one another on tilted streamlines. And once this sheared flow, and the associated vorticity structure, become horizontal, *mesoscale* vertical motion largely ceases (although localized pockets of ascent may remain).

The presence of horizontal vorticity plays one other crucial role in the dynamics of the trailing region. In order for sublimation and/or evaporation to occur beneath the trailing anvil cloud and ascending FTR flow region, unsaturated air must be present below. The superposition of the saturated,

precipitating layer and the subsaturated, potentially cooler air is a result of the *shear* between the upper and lower flow branches, and thus is crudely a function of the magnitude of the negative vorticity in the middle part of the trailing region. It is not necessary to have rear inflow relative to the leading edge transporting potentially cooler air into the area beneath the anvil cloud. FTR flow aloft could achieve the necessary superposition by transporting saturated air over stationary potentially cooler air below, for example. Thus shear, characterized by the presence of negative vorticity, is all that is required (kinematically) to enable the thermodynamic processes at the rear of the storm to lead to the further generation of vorticity. The strength of the relative rear inflow *per se* is not relevant in these processes.

f. Vorticity dynamics near the leading edge

Observations of the seven squall lines have been examined further in order to evaluate the simplifying assumptions presented by RKW, and to find replacements if these are not correct. Fig. 19a illustrates the flow pattern that embodies the assumptions of RKW. A cursory examination of the velocity fields shown herein make it clear that squall lines (at least those in the sample studied) do not, in general, contain vertically issuing symmetric updrafts in the vicinity of the cold pool. Nor do they contain stagnant flow with respect to the motion of the gust front in the cold pool region.

Neither of these observations invalidate the findings of RKW, however. In a broad sense, it is only required that the flux terms at the rear (left) and top of a chosen volume sum to zero (see Eq. 5 in RKW) in order to arrive at the RKW finding that "the import of the positive vorticity associated

with the low-level shear just balances the net buoyant generation of negative vorticity by the cold pool in the volume." When these two terms sum to zero, Eq. 5 of RKW simplifies to

$$\Delta \frac{u_R^2}{2} = \int_o^H B_L dz = -c^2 \tag{7}$$

The situation described by this equation is illustrated in Fig. 21b. The orientation and vorticity transport by the updraft (F_U) is arbitrary, but must be exactly opposed by the vorticity transport at the left face (F_L). The control volume must be chosen in such a way that the updraft issues from its top, since it is the impact of vorticity transport and buoyancy generation on the updraft structure that RKW are addressing.

In light of this more relaxed condition for the RKW integration, sums of left and upper face fluxes were computed for a number of storms and times. These sums were computed for volumes of 10 km width and varying depth, always chosen such that the right side was ahead of the gust front and the updraft branch passed through the top face. This process was repeated for all suitable integration volumes.

In general, these two terms did not sum to zero for any reasonable choice of upper and left face positions. In fact, this sum was typically of the same order as the transport estimated from environmental differential kinetic energy at the right face. Much of the contribution to the sum came from the left face, where either rearward flow was transporting negative vorticity (positive integral) into the cold pool region, or forward flow was transporting positive vorticity (again a positive integral) toward the front of the cold pool region. Other volumes were also analyzed to determine if any volumes existed with zero net flux at the upper and left faces, even if the

upper face contained a mixture of upward and downward motion. No volumes were found for which suitable assumptions could be made about the term involving integrated buoyancy in Eq. 5 of RKW.

These total transports are illustrated in Fig. 19 for three times during case 26nov88s. For any given point in these figures, the value at that point represents the sum of the left-face flux below that point and the top-face flux on the surface extending 10 km to the right of that point. Thus, the value is the sum of the two relevant fluxes for a rectangle having its upper left corner at that point. The gust front position, and position of the sloping vorticity zone, are marked. The updraft is a rearward-directed stream immediately above this zone. It can be seen that for reasonable control volumes, the total flux on the two relevant faces is near the maximum found in the forward part of the storm. Values are generally in excess of 100 m^2s^{-2}, which is the same order as the flux at the right side due to the environment. This is a general result based on similar calculations for all seven squall lines.

A number of other approaches to simplifying the integration of Eq. 5 in RKW were investigated. It was not possible to find any simplifying assumptions that could be reasonably applied to all storms at all times. Therefore, since the simplifications of RKW are not valid for the sample of storms investigated, and the data do not suggest any widely-valid replacements, a new approach was developed which is described in the remainder of this dissertation.

Chapter 4
A theory for the role of the environment in evolution

a. Theories based on vorticity budgets: the problem of cross-boundary transport.

As documented in the previous section, no apparent simplifications are available for solving the integration problem posed in RKW. Although one can make reasonable assumptions about the buoyancy distribution, it is also necessary to know the magnitude of the flux of vorticity across the boundary of the volume of interest. The flux associated with the inflow at the forward side can be assumed to be based on environmental values of differential kinetic energy, but the transport at the rear and upper sides of a rectangular region cannot be neglected, nor can their magnitudes be readily approximated. Since any equation for the tendency of circulation about the region involves these same quantities, that problem also is not amenable to simplifying assumptions about fluxes.

In this study, the problem is approached differently. An attempt is made to deduce the total flux about a specified region based on the flow in that region as determined by the vorticity structure. The flow in an incompressible, inviscid, Boussinesq fluid at any instant is described by the definition of horizontal vorticity (Eq. 1) and the continuity equation:

$$\frac{\partial u}{\partial x} + \frac{\partial w}{\partial z} = 0 \tag{8}$$

Combining these expressions by differentiating Eq. 8 with respect to z and Eq. 1 with respect to x leads to the following Poisson equation describing w:

$$\nabla^2 w = -\frac{\partial \eta}{\partial x} \tag{9}$$

Once this equation is solved for w, u can be computed by integrating the continuity equation from a lateral boundary upon which u is assumed to be known. Thus, by assuming a vorticity structure, not only can the velocity distribution be determined, but also the fluxes of vorticity across various boundaries.

b. A simple three-region squall line

The observations discussed in Chapter 3 suggest that a squall line is approximately described as a sloping zone of negative vorticity. This is shown in Fig. 23 as the region labeled "i" (this name was chosen to since the sloping region is generally near the interface between two distinct flow branches). The slope of this vorticity zone is indicated by the angle α, as shown in Fig. 23. As established in Chapter 3, evolution of a squall line is characterized by the gradual tilting of this vorticity zone from an upright orientation to a quasi-horizontal orientation.

The environmental wind profiles associated with the storms described in Chapter 3, as well as with most squall lines examined in the literature through observational, modelling, and theoretical studies, can be approximated by a layer of about 3000 m depth with constant shear (from the surface to height z_j), located below an upper layer with a different value of constant shear. If shear "reverses" in the upper layer (i.e. line-normal flow becomes increasingly negative with height), the flow near z_j resembles a jet.

These wind profiles will be discussed further in later sections. This commonly observed two-layer structure to the environmental flow requires that two other regions of vorticity must be included on this simple model: a lower environmental shear layer and an upper layer.

For this discussion, it will be assumed, based on observations, that the vorticity in each region remains constant. In Fig. 24, the average vorticity in the interior region of the six well-observed squall lines is depicted. The cases are arranged, from a-f, in order of increasing rate of evolution. As described in Chapter 3, it can be seen that vorticity becomes rapidly more negative during the formative and intensifying stages, remains approximately constant during the mature stage, and then increases gradually during the dissipating stage. It is during the mature stage that a squall line tilts from its most erect orientation to quasi-horizontal, and it is this stage that is characterized by relatively slow changes to the average vorticity.

In regions a and b, few observations are available to support the assumption of constant vorticity. It is reasonable to expect that the forward environment will be modified due to the presence of the squall line (e.g., Hoxit *et al.*, 1976, and LM). However, it will be assumed herein that the environmental shear is steady. Thus, in this model, changes in circulation are accommodated exclusively by changes in the areas of the regions, not by changes in average vorticity. This model is unquestionably highly simplified compared to real squall line and environmental flows, but it will allow for some new findings regarding the role of environmental shear. It does include some of the typical squall line flow features, including a low-level gust front, a sloping updraft, and a region of rear inflow (examples of the simplified flow are shown in the next section).

Circulation in this problem is defined as

$$C = \int_S \eta \cdot \mathrm{n} dS \tag{10}$$

where S describes a vertically oriented surface orthogonal to the squall line orientation, and n is the unit normal vector to the surface. Letting η represent the spatially averaged vorticity in each region,

$$C = A_a \eta_a + A_b \eta_b + A_i \eta_i \tag{11}$$

is the circulation about the regions a, b, and i combined, where A represents the area of the respective regions. Further, with vorticity constant, the circulation tendency is simply

$$\frac{dC}{dt} = \frac{dA_a}{dt} \eta_a + \frac{dA_b}{dt} \eta_b + \frac{dA_i}{dt} \eta_i \tag{12}$$

It is assumed that the width of region i is fixed, so its area is constant regardless of the slope. Thus any changes in circulation (as a result of buoyancy effects, for example) about the combined region lead to changes in the areas of regions a and b. In the atmosphere, the average vorticity in each region could adjust to accommodate the circulation tendency, but in this simple model *it is required that the slope of the storm is the only feature that can change*. The impact and validity of these assumptions are addressed in later sections.

In the three-region model described above, the area of region a is given by

$$A_a = \frac{1}{\alpha}(z_t - z_j)[(z_j + \frac{1}{2}(z_t - z_j)] \tag{13}$$

The area of region b is given by

$$A_b = \frac{z_j^2}{2\alpha} \quad . \tag{14}$$

The area of region i remains fixed because it is assumed, that its width remains approximately constant (based on observations of the storms discussed in Chapter 3). Differentiating Eqs. 13 and 14 with respect to time, with levels z_j and z_t fixed, and substituting in Eq. 12 yields an expression for the tendency of circulation as a function of slope α:

$$\frac{dC}{dt} = \frac{1}{2\alpha^2}[\eta_a(z_j^2 - z_i^2) - \eta_b z_j^2]\frac{d\alpha}{dt} \quad . \tag{15}$$

c. Determination of flow and vorticity fluxes

An alternative expression for the circulation tendency about a circuit that is not a material curve, where l is a unit vector along the curve and k is the unit vector in the +z direction, can be expressed as

$$\frac{dC}{dt} = \oint \mathbf{V} \times \eta \cdot \mathbf{dl} + \oint \mathbf{k} g B \cdot \mathbf{dl} \quad . \tag{16}$$

This equation shows that two processes can lead to changes in the circulation: transport of vorticity across the boundaries and the generation of circulation owing to buoyancy effects. The difficulties in evaluating the first term on the right, the flux of vorticity across the boundaries of a region, have already been documented.

In this study, a new approach is used in an attempt to approximate these terms. The Poisson equation for w (Eq. 9) is solved using a relaxation technique. The vorticity distribution is as described in the discussion of the three-region model shown in Fig. 23: constant vorticity with different values

in regions a and b, and negative vorticity in region i. The sloping vorticity zone, region i, is assumed to have a linear increase in vorticity from a specified minimum along the center line, h_{min}, to the surrounding ambient value. The width of this zone is kept fixed at 10 km, a value very typical of observed storms. Boundary values of w were specified to be zero at left and right boundaries well-removed from the sloping vorticity zone, and at z=0 and z=15 km. The vorticity flux term at the upper boundary is computed at level z_t (6000 m) along the line from the rear of the sloping vorticity zone to the right lateral boundary (upper bold line in Fig. 23). The vorticity flux was also computed at the sloping rear boundary of the region i using the normal velocity component. Vorticity flux at the surface is known to be zero since w=0. In a series of experiments the slope α of region i, vorticity in region i, and ambient upper and lower shear were varied over the entire range observed in the cases described in Chapter 3, plus a large surrounding range of values that encompass all squall line cases reported in the literature.

i) Flow as a function of inflow strength

The validity of the simple three region model is explored in this section by examining the velocity distributions derived from its vorticity structure. The vertical velocity distribution in this model is determined entirely by the vorticity distribution. Thus changing the magnitude of the horizontal flow at a boundary does not alter the distribution of w, but does change the orientation of the streamlines.

Figure 25 illustrates this effect using a vorticity zone sloped at 45 degrees, shear of $4 \times 10^{-3} s^{-1}$ (12 ms^{-1} over 3000 m depth) in the lower layer, and

no shear in the upper layer. In the case of strong inflow (18 ms^{-1} velocity at the lowest level, shown in panel a), the updraft tilts rearward above a gust front that has a surface location at x=37 km. With inflow of 12 ms^{-1}, the updraft issues vertically (as required in RKW), but is highly asymmetric. With weaker inflow (6 ms^{-1} in panel c) the gust front is located near x=40 km, slightly more forward than in the stronger inflow solutions, and the updraft streamlines tilt forward with height.

The orientation of the updraft would seem to imply that there is a minimum inflow strength required for rearward-sloping updraft trajectories, prohibiting precipitation from falling into the inflow. However, this sensitivity was not tested in this study. Since it is the actual trajectories of the inflow rather than the streamlines that are important here, the propagation speed would also play a role in determining whether or not precipitation is deposited in the inflow.

Several important features of squall lines are shown in these solutions based on the simple three-region model. A surface gust front is present at the source region for the updraft. The updraft slopes rearward above the sloped vorticity zone. Also, a rear inflow jet is present that descends toward the surface near the leading edge. The slope of the inflow jet may appear extreme in these solutions, but the 45 degree slope of region i is quite large for a mature squall line as shown in Chapter 3. With more realistic slopes, the rear inflow jet would descend more gradually.

ii) Flow as a function of vorticity zone strength

The effect of varying the minimum vorticity in the sloping region i is illustrated in Fig. 26. The most obvious effect is the increase in the strength of the perturbed flow with increasing magnitude of negative vorticity. In all three solutions, the width of the sloping vorticity zone, inflow strength, and ambient shears are the same. Interestingly, in panel c of Fig. 26, the ambient vorticity below 3 km is equal to the minimum vorticity in the sloping zone. Thus, this solution most nearly represents a "balance" between ambient and storm-generated vorticity. However, this set of solutions shows that if an "optimal" configuration is one with an intense updraft, it is preferable to have much stronger storm generated vorticity than ambient shear, as in panel a. On the other hand, if it is optimal to have a vertically issuing updraft, another combination of shear and storm-generated vorticity is desirable. The "balanced" solution leads to a rather weak, sloped updraft in these particular combinations of parameters.

More subtle effects of varying the vorticity are also illustrated. The flow at the lowest level has stagnation points ahead of and behind region i. When storm-generated vorticity is small, as in panel c, the stagnation points are closer to the centerline of region i. As storm-generated vorticity becomes large, the stagnation points move away from the centerline.

iii) Flow as a function of slope

A major finding discussed previously is that the storm evolution is described by the gradual tilting of the zone of negative vorticity, from erect to quasi-horizontal. Fig. 27 shows the effect of tilting on the relaxation solutions. The slope of region i in panel a is 1.0 (45 degrees inclined from horizontal). Such a slope is quite extreme, and was usually only observed in the formative and intensifying stages of the squall lines. At this slope, the flow represents an updraft above a surface "windshift", with a trailing downdraft and developing rear inflow.

In panel b, the slope is 0.5 (about 27 degrees). This also is a rather large slope for the mature stage of a squall line, but was observed in at least one case (26jan89s). At this slope, rear inflow has expanded and occupies a region 20-30 km in horizontal extent behind the leading edge. In panel c, the slope is 0.25 (about 14 degrees). This slope is quite typical of the mature stage of most of the squall lines examined. At this slope, descending rear inflow in the region below 6 km extends at least 60 km behind the leading edge. Thus, the upscale growth of the squall line circulation can be approximated by the tilting of the vorticity zone toward the horizontal.

These solutions are similar in many important respects to squall line flows in the lowest 6 km. They all feature an updraft that begins near a surface windshift region, and slopes upward and rearward. As the vorticity zone (region i) tilts toward the horizontal, the updraft streamlines become more horizontally inclined, and vertical velocities become weaker, in strong agreement with the findings presented in Chapter 3. In addition, the solutions show a downdraft region that, at large slopes, resembles convective

downdrafts, and as the system tilts toward the horizontal, resembles a descending rear inflow jet. Again, these findings show striking similarity to the gross features of structure and evolution described in previously. Panel c of Fig. 27 also bears considerable resemblance to the conceptual model for a "mature" squall line storm (Fig. 1).

One other feature merits discussion. In this simple model, the strength and orientation of the rear inflow jet is a function of the environmental flow and the strength and orientation of the vorticity in region i. If the shear in region b is strong enough to cause storm-relative RTF flow in the environment, this flow penetrates to near region i. It remains "elevated" when the region i vorticity is relatively weak, and it "plunges" when the vorticity is relatively strong.

iv) Total flux determined from relaxation solutions

Several hundred solutions to Eq. 9 were assembled that span a large range of lower and upper ambient shear, strength of the vorticity zone, slope, etc. The ranges of these variables that were used encompass all of the storms observed in Chapter 3, and most (perhaps all) other published squall line cases. This was done in order to find an expression for total flux as a function of the other parameters.

Allowing only slope to vary, it is found that in all cases the total flux of vorticity across the boundary shown with the heavy bold line in Fig. 23 is a nearly linear function of slope up to about α=0.66 (approximately 38 degrees). For more erect slopes, flux is approximately constant at the value corresponding to α=0.66. This is illustrated in Fig. 28 for zero upper shear,

$4x10^{-3}s^{-1}$ lower shear, and vorticity zone strength $-1x10^{-2}s^{-1}$. This finding greatly simplifies the process of determining an approximation for total flux based on the other parameters. The dependence on α is linear, so it is only necessary to approximate the total flux at (say) α=0.66.

Another major simplification results from the fact that total flux is not a function of inflow strength. For given upper and lower shears, the wind speed at any level (z=0, for example) determines the speed at all levels. In this model, for a given vorticity distribution, w is determined. Thus the transport through the upper part of the domain is a function of vorticity distribution alone. Since w is fixed, increasing inflow at the right side of the domain correspondingly increases rearward flow at the sloping rear surface (mass is conserved in the domain). The vorticity distribution is the same at both of these faces, so an increase in vorticity flux at one face causes an equal and opposite transport at the other face.

With the simplifications just discussed, the process of determining total vorticity flux (first term on RHS of Eq. 18) becomes one of fitting the flux at a slope α=0.66 as a function of upper and lower shears and minimum vorticity in region i. Several hundred relaxation solutions to total flux were computed. The following expression describes the dependence of total flux (F_t) on the other parameters:

$$\begin{aligned} F_t = & -16.4 + 1.78x10^3 \eta_{min} + 1.62x10^6 \eta_{min}^2 \\ & +1.12x10^7 \eta_{min}\eta_a - 9.65x10^3 \eta_b - 1.57x10^7 \eta_{min}\eta_b \\ & -1.13x10^7 \eta_a\eta_b + 1.37x10^7 \eta_b^2 \end{aligned} \qquad (17)$$

Here, the subscript "min" represents the minimum value on the center line of region i. Fig. 29 shows that this expression provides an excellent fit to the total fluxes computed in the many relaxation solutions. It should be noted that this expression is valid for the following ranges of parameters:

$\alpha \leq 0.66$

$-1.5\text{x}10^{-2} < \eta_{min} < 0$

$0 < \eta_b < 1.5\text{x}10^{-2}$

$-5\text{x}10^{-3} < \eta_a < 5\text{x}10^{-3}$

For slopes greater than α=0.66 (about 38 degrees), F_t can be approximated using the value for α=0.66.

d. Slope, tilt, and the predictive equation for tilting

In this dissertation, the term slope (represented by angle α) is used to represent the inclination from the horizontal of the sloping vorticity zone. The term "tilt" is used as a verb to represent the change of slope, $d\alpha/dt$. An equation for $d\alpha/dt$ can be arrived at by combining Eq. 16 with Eq. 15 to yield

$$\frac{d\alpha}{dt} = \frac{2\alpha^2(F_t + \oint_l \mathbf{k}gB \cdot \mathbf{dl})}{\eta_a(z_j^2 - z_t^2) - \eta_b z_j^2} \tag{18}$$

This expression is general, and not dependent on the relaxation solutions and curve fitting described above. The technique described in the previous section gives an expression for F_t which can be used to evaluate the effects of environmental shear in the tilt of the sloping vorticity zone.

Eq. 18 indicates that one condition for steadiness ($d\alpha/dt = 0$) is for the transport of vorticity out of the domain (F_t) to be exactly offset by the generation due to buoyancy at the rear side of the domain. Another implication of Eq. 18 is that as the slope approaches horizontal, the tilting diminishes. And most important, the denominator can be of either sign according to sign in the following inequality:

$$\frac{z_j^2}{z_t^2} < \frac{\eta_a}{\eta_a - \eta_b} \quad . \tag{19}$$

The value of the denominator in Eq. 18 is shown in Fig. 30. It can be seen that the denominator can take either sign over the range of shears observed in squall line environments. In the region where the denominator is near zero, Eq. 18 implies that tilting will be rapid, either forward or rearward depending on the balance of integrated negative buoyancy and F_t. This region corresponds to the physical situation of little net average vorticity in the environment, so that very large changes of area are required to accommodate any changes in circulation. Some implications of this are explored in later sections.

e. A role of the environment in storm evolution

In this section, the role played by the environment in determining tilting rate is explored. As an introduction, the nature of the solutions for a given set of vorticity values in the three regions is shown graphically in Fig. 31. The nature of the curves can change dramatically as the shears are varied, so this example should not be interpreted as illustrating the role of shear and buoyancy across the parameter space. This particular set of curves is presented to make one major point concerning the possibility of a steady slope under the given conditions. The graph shows tilt versus slope for a set of four combinations of shears and integrated negative vorticity, DCAPE (Downdraft Convective Available Potential Energy). The term "DCAPE" is used here because, as shown in Chapter 3, it seems that the region containing the most negative buoyancy probably slopes up and rearward along the underside of the sloping vorticity zone, and is not confined to a surface-based

"cold pool." It should be noted that DCAPE is sensitive to the time of day, since it involves the integrated difference between the environmental virtual potential temperature ahead of the storm and the virtual potential temperature of the negatively buoyant air in the storm. Thus, significantly smaller DCAPE is to be expected with a nocturnal boundary layer compared to a daytime boundary layer.

For certain values of DCAPE, one curve (open circles) shows that, for any slope, the tendency is for the vorticity zone to continue to tilt rearward ($d\alpha/dt < 0$). For other combinations (e.g. the curve with filled squares), erect zones initially tilt rearward, but then slow and stop tilting as certain slopes are reached. The observations presented previously indicate that in the formative and intensifying stages, updrafts and negative vorticity zones are erect. Thus this theory indicates that for certain combinations of shears, storm-generated vorticity strength, and DCAPE, the storm will arrive at an equilibrium slope and remain steady at that slope (presumably until environmental shears or DCAPE changes). Additionally, it appears that if a storm "finds itself" with slope shallower than the equilibrium slope, it will become more upright until it reaches the equilibrium. In this section, the general findings of this theory will be explored with regard to the possibility of an equilibrium slope being reached. With yet other combinations, a rearward-sloped storm will tend to become more erect (filled circles).

Figure 32 show the equilibrium slopes (defined as the slope above which region i tilts rearward and below which region i tilts forward) as a function of environmental upper and lower shear for three different values of DCAPE. All of these graphs are for minimum region i vorticity of $-8 \times 10^{-3} s^{-1}$, a typical value for the observed storms. Where the curves are plotted, it can be said that a steady storm ($d\alpha/dt=0$) is possible. More

specifically, it can be seen that as DCAPE increases (from panel a to c), larger lower shears are required for steadiness. For the case of a DCAPE of -1500 m^2s^{-2}, low-level shear must generally be larger than $1x10^{-2}s^{-1}$ (30 ms^{-1} in 3 km) to "balance" the cold pool and lead to a steady system. Note that in these results it is the magnitude of the low-level shear that is important, not its transport (i.e., not differential kinetic energy). This is a consequence of the fact that in this model, total flux of vorticity (F_t) does not vary with environmental flow strength, but only with vorticity.

It can also be seen in Fig. 32 that as upper shear goes from negative to positive, the possibility of a steady, rearward-sloping, quasi-2D squall line becomes more remote. Finally, as low-level shear increases for a given upper shear and DCAPE, the equilibrium slope becomes shallower. In light of RKW, this seems counterintuitive. However, the explanation is straightforward: as low-level shear increases, the total flux (F_t) increases. For a given large slope (α), the flux is more than sufficient to balance the cold pool, leading to a numerator in Eq. 18 that is positive. All of these curves fall in the region of Fig. 30 in which the denominator of Eq. 18 is less than zero, so rearward tilting is expected for the assumed large slope. Thus as low level shear increases, the tilting tendency is increasingly negative at large slopes. Therefore tilting tendency does not go to zero until shallower slopes are reached.

If this theory is correct, it appears that the intuitive concepts proposed by RKW must be reconsidered. Storm structure and evolution *is* a function of the degree of balance between DCAPE and total flux. However, total flux is a function of the slope of the storm and the shear in both the lower and upper levels. The implications of Eq. 18 will be further illustrated in later sections where observations and previous modelling results are considered.

The data presented in Fig. 32 pose a forecast dilemma: as low-level shear increases, a sudden transition is made from conditions in which no steady rearward-sloped storm is possible, to those supporting an erect, steady storm. Presumably the erect configuration would also imply a relatively more intense storm, since updraft magnitudes would be larger and confined to a narrower band.

As a final illustration of the predictions of this theory, the average DCAPE that can lead to a steady storm ($d\alpha/dt=0$) is shown in Fig. 33a for a variety of shears. The minimum vorticity in region i is again assumed to be $-8x10^{-3}s^{-1}$. Where curves are not plotted, a steady rearward-sloping squall line is not possible. One general finding is that larger DCAPE can be balanced by increasing low-level shear, as argued in RKW. Another finding is that upper-level shears less than zero (reverse shear) supports allows stronger cold pools to be associated with steady storms. In Fig. 33b, the full width of the range of cold pools associated with steady storms is shown. The clear interpretation is that a very wide range of DCAPE can lead to steady storms if the low-level shear is large (these steady storms will have a variety of equilibrium slopes). On the other hand, as upper shear increases and/or low-level shear becomes smaller, the storms require a more exact DCAPE for steadiness.

f. Comparison to observed cases

In this section, the predictions of the theory are compared to the seven cases from Chapter 3, in which the mature stage and tilting rate were well documented. In order to evaluate the theory, soundings were used that were nearest in time and space to the leading edges, yet appeared to be unaffected by

the squall lines. The shears below and above 3 km were estimated by approximating the line-normal velocity profile with straight lines in those layers. A good technique for estimating integrated negative buoyancy has not yet been developed. For these tests, DCAPE was evaluated as the integral of the difference between the sounding wet bulb temperature profile and the environmental temperature below 6 km. The tilting rate equation was evaluated for this particular value of DCAPE +/- 30%. This range should allow the effects of condensate loading, vertical redistribution of cooled air, and other effects to be represented. Since soundings were not generally available to the immediate rear of the leading edge of these systems, any refinement to the estimated DCAPE would be highly speculative.

Earlier in Fig. 24, the slope α of the six well-observed squall lines was depicted as a function of time (solid curves). The cases are arranged from a-f according to a crude estimate of rate of tilting during the mature stages. These cases are examined in that order: slowest-evolving to most-quickly evolving.

The environment of the storm denoted 26jan89s (the slowly evolving system on 26 January 1989 from DUNDEE) is examined in Fig. 34. As shown earlier in Fig. 24a, the vorticity zone in this storm essentially oscillated about a very large slope; hence it was quasi-steady. The estimated DCAPE of this storm was in the range -569 to -1057 m^2s^{-2}. The storm-relative line-normal wind component had large shear below the jet ($4x10^{-3}s^{-1}$), and relatively large "reverse" shear above the jet ($-1.2x10^{-3}s^{-1}$). It can be seen that the environmental flow is front-to-rear at all levels. Although rear-to-front relative environmental flow occasionally was observed in DUNDEE, in general the flow was front to rear in substantial agreement with the observation of Zipser (1977) of tropical squall lines having relative inflow (front-to-rear) at all levels. The solutions for the tilting in this environment

are also shown in Fig. 34c, using an assumed minimum vorticity in the sloping zone of $-8 \times 10^{-3} s^{-1}$. This value is fairly typical of the systems analyzed; the observed range was approximately $-6 \times 10^{-3} s^{-1}$ to $-10 \times 10^{-3} s^{-1}$. The curves are not especially sensitive to this parameter in most cases. The graph has a simple and clear interpretation: an initially erect storm will tilt fairly rapidly rearward. As it does, the rate of tilting rapidly goes to zero, so that the storm will eventually stop tilting and reach a steady configuration. For the sounding-derived DCAPE, equilibrium occurs at slopes greater than 30 degrees, in strong agreement with the observed equilibrium slope (Fig. 24). Two other curves are shown for smaller DCAPE, showing that as DCAPE is reduced, equilibrium occurs at shallower slopes.

Another rather slowly-evolving storm occurred during DUNDEE on 26 November, 1988 (26nov88s). Fig. 35 depicts the environmental conditions, as well as the solutions for rate of tilting for this storm. DCAPE is estimated to have been between -670 and -1244 $m^2 s^{-2}$, with an upper shear of about $-1.8 \times 10^{-3} s^{-1}$ and a lower shear of about $3.9 \times 10^{-3} s^{-1}$. The solutions for this case are unique among the six cases in that it appears that a storm with DCAPE near or less than -670 $m^2 s^{-2}$ and a slope of more than about 25 degrees will become more erect with time. The early history of this squall line is not known, since it formed beyond the range of the radar coverage. However, in Fig. 24 it can be seen that the storm generally had a slope less than 25 degrees, and in fact tilted only very slowly rearward with time. This seems to be in substantial agreement with the prediction of the theory for the observed slopes.

Another relatively slowly evolving storm occurred during the PRE-STORM on 10-11 June, 1985 (10jun85m). Fig. 24 shows that this storm tilted rather slowly rearward until it reached a slope of around 10 degrees, at which

time it appeared to be steady. This is a remarkably shallow slope for the vorticity zone; the storm's apparent vigor even at these shallow slopes can be attributed to the unusually strong storm-relative inflow, a condition which implies stronger-than-usual ascent for a given slope. The environmental conditions and solution for tilting are shown in Fig. 36. The curves are similar to those for 26jan89, in that they show a comparatively slow tilting rate, and the likelihood of steadiness. In contrast to 26jan89s, it appears that this storm should become steady at a much shallower slope (12-21 degrees), which is well supported by the observations (i.e. this storm became steady at a much shallower slope than 26jan89s).

A more quickly evolving storm occurred in DUNDEE on 7 February, 1990 (7feb90m). The environment (Fig. 37) contained weaker average shear in the low levels (about $5 \times 10^{-3} s^{-1}$) than the three previous cases, as well as weaker reverse shear above the jet (about $-1 \times 10^{-3} s^{-1}$). DCAPE was estimated to have the second-largest magnitude of the six cases (-889 to -1651 $m^2 s^{-2}$). The solution for tilting for this case disagrees with the observations (Fig. 24). However, note from Fig. 30 that the denominator in Eq. 18 for this case is very close to zero. This implies fairly rapid evolution (unless the flux and DCAPE are very nearly balanced) but the sign of tilting is somewhat uncertain. This is an interesting part of the parameter space. The physical implication based on this theory is that evolution is rather unpredictable in this vicinity.

The last two storms illustrated in Fig. 24 evolved very quickly (other storms were observed which evolved so quickly that the mature stage was too short for estimates of tilting rates to be obtained). The environmental conditions for the DUNDEE storms on 5 December 1989 (5dec89f) and 18 November 1989 (18nov89f) are shown in Figures 38 and 39 respectively. It can be seen that both cases had relatively weak shear in the lower levels

(2.4×10^{-3} s^{-1} and 5×10^{-3} s^{-1} respectively) and moderate reverse shear above (about -2×10^{-3} s^{-1}). DCAPE in the case 5dec89f was estimated as -547 to -1012 $m^2 s^{-2}$, the weakest of the six cases, whereas in 18nov89f it was -982 to -1824 $m^2 s^{-2}$, the largest of the six. The solution curves for both cases correctly show that a *steady storm is not possible*. Rather, in both cases storms at any slope have the tendency to tilt further rearward.

In summation, the theory expressed by Eq. 18 correctly predicts the possibility of steadiness, the approximate slope at which steadiness occurs, and the correct sense of the rate of tilt (except for 7feb90m). It should be pointed out that, despite these strengths, the theory predicts tilting rates that are too large by an order of magnitude or more (~0.1 deg s^{-1} vs. the observed rates of ~0.01deg s^{-1}). Possible reasons for this overprediction are discussed in later sections.

g. Comparison to other observations

Herein predictions of Eq. 18 are compared to observations based on other published studies. Bluestein and Jain (1985) described an echo category they termed "broken line" which most nearly resembles the typical echo patterns of quasi-two-dimensional squall lines described herein. Using their published average line-normal wind components and standard deviations, the average low-level shear for their "broken line" classification is approximately between 0.7×10^{-3} s^{-1} and 4×10^{-3} s^{-1}. The average shear from 3 to 6 km is approximately between -0.7×10^{-3} s^{-1} and 2.7×10^{-3} s^{-1}. The 26 May 1976 squall line in Oklahoma (Ogura and Liou, 1980; Smull and Houze, 1985; 1987) is one example of a storm that occurred within this range of shears. Referring to Fig. 33 it can be seen that these shears should be associated with

storms falling well outside the ranges associated with steady systems except perhaps those with unusually small DCAPE. Another classification that seems to encompass the quasi-two-dimensional squall lines discussed herein is the "strongly classifiable symmetric" class of Houze *et al.* (1990), identified from climatological studies of Oklahoma squall lines. Their values of lower shear ($1.2 \times 10^{-3} s^{-1}$) and upper shear ($1.8 \times 10^{-3} s^{-1}$) fall into the same parameter space as those given by Bluestein and Jain for squall lines in the same region. Solutions to Eq. 18 spanning the likely range of cold pools strengths are shown in Fig. 40. It can be seen that for all values of DCAPE with these two given shears, the vorticity zones tilt forward regardless of the slope.

For all of the available mid-latitude data discussed above (except for the 10-11 June 1985 PRE-STORM case described above), it appears that the low-level shear is too weak to allow for steady, rearward-sloped storms. The possible exception to this finding is for mid-latitude cases occurring at night when DCAPE is much smaller due to the relative coolness of the nocturnal boundary layer. Under the "typical" middle latitude environmental conditions, it appears that steady, rearward-sloped systems are quite possible at night, but highly unlikely during the daytime, due to the expected changes in DCAPE.

It is likely that many of the daytime middle latitude systems examined as individual cases or part of climatological studies, are not quasi-2D, rearward-sloped steady systems. It is interesting that in examining the slab averages of reflectivity for the tropical systems, even at 10 minute temporal resolution, individual cells were not seen propagating rearward from the leading edge, and horizontal depictions of reflectivity showed very uniform structure to the leading edge compared to published middle latitude cases. The conceptual model based on middle latitude systems features rearward-

propagating discrete cells, and the horizontal reflectivity structure is comparatively more cellular.

In general, observations suggest, and this theory predicts, a better likelihood of long-lived squall lines with *steady updrafts* in the tropics than in middle latitudes, because of the beneficial presence of reverse shear above the low-level line-normal jet. It suggests that many middle latitude squall lines that occur during the daytime, although they may be long-lived, are somehow dynamically different than those described by the model herein. This difference may involve unsteady, forward-sloped updrafts, reorientation of vorticity due to earth's rotation or 3D effects into the line-normal plane, effects due to large-scale baroclinity, etc. However, it seems that the steady, rearward-sloped vorticity zone model probably does not describe many squall lines that occur with weak low-level shear and forward shear aloft. Despite the apparent common occurrence of squall lines under these conditions in the middle latitudes, there remains an almost complete lack of Doppler data sets with sufficient temporal resolution to adequately assess the evolution and mode of propagation of these systems.

Finally, other systems observed in the tropics include the 23 June 1981 COPT 81 squall line in west Africa (Roux 1988). The approximate low-level shear in the environment of this system was $5.2 \times 10^{-3} s^{-1}$, with an upper shear of $-1.3 \times 10^{-3} s^{-1}$. Using a range of possible values of DCAPE, the resulting predictions of tilt rate as a function of slope are shown in Fig. 41. It appears from this theory that for DCAPE of less than $-1000\ m^2 s^{-2}$, a steady system is possible with a rather large slope (about 25 degrees or more). That is quite similar to the slope seen in Fig. 6b in Roux (1988).

h. The findings of RKW and LM interpreted through this theory

This theory embodies, albeit crudely, some the system-scale effects described by LM as being important to squall line longevity. To the extent that quasi-2D squall lines are represented by sloping vorticity zones embedded in a two-layer environment, these features are included. As described previously, these include a rearward-sloping updraft, a possible overturning updraft branch, and descending rear inflow branches of various strengths and configurations. Clearly, this is a highly simplified model, but it implicitly represents a much broader scale of influences than a simple cold pool/low-level shear balance.

Based on numerical modelling studies, Thorpe *et al.* (1982, hereafter referred to as TMM), demonstrated that even with low-level shear held constant, the shear above had profound influences on the resulting storm structure and evolution. Using their shears, and a DCAPE of -800 m^2s^{-2}, the theory herein predicts results (Fig. 42) similar to those reported by TMM. For instance, it appears that for strong forward shear, denoted "P(+10)" in TMM, a forward-tilting vorticity zone is likely. Presumably, in a 2-D simulation, this system would deposit precipitation into its inflow, thereby reducing potential buoyancy and storm longevity. TMM report that the P(+10) storm consisted of essentially one pulse of convection followed immediately by decay. The P(+5) simulation produced a "vigorous second cell" which also decayed rapidly. This is an interesting finding in light of the discussion above concerning the middle latitude squall line cases, and lends credence to the speculation that, where the present theory predicts slow forward tilting, squall

lines are possible but their leading edge convection will exhibit pulsing behavior, or the commonly reported "succession of cells" in the 2-D structure.

The remaining curves suggest steady, rearward-sloped storms. The smallest predicted equilibrium slope is associated with "reverse" shear of 10 ms^{-1} aloft, while the most erect is associated with no shear aloft. These correspond to the "P(-10)" and "P(0)" storms in TMM. Their results indicate that the longest-lived storm occurred with no shear aloft, and the theory herein predicts that this storm should indeed be steady. With the shallower equilibrium slope, the theory implies that the "P(-10)" storm should deposit precipitation over the largest rearward-extending region, which it did in the simulations of TMM. Computations for other values of DCAPE indicate that, for this particular set of shears, the tilting rates and equilibrium slopes are highly sensitive to DCAPE. Despite this fact, it is clear that a variety of possibilities for steadiness and equilibrium slopes are possible when only upper shear is varied, in complete agreement with the findings of TMM.

RKW did not consider the role of upper shear. In their study, upper shear was held constant at zero, while lower shear was varied in a search for an optimal value. Using a velocity profile containing no shear in the upper levels, Eq. 18 predicts that the optimal lower shear is approximately where RKW predicted it to be. Although DCAPE in the RKW simulations is not known, for a strength of -600 m^2s^{-2} the most erect, steady storm should occur with a lower shear of about $7x10^{-3}s^{-1}$, exactly as found by RKW (see Fig. 43). With a DCAPE of -1200 m^2s^{-2}, this "optimal" shear value increases to around $9x10^{-3}s^{-1}$. Other "optimal" values of DCAPE for wind profiles with no upper shear can be found in Fig. 33 along the line where ambient upper shear equals zero.

The RKW theory involved only cold pool strength and vorticity transport from the environment in the lower levels in an attempt to explain strong, long-lived squall lines. The RKW approach, and the need to verify their conclusions from an observational perspective, motivated this study. In light of the agreement between observations, modelling work, and observations shown in the present paper, it does appear that lower shear and DCAPE need to be considered together with upper shear and system slope when drawing conclusions about intensity and longevity.

Chapter 5

Discussion

Examination of the various cases documented observationally in this study reveals common features in the reflectivity and kinematic structure of these squall lines which can be associated with the stages of evolution. Of primary importance is the observation that although the storms undergo common patterns of evolution, the time scale over which the evolution occurs varies greatly among systems. Combined durations of the formative, intensifying, and mature stages of the storms varied from about an hour (18nov89F, 5dec89F), to over four hours (26jan89S). Measurements of the rate of change of slope of the vorticity zone in the jump updraft region shows that these systems may span an order of magnitude in evolution rates. Another observation of major importance is that the *structure* of this type of squall line is characterized by a sloping zone of horizontal vorticity, with streamlines approximately parallel to the vorticity zone. The *evolution* is characterized by the gradual tilting of this vorticity zone toward the horizontal. During the intensifying stage the sloping zone of negative horizontal vorticity develops, strengthens, and reaches its most upright orientation. During the mature stage, its strength remains about constant while it tilts toward the horizontal. During the dissipating stage, its orientation remains quasi-horizontal, and the vorticity weakens. These

generalizations seem to apply across a fairly large range of storm intensities and relative flow strengths.

Observations of features that can be used to classify storm stage are summarized in Table 2 and in Fig. 45. Because the structure of the flow and reflectivity change so much from one stage to another, the "snapshot" structure of a squall line depends strongly on the stage of evolution. For this reason, the

Table 2: Characteristics of squall line evolutionary stages.

	STAGE			
Characteristic	Formative	Intensifying	Mature	Dissipating
Horizontal reflectivity structure	Scattered or broken cells in a line	Soild line of cells. Trailing region forms	Solid line of cells. Large trailing region. Transition zone	Cellular leading becoming patchy. Stratiform weakens
Vertical reflectivity structure	Deepening	Reaches deepest, most intense, and most upright	Gradually becomes shallower, weaker, and more tilted	Shallow, relatively weak cells or stratiform ascent
Vertical velocity in leading edge	Increasing	Increases more quickly to maximum values	Gradually decreases	Small
Motion	Generally less than the mean flow	Continued relatively slow	Suddenly faster; resembles cold pool propagation speed	Varies
Slope	Varies	Most upright	Gradually more horizontal	Quasi-horizontal mesoscale flow branches

features depicted in conceptual models of squall line structure (e.g. Fig. 1) should be interpreted with caution as such a model may be a synthesis of features that occur at different times during the life cycle instead of typifying any certain stage. The rate at which evolution occurs in the squall lines described here makes any assumptions about steadiness of questionable value. Before a system is assumed steady from a dynamical viewpoint, a careful analysis of the relative magnitudes of terms in predictive equations should be made. In general, *a priori* assumptions of steadiness may not be justified when describing squall line dynamics.

The squall line examples presented herein, as well as the additional cases analyzed, but not discussed in detail, make it clear that the generation of vorticity is a system-scale phenomenon, as proposed by Lafore and Moncrieff (1989). This can be seen by examining the slab-averaged horizontal vorticity for the cases presented. Negative horizontal vorticity develops across the system shortly after the leading edge first becomes solid. The appearance of negative vorticity aloft to the rear of the leading edge seems to occur much too quickly to be attributed to advection rearward from some leading edge generation region alone. It appears that there is not a distinct separation between the negative horizontal vorticity in the low-level cold pool near the leading edge, and the vorticity that appears at higher elevations rearward of the leading edge (except perhaps during the dissipating stage). Instead, a nearly continuous zone of negative vorticity strengthens fairly uniformly across the system with time. This implies that important buoyancy gradients occur across the entire squall line and through most of its depth, not just near the leading edge of the low-level cold pool.

It is apparent from the data presented, that once a squall line becomes more-or-less solid at its leading edge, the buoyancy distribution leads to the

generation of negative vorticity to the rear of the leading edge. The flow structure associated with this vorticity is such that ice particles are carried rearward, relative to the leading edge, in the upper portion of the trailing region. Sublimation, melting, and evaporation below and to the rear of this expanding cloud, as well as condensate loading near the leading edge, should lead to a negative buoyancy anomaly along the sloping lower boundary of the trailing stratiform cloud. Heating due to condensation and freezing should maintain a positive buoyancy anomaly in the cloudy region as long as ascent persists. These anomalies produce a horizontal buoyancy gradient across the system, aiding in vorticity generation in the interior. One consequence of the generation of negative vorticity in the storm interior, under certain environmental conditions is that the strongest drafts gradually tilt from nearly vertical during the formative stage, to nearly horizontal in the dissipating stage, and the scale grows from that of convection to mesoscale. The demise of the squall line is apparently caused by the tilting process as it reorients the major drafts to quasi-horizontal slopes.

With respect to the role of upper level jets and ambient baroclinity in causing the development of a rear inflow jet, almost all of the cases studied developed significant rear inflows of 5-10 ms^{-1}. In some cases, rear inflow magnitudes of 10 to 20 ms^{-1} relative to the motion of the leading edge were present. The development of rear inflow did not depend on the presence of an upper jet impinging on the storm from the rear, which is the causative factor cited by Zhang and Gao (1989) in their modelling study of the 10-11 June PRE-STORM case. In several cases with significant rear inflow, there was no environmental RTF flow relative to the motion of the surface position of the leading edge. From the vorticity viewpoint, rear inflow should be expected to result from the storm-generated buoyancy gradients (as shown by Fovell and

Ogura, 1988) which lead to the generation of horizontal vorticity across the storm. While the "blocking" of middle- and upper-level momentum may indeed play a role in the rear inflow dynamics, it is not a sole causative role.

The observations indicate a strong connection between the occurrence of horizontal convergence and negative vorticity. It can be shown that such a correspondence is to be expected when the vorticity is due to shear alone between uniformly tilted streamlines. Thus the mesoscale ascent often observed in the upper part of the interior region, and mesoscale descent below, are a function of the magnitude of negative horizontal vorticity as well as the slope of the vorticity distribution. As tilting proceeds, the mesoscale ascent weakens until the streamlines in the interior region become horizontal. However, the velocity data suggest that there are pockets of vertical motion occurring in the upper portion of the interior region on a scale much more like that of the leading edge convection.

In one respect, the large magnitudes of negative vorticity generated in the storm interior tend to lead to additional generation of vorticity. This is because the shearing flow associated with the vorticity brings potentially cooler air beneath the saturated, precipitating anvil cloud, or in another frame of reference, draws the anvil cloud rearward over the potentially cooler air. In this way, the negative buoyancy anomaly at the rear of the system, beneath the anvil cloud, can be reinforced through diabatic processes. This in turn maintains the horizontal buoyancy gradients that cause additional vorticity generation.

It has been shown that the simplifying assumptions made by RKW do not seem to apply generally when the observations are examined. It is also clear from observations, as well as the work of TMM, that squall line

structure and evolution seem to be sensitively influenced by upper shear, not just by a balance between low-level vorticity transport and DCAPE.

Motivated by these observations, a new theory has been developed and tested which considers the roles of both lower and upper shear, as well as DCAPE, the strength of storm-generated vorticity, and storm slope as measured by the slope of the negative vorticity zone. There is much evidence that this theory offers improved predictions of storm evolution and the possibility of steadiness. The theory also makes it clear that storm slope and upper shear play roles as important as DCAPE and low-level shear in determining squall line behavior.

There are numerous potential problems with this theory that must be reiterated. Some of these potential problems are inherent to the dynamical approximations made (e.g. two-dimensionality, inviscid fluid, Boussinesq approximation applied over a deep layer, etc.). A major issue that has not been addressed in this theory is the role of updraft available potential energy (CAPE), which is often significant below 6 km. In the context of the three-region model, the only role of CAPE that has been neglected would be to give a positive vorticity tendency in the upper region (region a) ahead of the storm. This would clearly have an effect on the circulation tendency and tilting rate, since it was assumed that vorticity is constant in each of the three regions. Another potentially important physical process that has been neglected is mixing. Mixing could transport the negative vorticity from region i into regions a and b ahead of the storm, thereby giving a non-zero tendency to the average vorticity in these regions. It is felt that mixing does play a large role in this regard, and that if mixing were somehow included in this model, the predicted tilting rates might be much closer to those observed. On the other hand, in a system with a very shallow slope, mixing between the

cold pool and inflow over the long inflow trajectories could mean that the system would no longer survive.

Also, it seems likely that storms do modify their environments and this also would lead to non-zero vorticity tendencies in the environment. In fact, from the standpoint of this theory, the only way a steady storm could eventually begin tilting again and dissipate is for changes to occur in the environment, either through storm modifications or larger scale or diurnal processes. From a prediction point of view, it is hoped that despite the changes that occur in the environment, the storm probably stays in one general part of the parameter space, and hence the general characteristics of structure and evolution remain predictable. Finally, no attempt has been made to understand how the strength of the vorticity in the sloping region i relate to environmental characteristics. The observations suggest that this parameter is generally between $6x10^{-3}s^{-1}$ and $1x10^{-2}s^{-1}$, and the solutions to the tilting equation do not seem especially sensitive to this parameter over a large range of ambient shears and DCAPE. Despite the shortcomings, it seems that for observed cases and other modelling results in which enough information is available to document structure as well as evolution, this simple theory produces meaningful results.

In general, this theory indicates that, as low-level shear increases, larger DCAPE is associated with steady rearward-sloped storms, and that steady storms can occur over a larger range of DCAPE. It also shows that steady storms are more likely with reverse shear aloft (i.e. with a low-level line-normal jet profile) than with forward shear aloft. Thirdly, if the reverse shear is too strong and/or lower shear too weak, no steady system is possible (storms continue tilting rearward until they collapse).

Fig. 44 presents one more look at the question of the structure and evolution of mid-latitude versus tropical squall lines. This figure is a duplicate of Fig. 33 with certain ranges of shears for various storms superimposed. The box in the middle left portion of the picture is an approximation of the range of shears, using mean line-normal wind profiles +/- one standard deviation, derived from Bluestein and Jain (1985) and associated with the broken line form of severe squall lines in Oklahoma. The Houze et. al mean condition for strongly classifiable symmetric systems in Oklahoma falls within this same box, as well as the 26 May 1976 Oklahoma squall line investigated by several different authors. The range of shears for the tropical squall lines, including those from DUNDEE, the 23 June 1981 COPT 81 squall line (Roux, 1988, marked "Roux"), and the 22 June 1981 COPT 81 squall line (Chong *et al.*, 1987, marked "Chong") is denoted by the second box in the lower center, with individual data points marked. Finally, the 10-11 June 1985 PRE-STORM squall line is marked "10jun", and is found quite removed from the other middle latitude storms.

It is likely that DCAPE in middle latitudes is similar in magnitude to that in the tropics: although water loading contributions are smaller, the contribution due to evaporation is likely larger. If the present theory is correct, it suggests that many middle latitude storms occurring during the daytime do not feature draft structures described by steady, rearward-sloping vorticity zones. However, steady rearward-sloping storms become more likely during the night when DCAPE is reduced due to cooling in the boundary layer. Perhaps the three-region model does not even apply to the daytime storms in the part of the parameter space determined from the Bluestein and Jain (1985) data. Or perhaps these systems have forward-tilting draft structures that are continuously regenerated through discrete

development at the gust front or gravity-wave induced propagation. Also possible is that the role of earth's rotation, perhaps in terms of inertial stability, or the role of the often-observed vortex features in the stratiform region, must be considered. All of these issues will remain unresolved until the evolution of a number of middle latitude squall lines can be documented with adequate temporal resolution.

Chapter 6

Conclusions and suggestions for additional research

The scope of this study is limited to a description of the evolution of quasi-two-dimensional squall lines that feature a continuous, rearward-sloping vorticity zone, and a possible mechanism for environmental control of this evolution. It does not address the conditions necessary for the initiation of a squall line. Also, storms with a system-scale three-dimensionality, and those consisting of well-separated thunderstorms in a line, have not been examined. The main emphasis herein has been on a description of events and processes that occur during *one* cycle of intensification and decay. Many of the squall lines analyzed exhibited very prolonged dissipating stages, and it appears that squall lines can progress from a deep convective mode, to one of much shallower, less-organized, but persistent leading edge convection. Also, in several of the systems, deep leading-edge convection recurred after a prolonged period of the dissipating stage. It is plausible that such regeneration is due to changes in the environment, or to weakening or slowing in the propagation of the cold pool after it surges ahead of the dissipating leading edge. These issues merit further research.

A simple vorticity budget approach to understanding squall line dynamics is employed in this study. Approaches of this type require many simplifying assumptions in order to obtain meaningful solutions. Based on the predictions of the theory presented herein, it seems that this approach is

an improvement over that used by RKW, primarily because the effects of upper shear are accounted for, and the allowable storm morphologies much more closely correspond to observations. However, it seems that the limit to this type of approach has probably been reached, and further advances must come through numerical modelling.

If the findings of this study are correct, future numerical simulations should systematically explore the parameter space described by low-level shear, upper shear, and DCAPE. It appears that for this class of storm, two-dimensional simulations may be adequate. However, in light of the fundamental role of DCAPE (also see Emanuel, 1989), it will be vitally important to correctly model the buoyancy distribution in the part of the storm featuring negative buoyancy.

Some fundamental aspects of squall line dynamics remain to be explored observationally. The evolution of middle latitude squall lines has not been adequately documented. The present theory suggests that middle latitude squall lines with large DCAPE are dynamically different from "typical" tropical squall lines; it appears that a quasi-two-dimensional system with a continuous vorticity zone should not occur in weakly sheared environments with large DCAPE. Rather, it is suspected that in these environments squall lines consist of much more cellular, unsteady leading edges, and that organized rear inflow probably does not penetrate across the entire storm to the leading edge. Though fundamentally unsteady at the convective scale, it should still be possible to have a long-lived system that appears quasi-steady at larger scales. And from a climatological perspective, it seems that at night, since DCAPE decreases with boundary layer cooling, the possibility of steady systems like those described in this dissertation becomes much greater.

This study, because of its focus on two-dimensional dynamics, has emphasized events that occur relatively early in the life cycle of a mesoscale convective system (Maddox, 1980). A squall line that tilts rearward and dissipates is not likely to grow upscale into a longer-lived mesoscale convective system (except perhaps if convection repeatedly regenerates at the gust front). However, for those environments capable of supporting a steady system, growth will occur upscale through the mechanisms described in this dissertation, and the possibilities that the system will evolve toward inertial stability and geostrophic balance [a definition of an MCC proposed by Cotton and Anthes (1989), p. 673] are much enhanced. For this reason, among others, further research into the dynamics of squall lines is definitely needed, especially in the middle latitudes. Future observational programs must obtain Doppler radar data at intervals of about ten minutes or less over the longest possible periods in order to be useful. Observational data sets that provide infrequent snapshots of storm structure are of comparatively little use. Reliable methods to assess the in-storm buoyancy structure also are needed, as well as realistic techniques to estimate DCAPE from pre-storm soundings.

Finally, this work provides a basis for a re-examination of the derecho phenomenon (Johns and Hirt, 1983). A cursory examination of the data published thus far indicates that derechos may occur in environments supporting steady, rearward-tilted systems. If derechos are in this class, it will be interesting to find out what makes them an especially intense variation on this basic storm type.

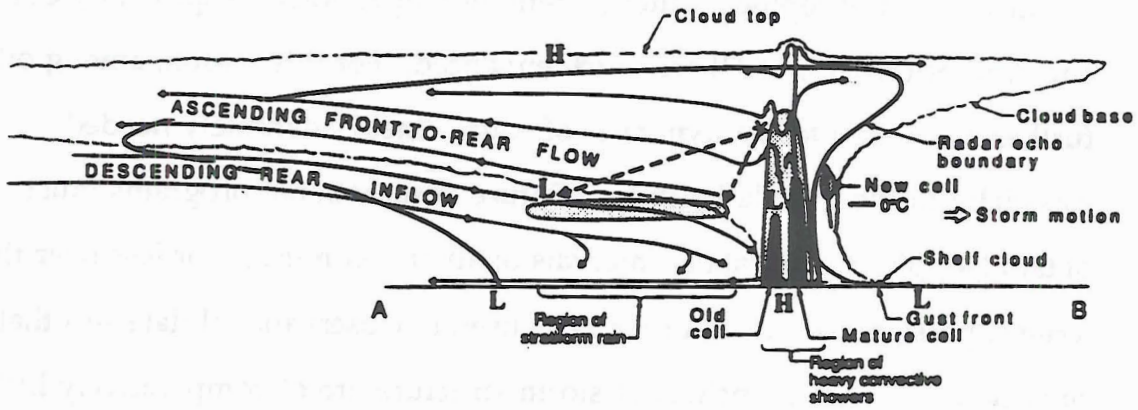

Figure 1. Conceptual model of the line-normal structure of a squall line (adapted from Houze *et al.*, 1989).

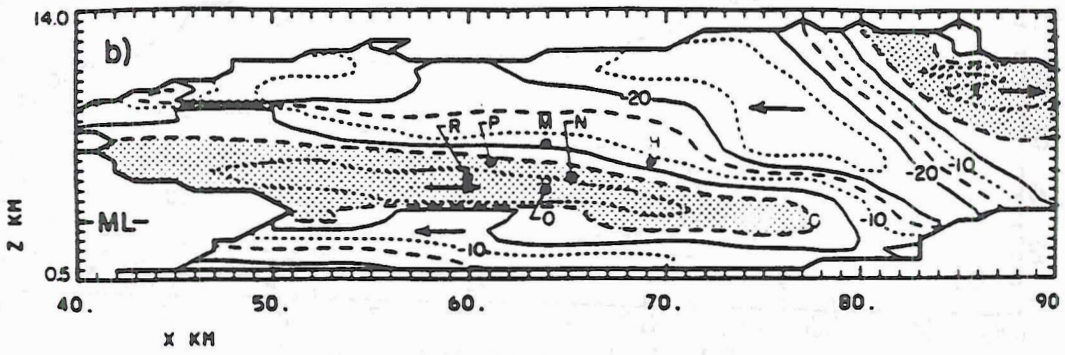

Figure 2. A single cross-section of line-normal horizontal velocity from the 2-3 August 1981 CCOPE squall line (from Schmidt and Cotton, 1989). Stippled regions represent flow left-to-right. Velocity values are storm-relative.

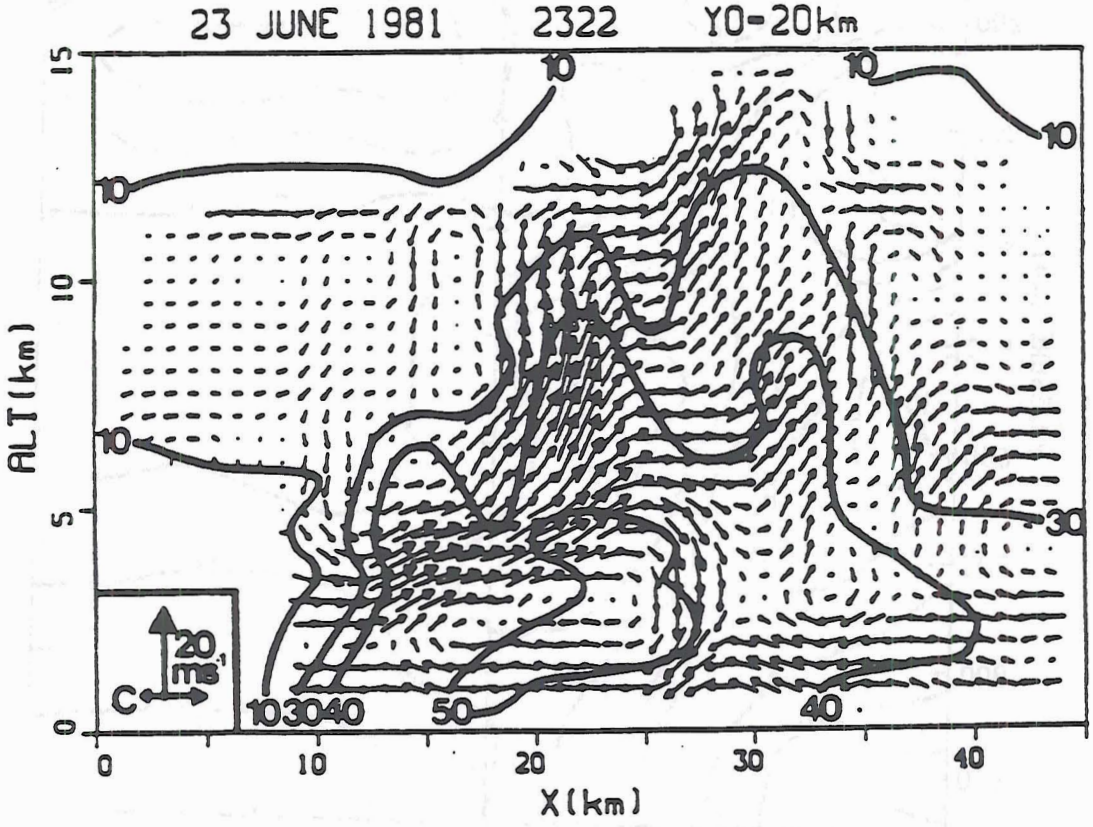

Figure 3. Storm relative velocity vectors for the 23 June 1981 COPT-81 storm (from Roux, 1988). Solid contours are radar reflectivity values in dBZ.

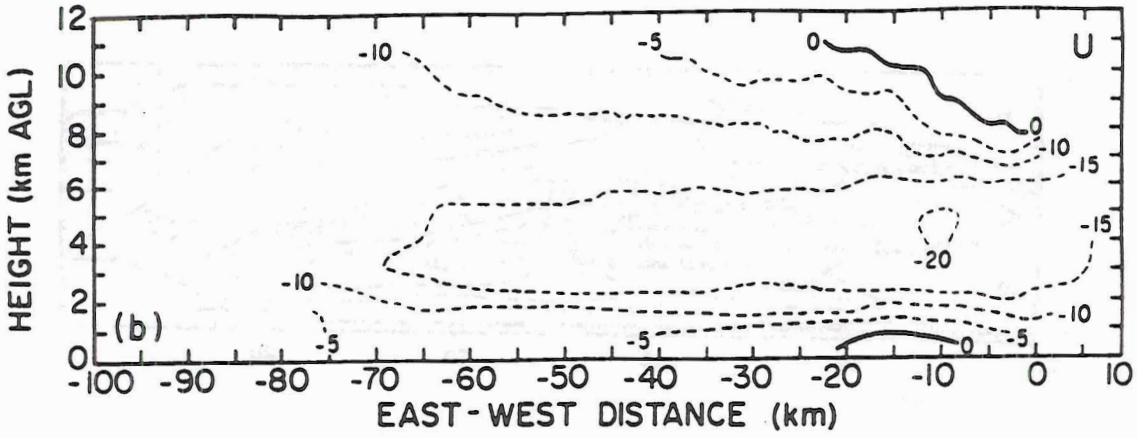

Figure 4. Average line-normal velocity in the 22 May 1976 Oklahoma squall line (from Smull and Houze, 1987b). Negative values indicate flow from right-to-left.

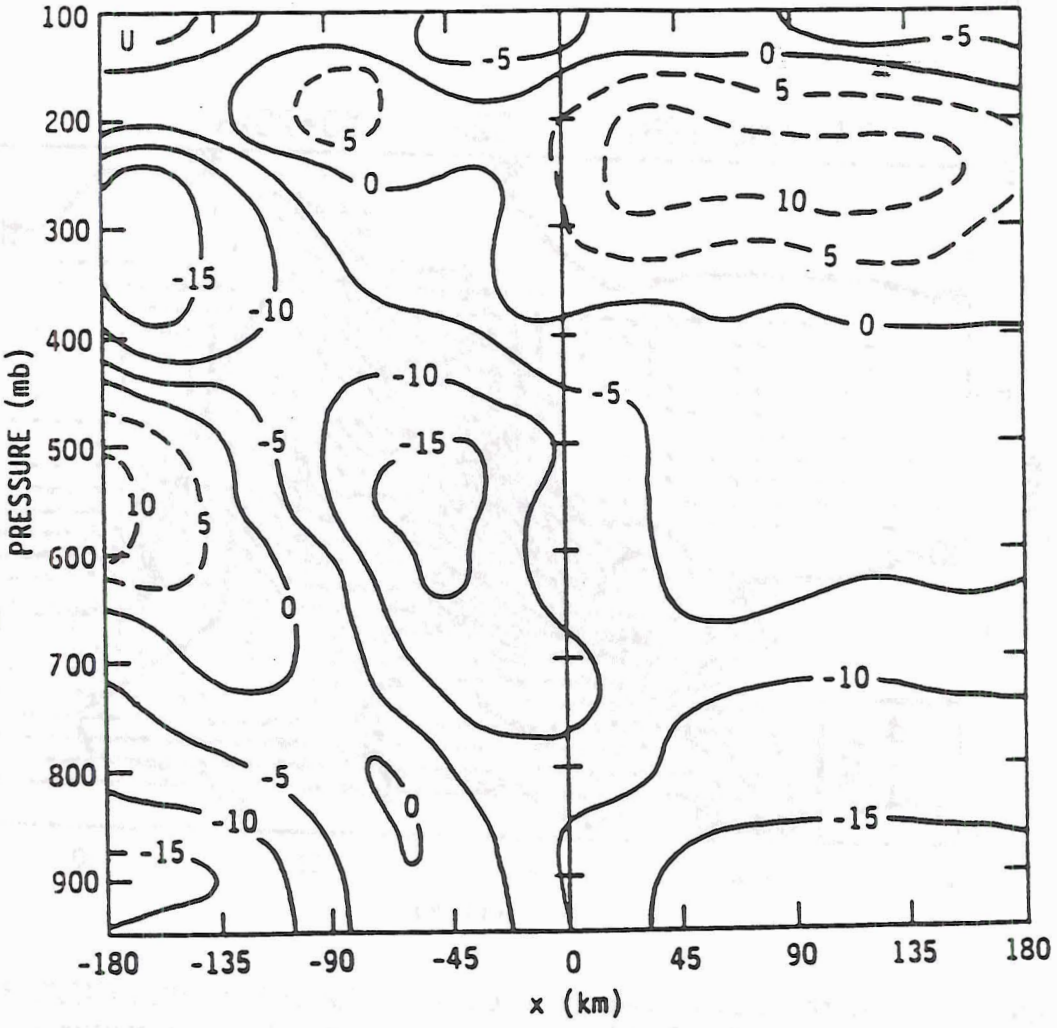

Figure 5. As in Figure 4, but based on rawinsonde analysis (from Ogura and Liou, 1980).

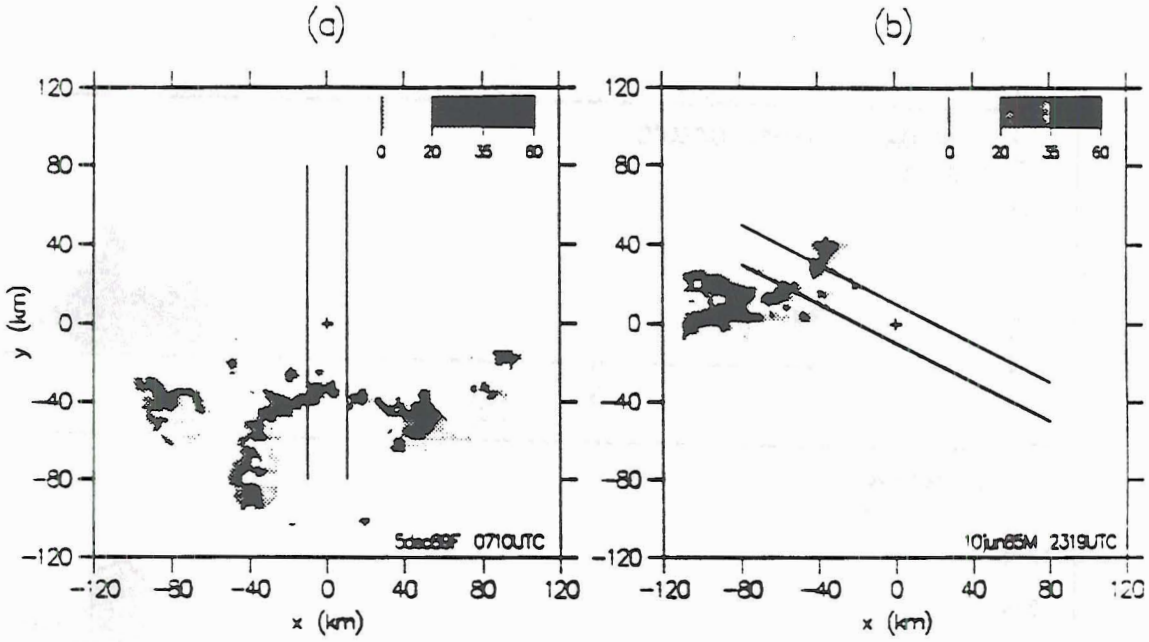

Figure 6. Horizontal reflectivity maps for the formative stage. The radar is at the "+" symbol, with the parallel lines denoting the region for vertical cross-section slab averages used in later figures. Horizontal axes labeled in km from radar. a) 5 December 1989 tropical case, 0710 UTC. b) 10 June 1985 middle latitude case, 2319 UTC.

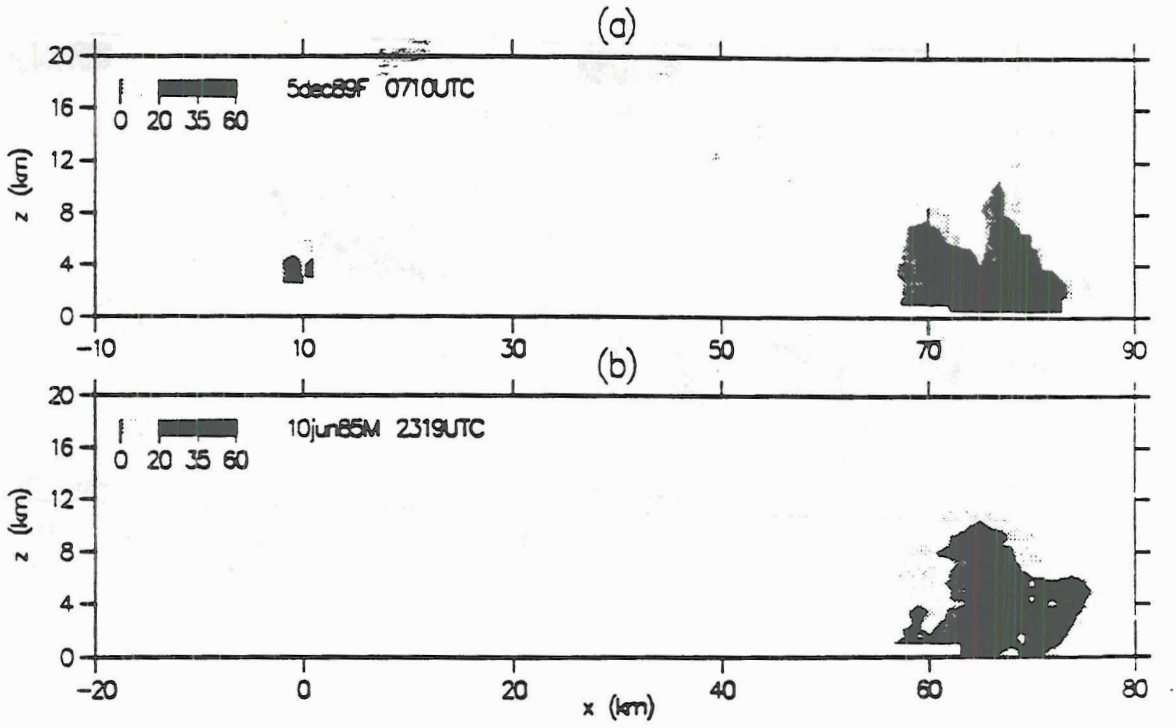

Figure 7. Slab-averaged (vertical cross-section) reflectivities in the formative stage. Shading levels are as in Figure 6. Axes labeled in km, the horizontal distance being distance in the direction of propagation (left to right), with the radar always at x=114 km. a) 5 December 1989. b) 10 June 1985.

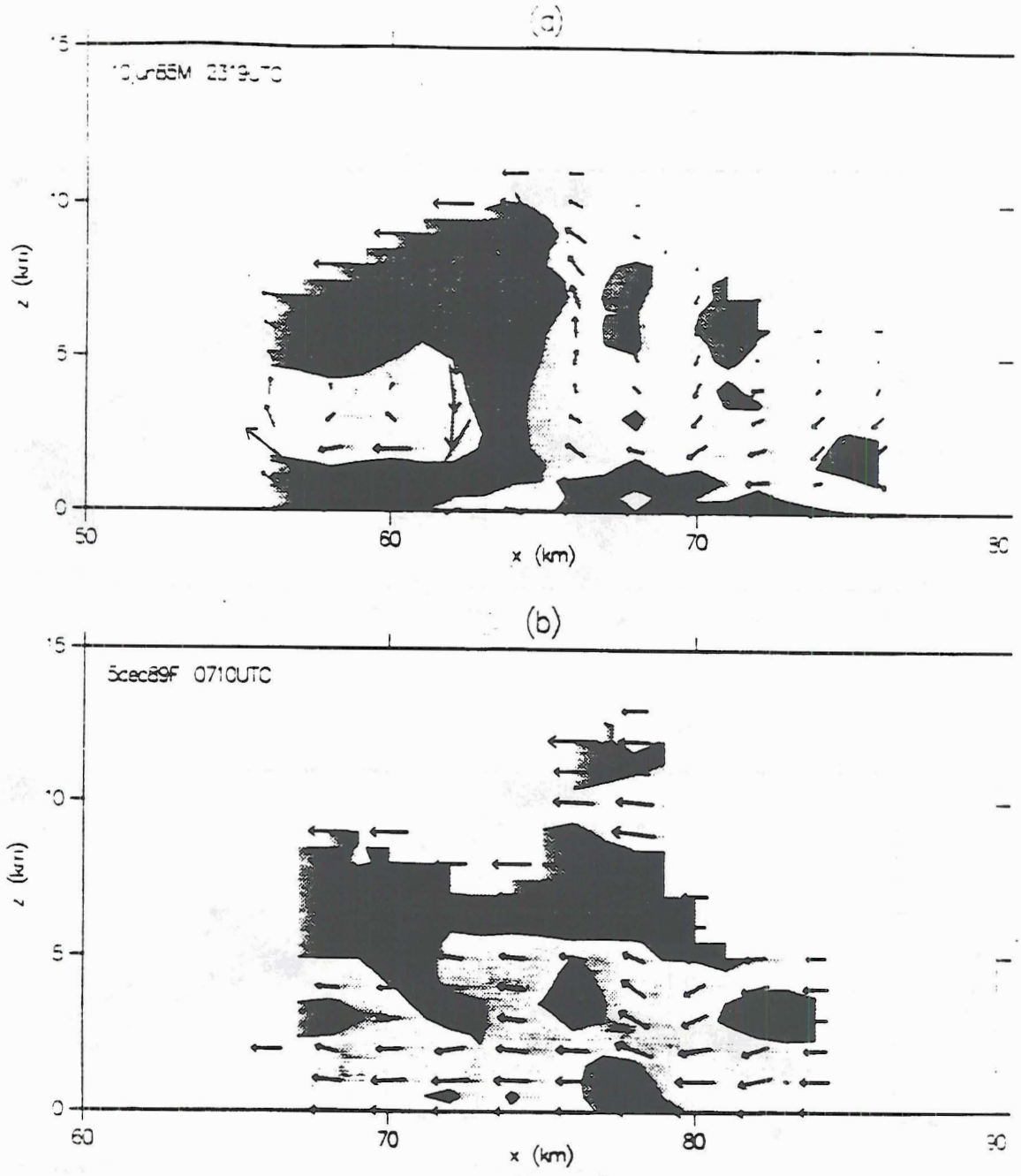

Figure 8. Slab-averaged (vertical cross-section) velocities and vorticity in the formative stage. Velocity vectors scaled to the plot dimensions (as shown in the upper right). Vorticity contours at $5 \times 10^{-3} s^{-1}$, with positive vorticity shaded lightly, and negative values shaded darkly. Note that the horizontal and vertical scales are different than in Figure 7. a) 10 June 1985. b) 5 December 1989.

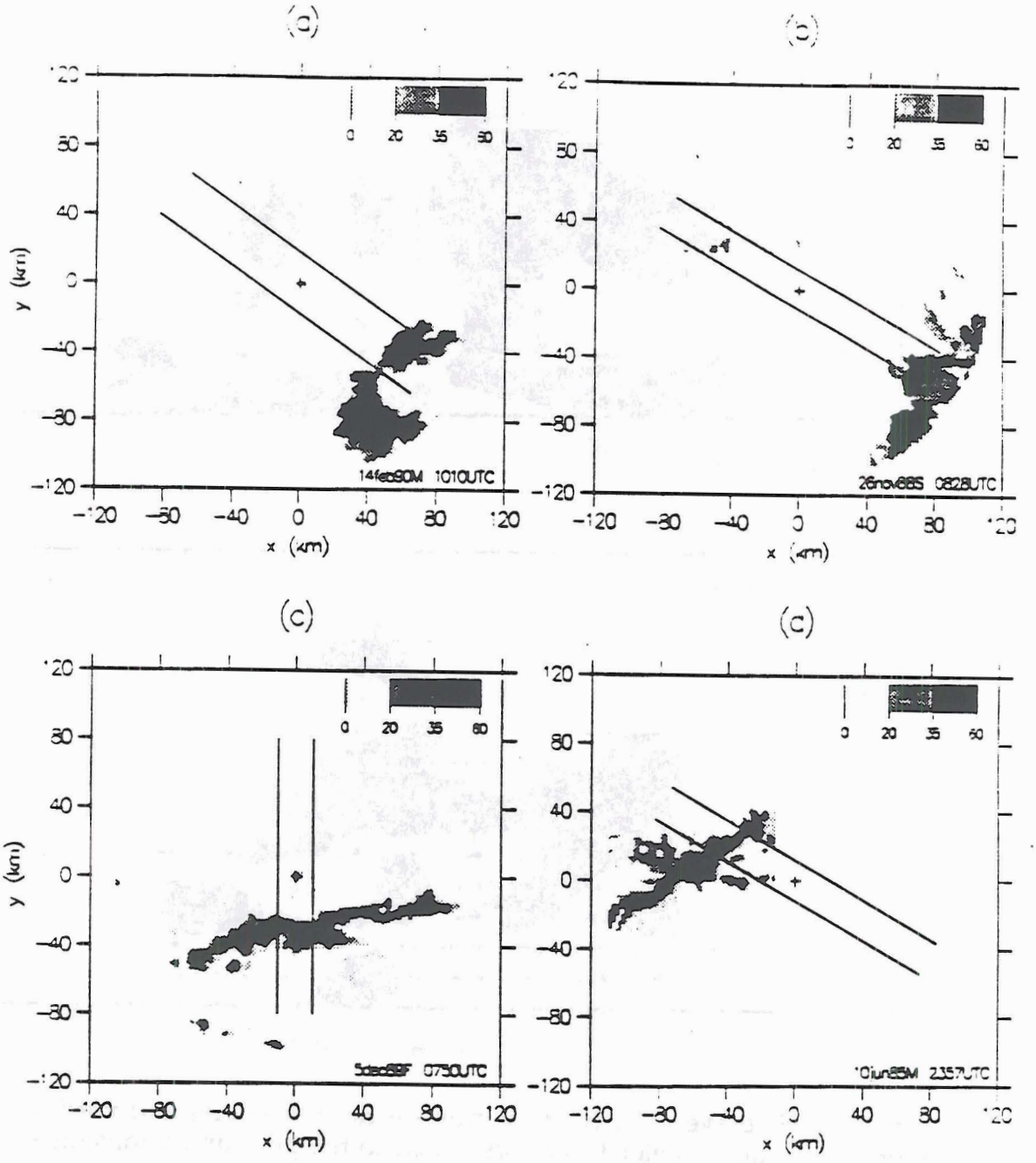

Figure 9. Horizontal reflectivity maps in the intensifying stage. As in Fig. 6. a) 14 February 1990. b) 26 November 1988. c) 5 December 1989. d) 10 June 1985.

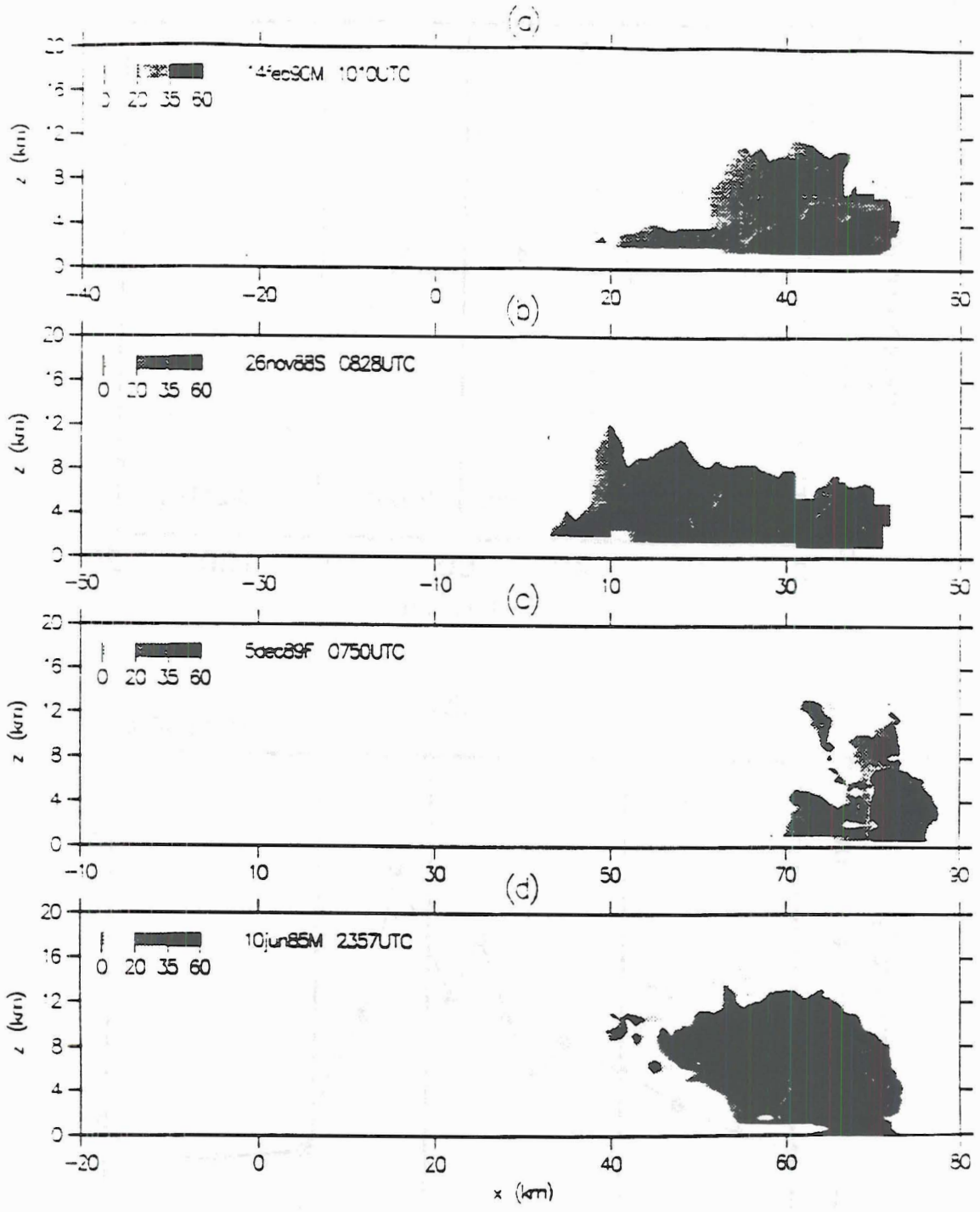

Figure 10. Slab-averaged reflectivities in the intensifying stage. As in Fig. 7. a) 14 February 1990. b) 26 November 1988. c) 5 December 1989. d) 10 June 1985.

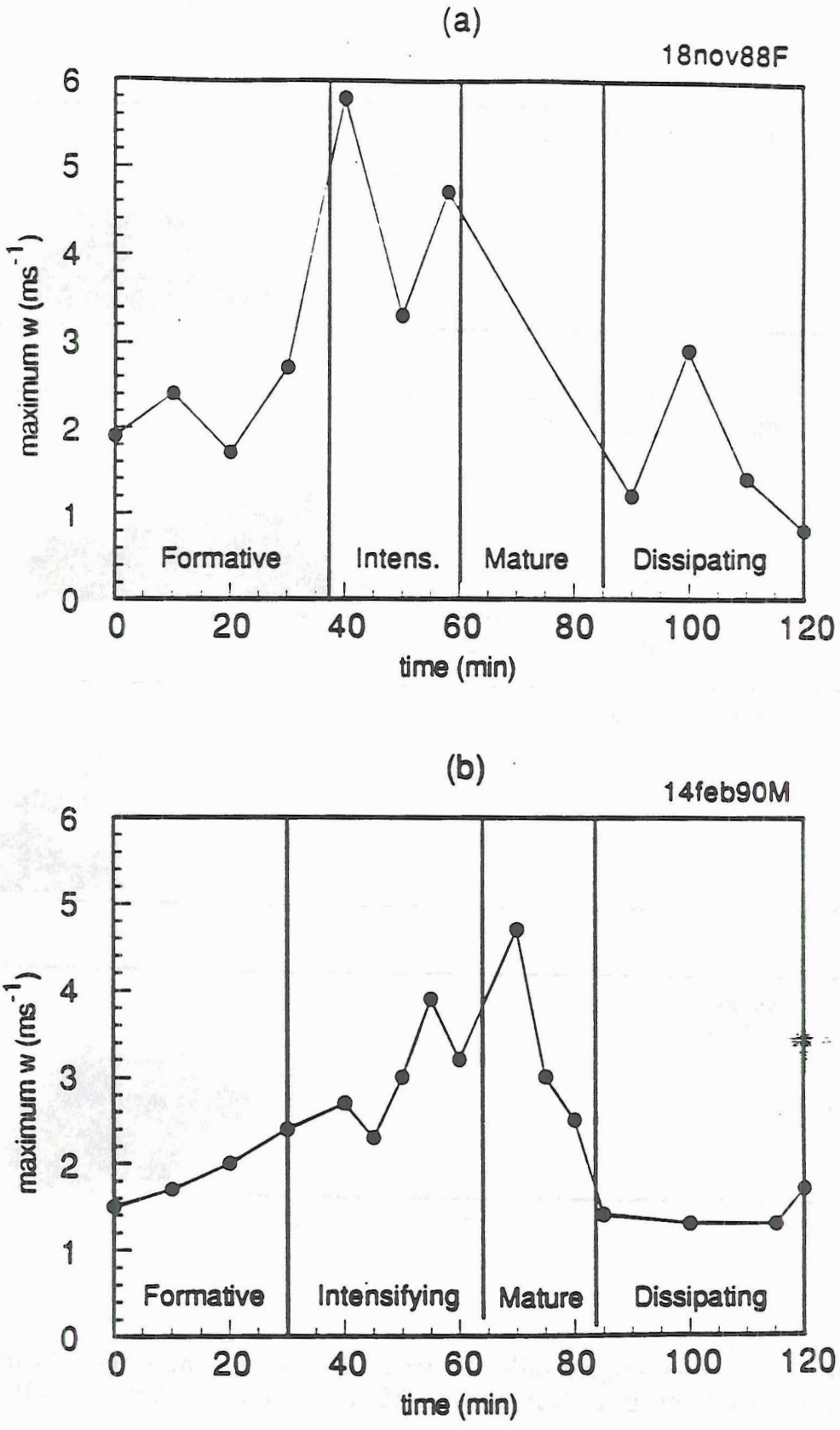

Figure 11. Graphs of maximum slab-averaged vertical velocity for a) 18 November 1988 and b) 14 February 1990.

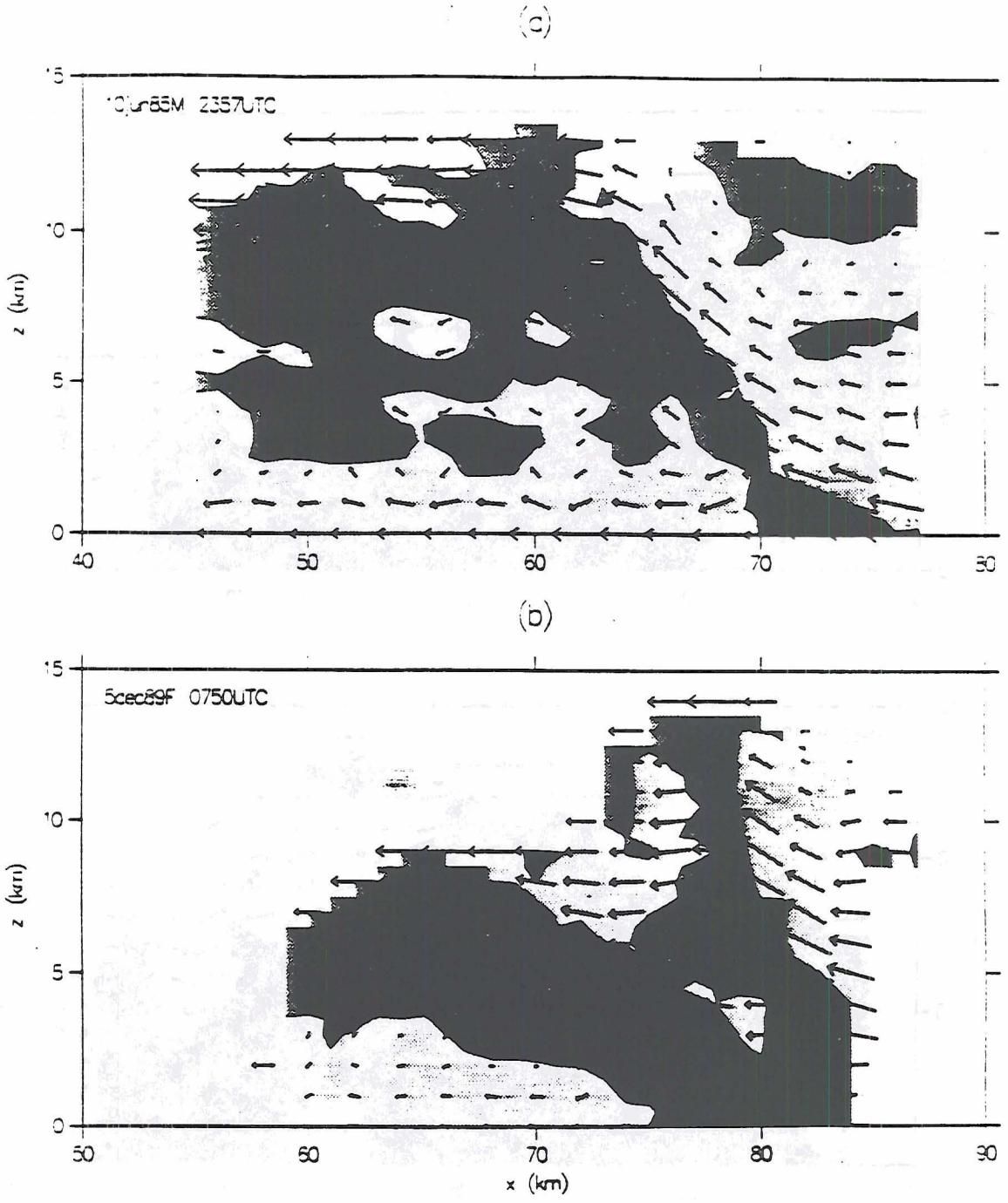

Figure 12. Slab-averaged velocities and vorticity in the intensifying stage. As in Fig. 8. a) 10 June 1985. b) 5 December 1989. c) 26 November 1988. d) 14 February 1990.

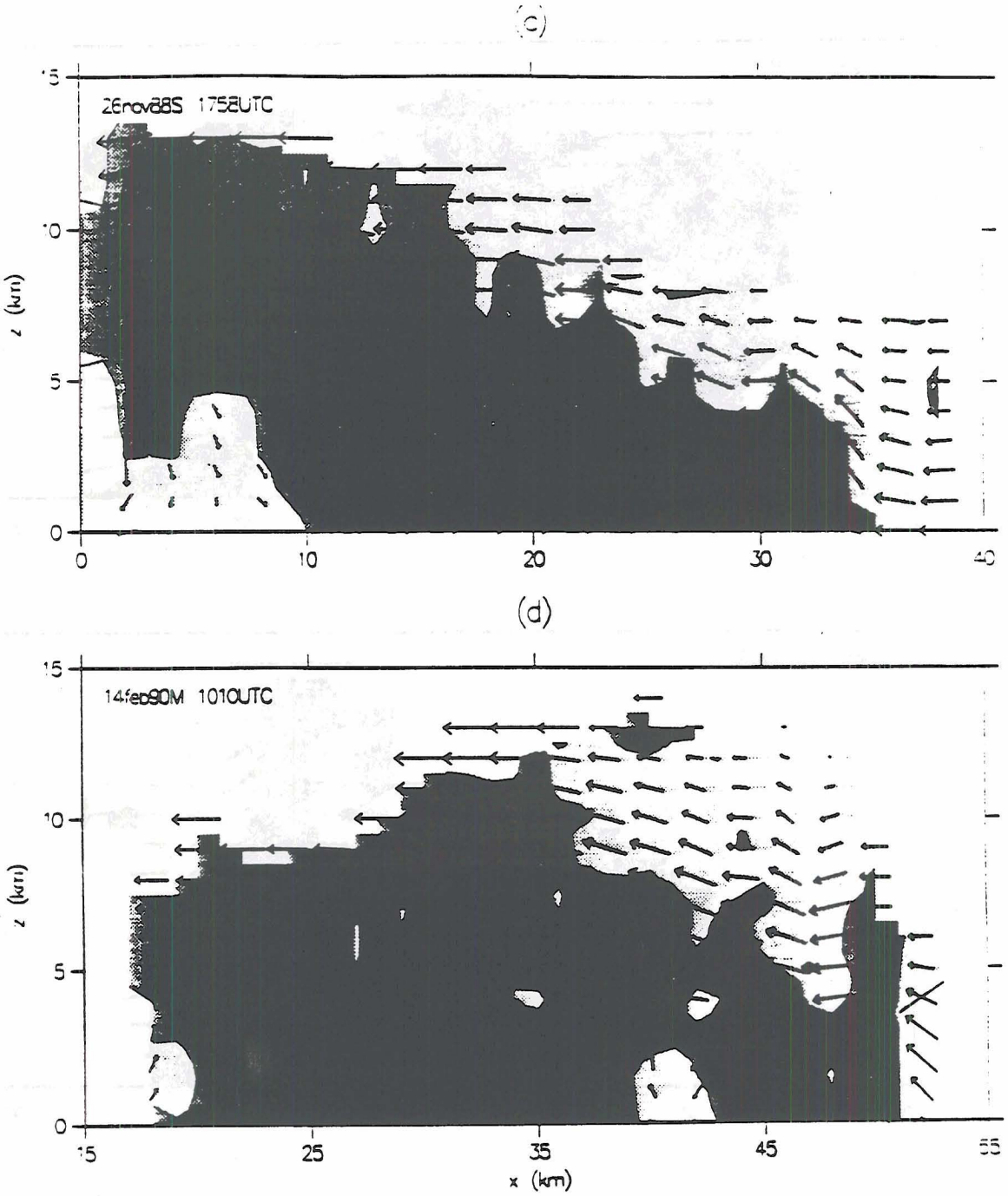

Figure 12 (continued).

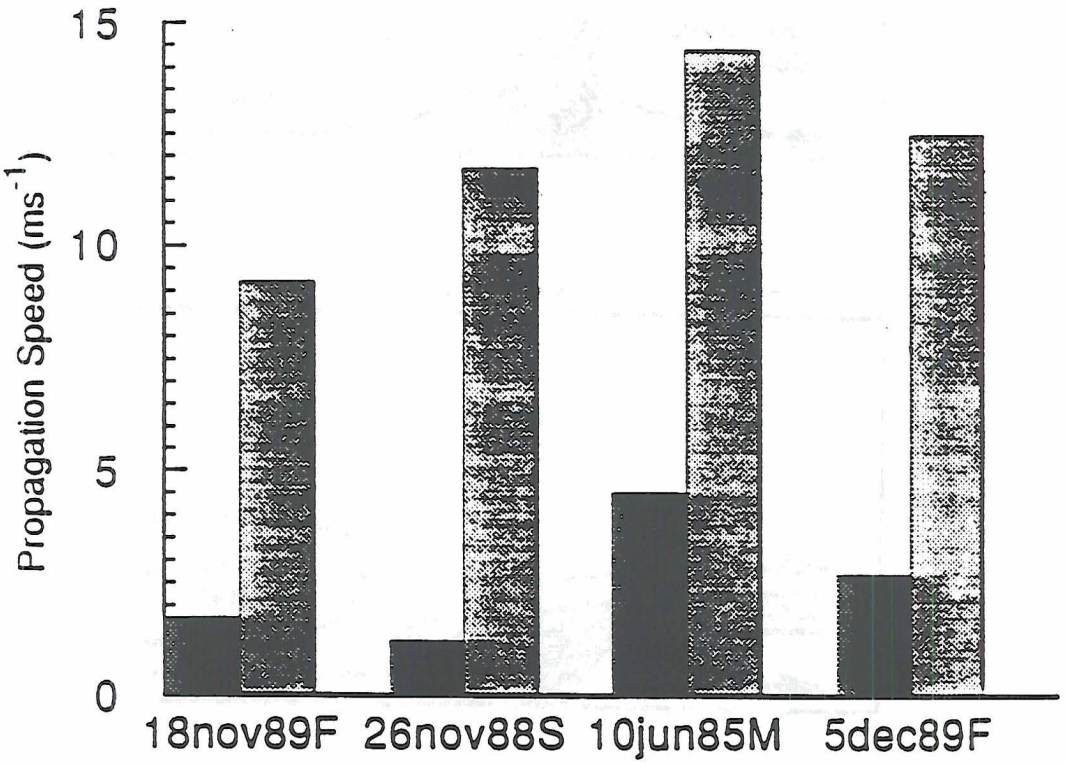

Figure 13. Graph of the average leading edge propagation speed for the formative and intensifying stages (dark) and the mature stage (light) for four cases in which both speeds could be measured.

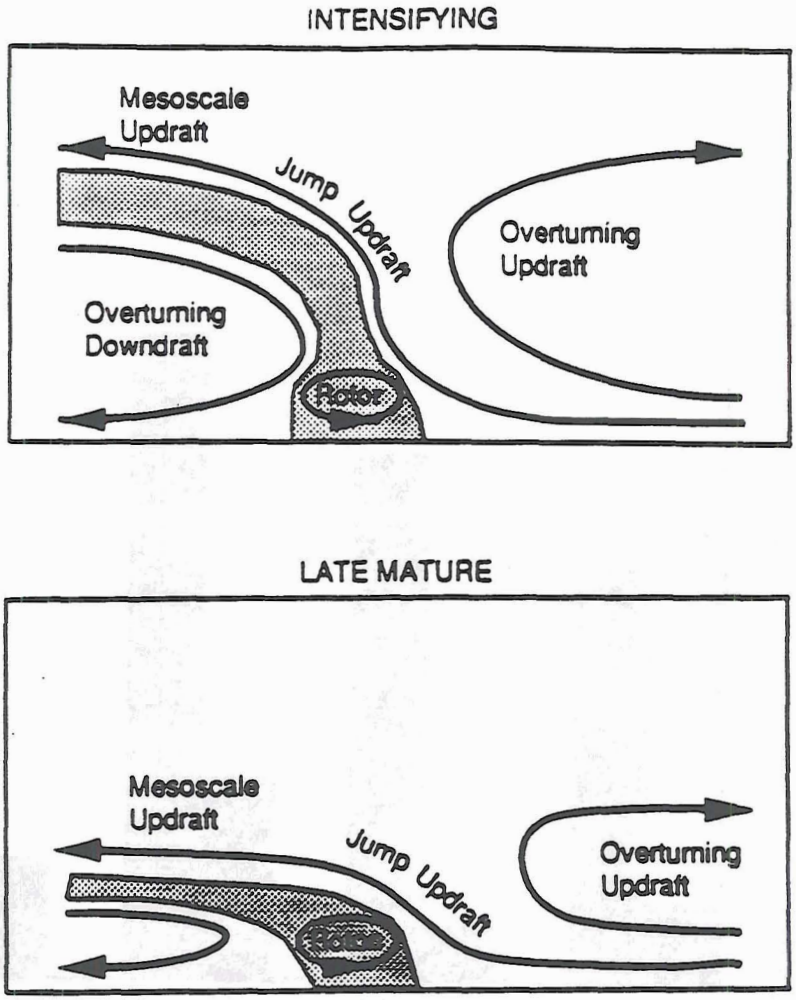

Figure 14. Schematic diagram of squall line flow features adapted from Thorpe, Miller, and Moncrieff (1982). The vorticity zone referred to in the text is shaded. Modifications shown here are the designation of "mesoscale updraft" and the evolution shown: the top schematic is representative of an intensifying squall line and the bottom schematic represents the structure late in the mature stage.

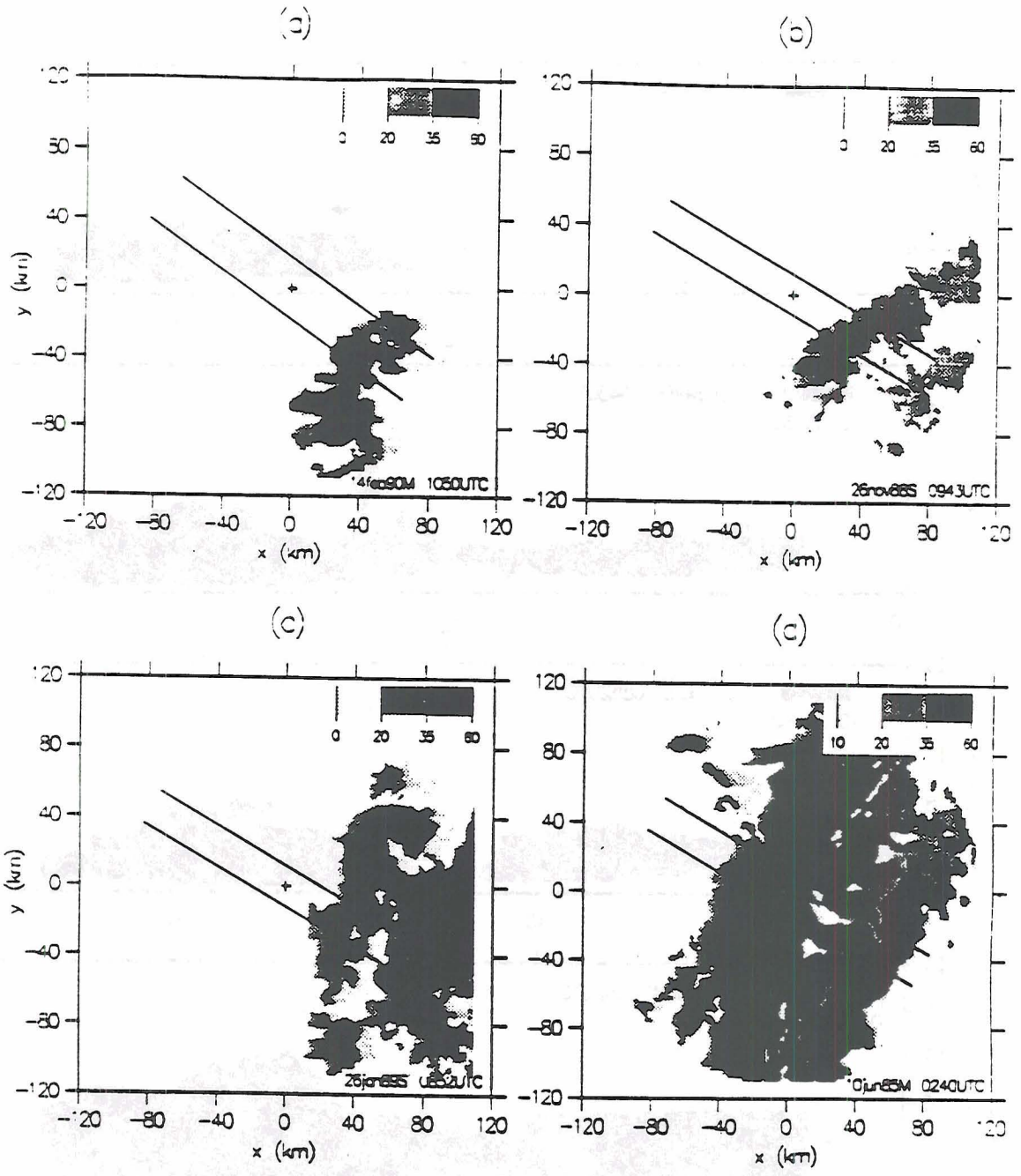

Figure 15. Horizontal reflectivity maps in the mature stage. As in Fig. 6. a) 14 February 1990. b) 26 November 1988. c) 26 January 1989. d) 10 June 1985.

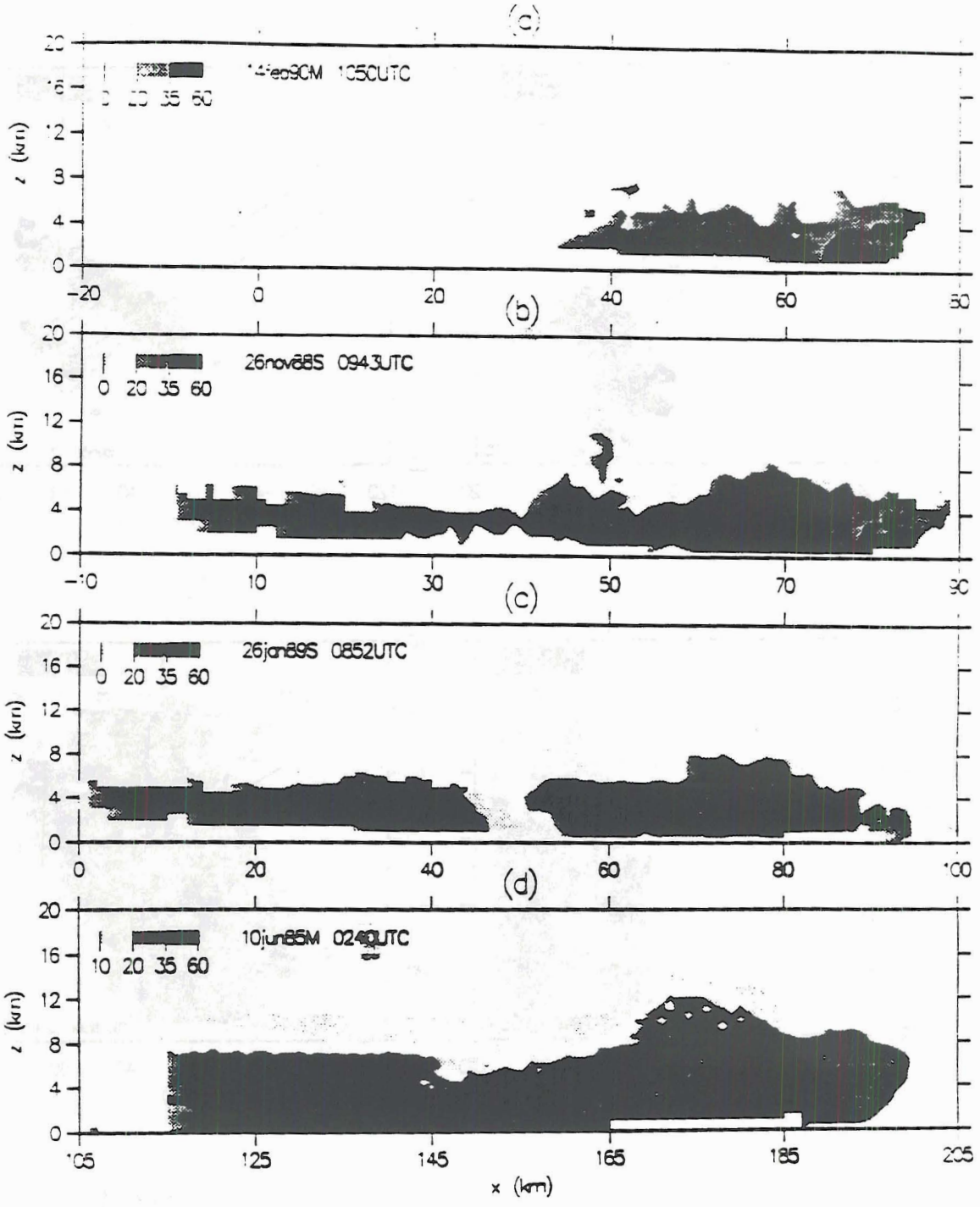

Figure 16. Slab-averaged reflectivities in the mature stage. As in Fig. 7. a) 14 February 1990. b) 26 November 1988. c) 26 January 1989. d) 10 June 1985.

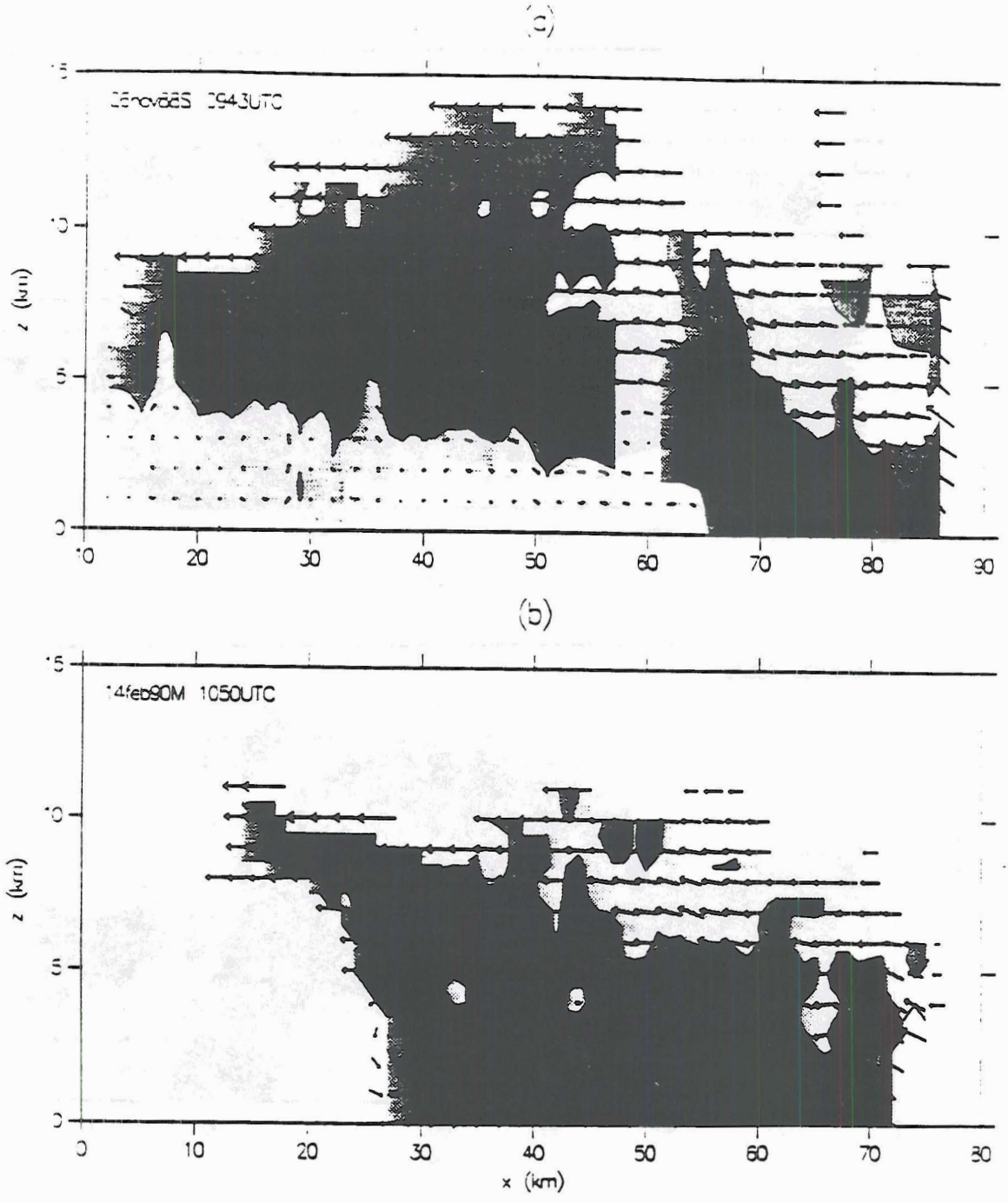

Figure 17. Slab-averaged velocities and vorticity in the mature stage. As in Fig. 8. a) 26 November 1988. b) 14 February 1990. c) 10 June 1985. d) 26 January 1989.

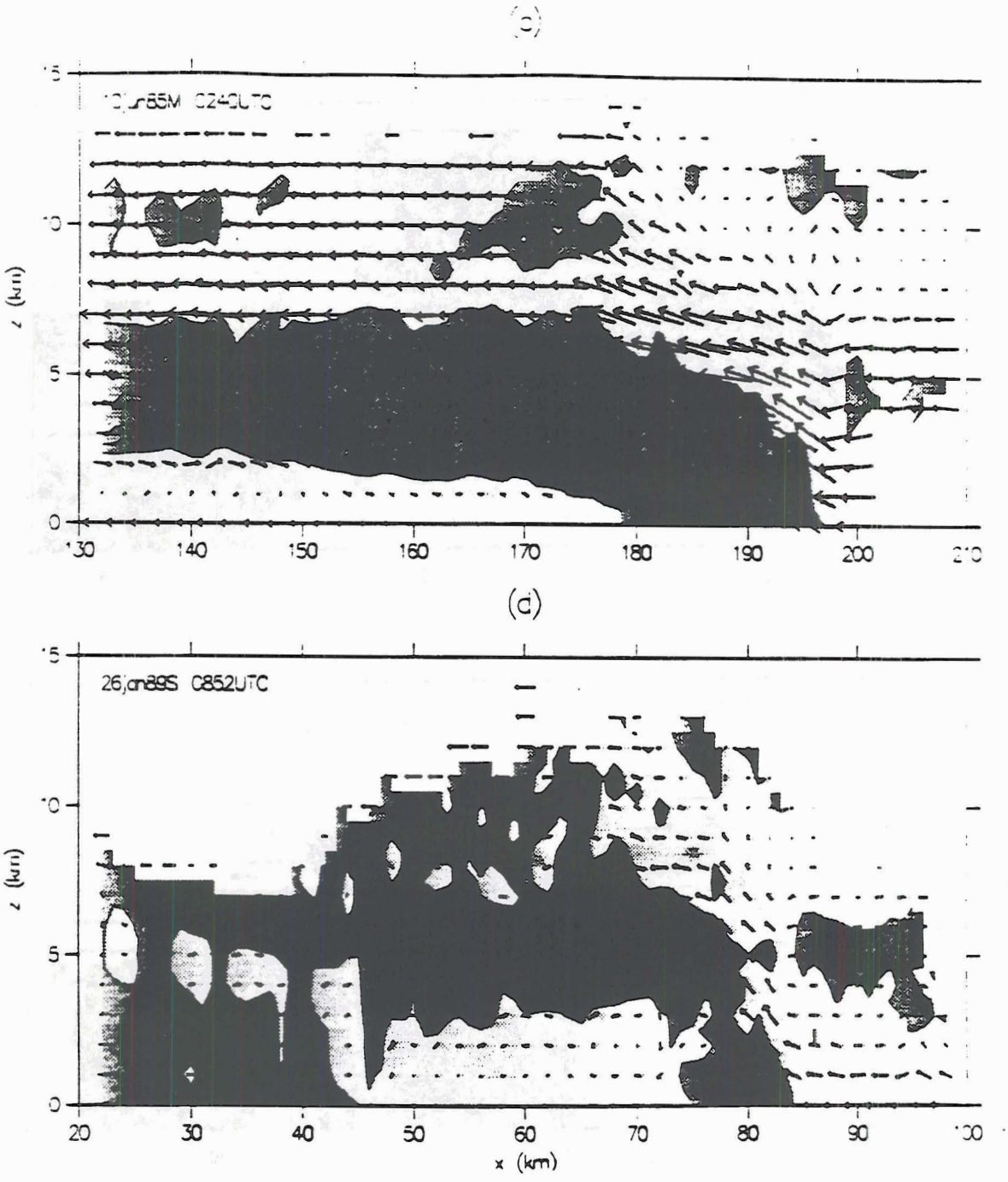

Figure 17 (continued).

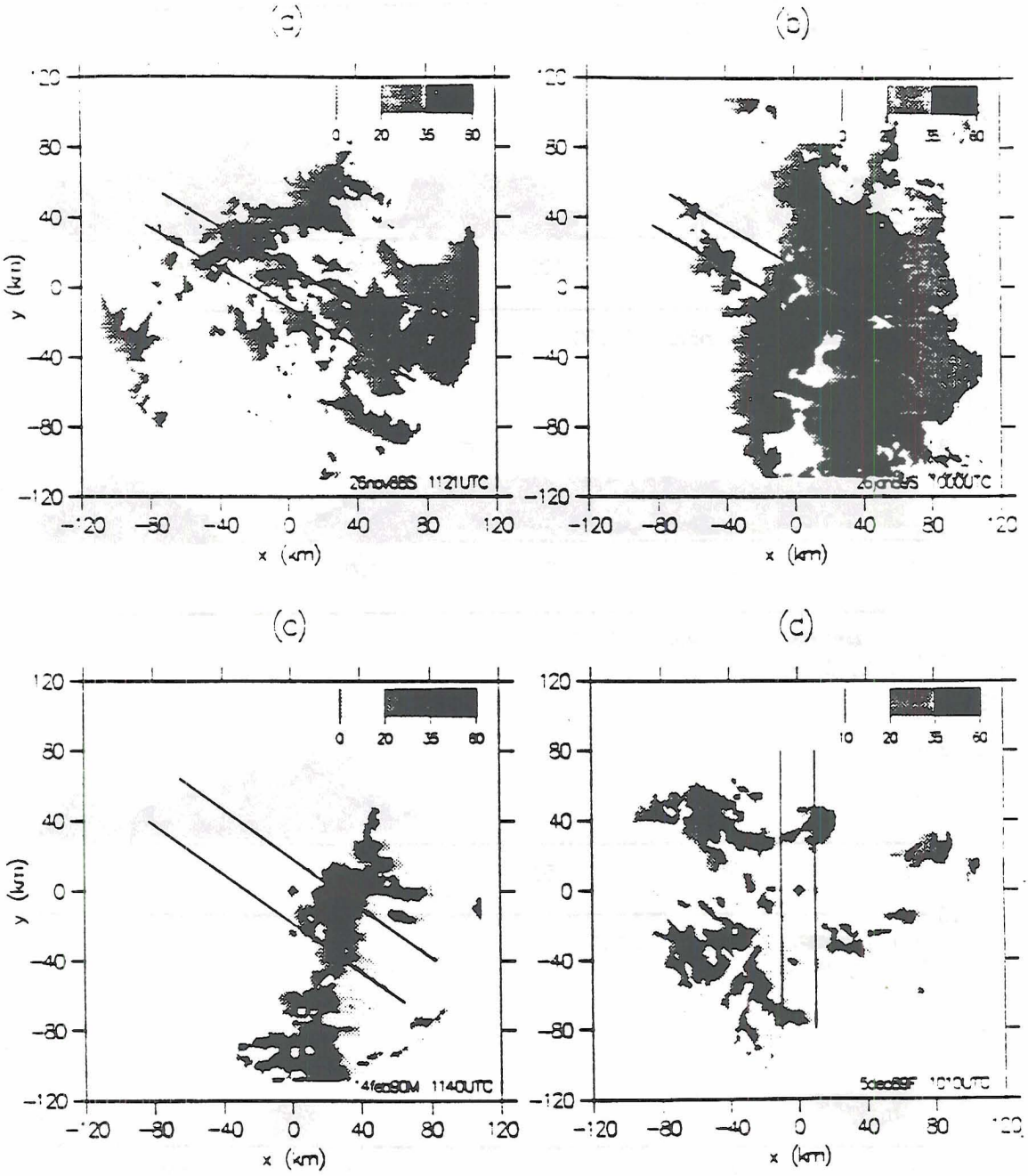

Figure 18. Horizontal reflectivity maps in the mature stage. As in Fig. 6. a) 26 November 1988. b) 26 January 1989. c) 14 February 1990. d) 5 December 1989.

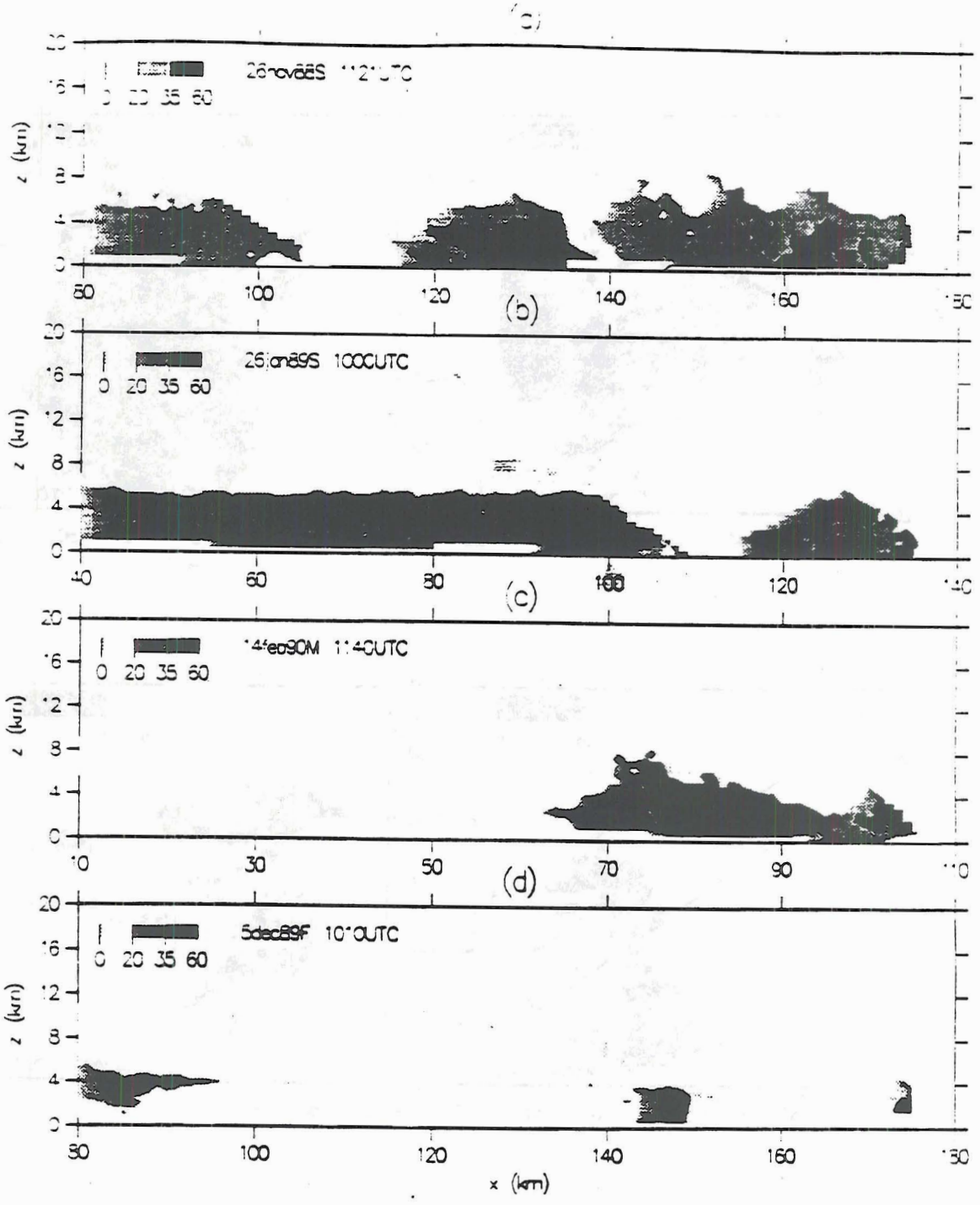

Figure 19. Slab-averaged reflectivities in the mature stage. As in Fig. 7. a) 26 November 1988. b) 26 January 1989. c) 14 February 1990. d) 5 December 1989.

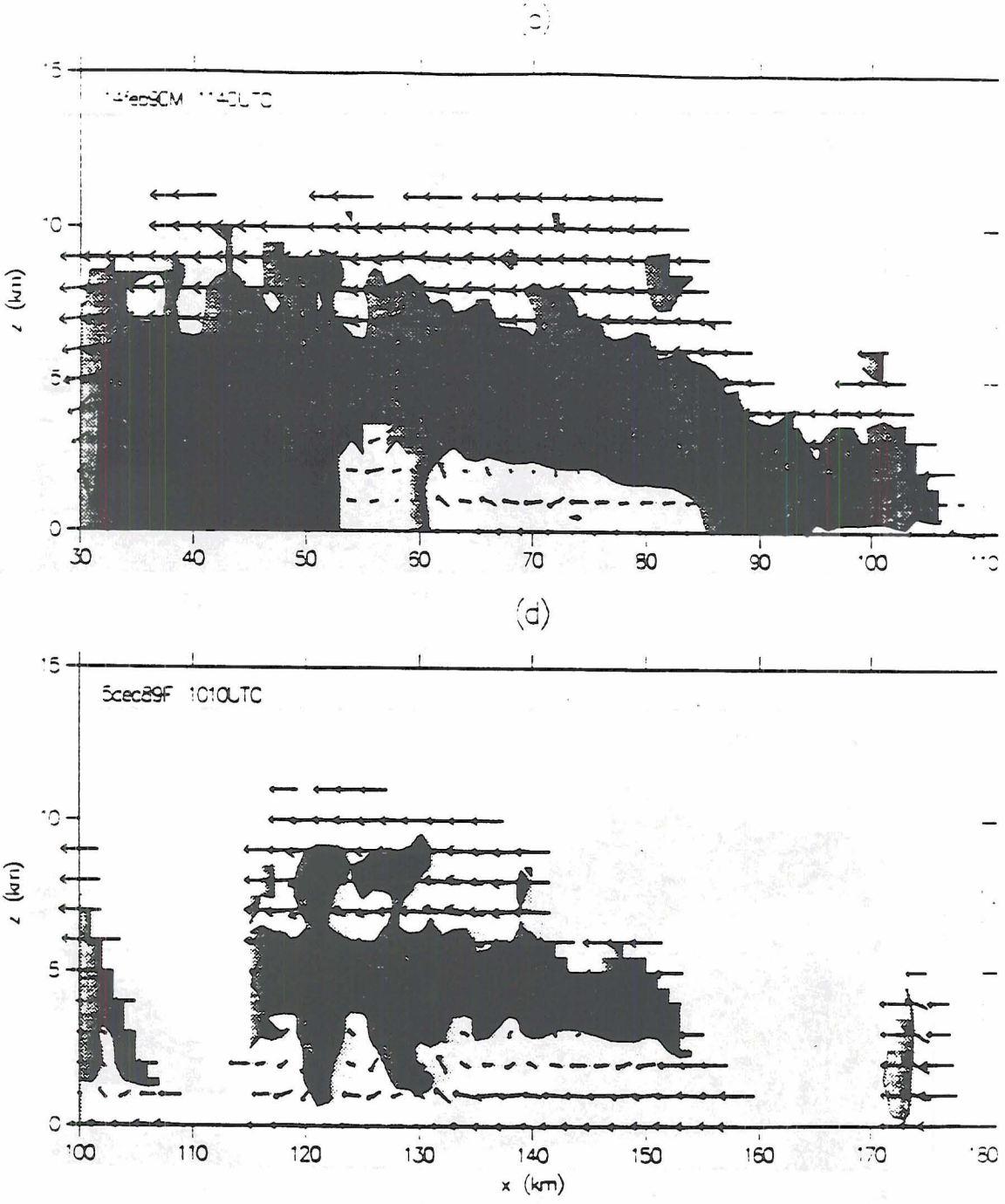

Figure 20. Slab-averaged velocities and vorticity in the mature stage. As in Fig. 8, except horizontal scale is different. a) 26 November 1989. b) 26 January 1989. c) 14 February 1990. d) 5 December 1989.

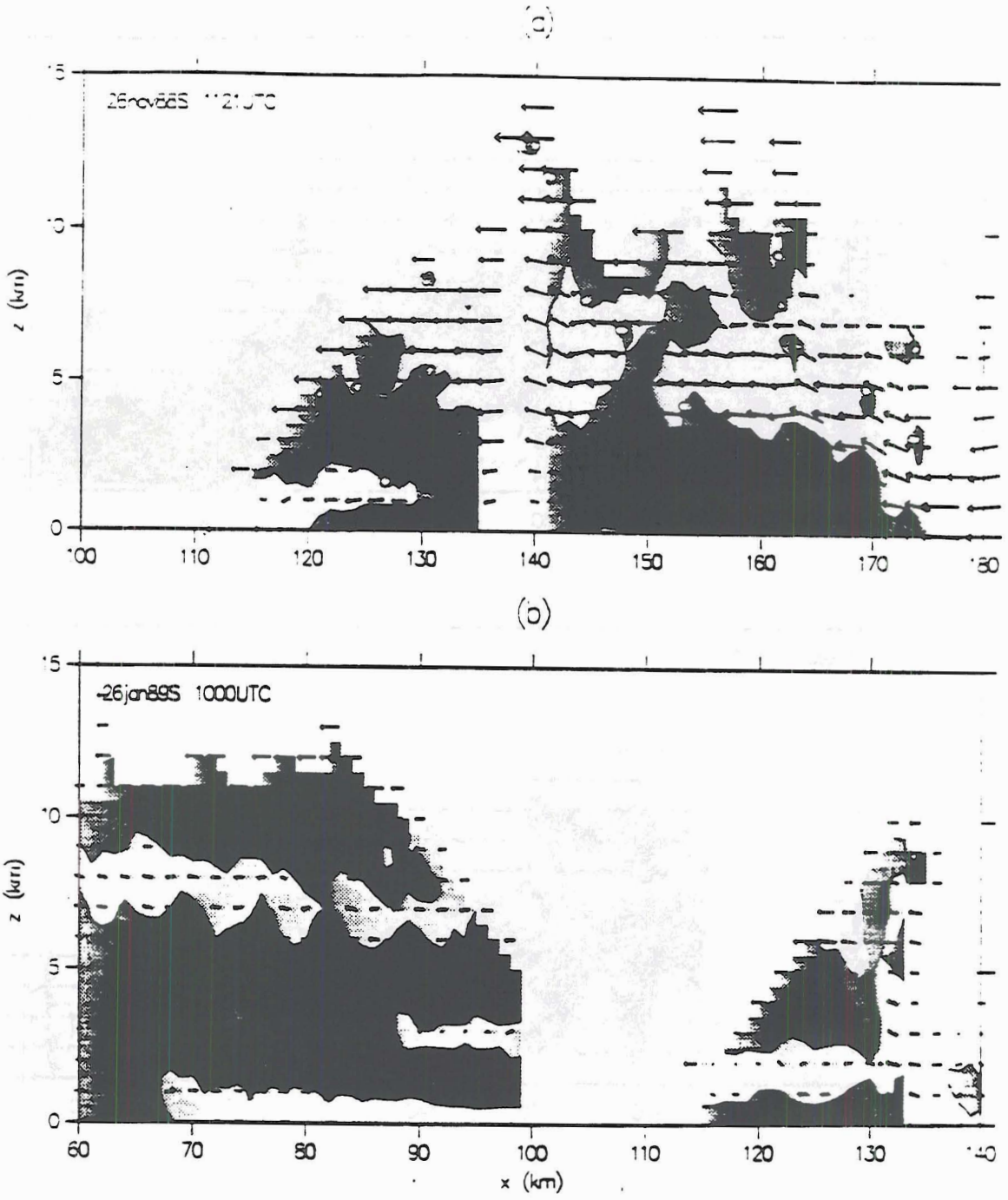

Figure 20 (continued).

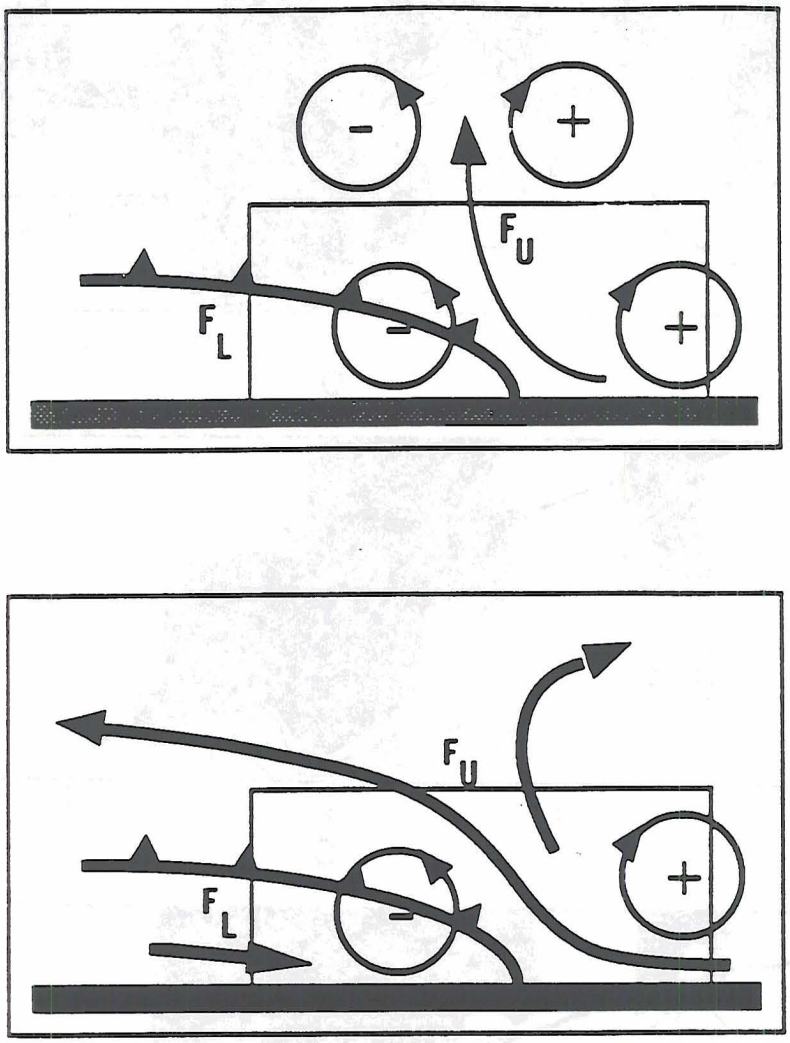

Figure 21. Integration volume for vorticity equation, adapted from Rotunno et al. (1988). Plus and minus signs enclosed in circular arrow symbols denote vorticity, streamlines are bold arrows, and the boundary of the cold pool is shown with the conventional cold front symbol. The integration region is the smaller rectangle, with FU denoting flux at the upper face, and FL denoting flux at the left face. a) RKW assumptions; b) Relaxed assumptions as described in the text.

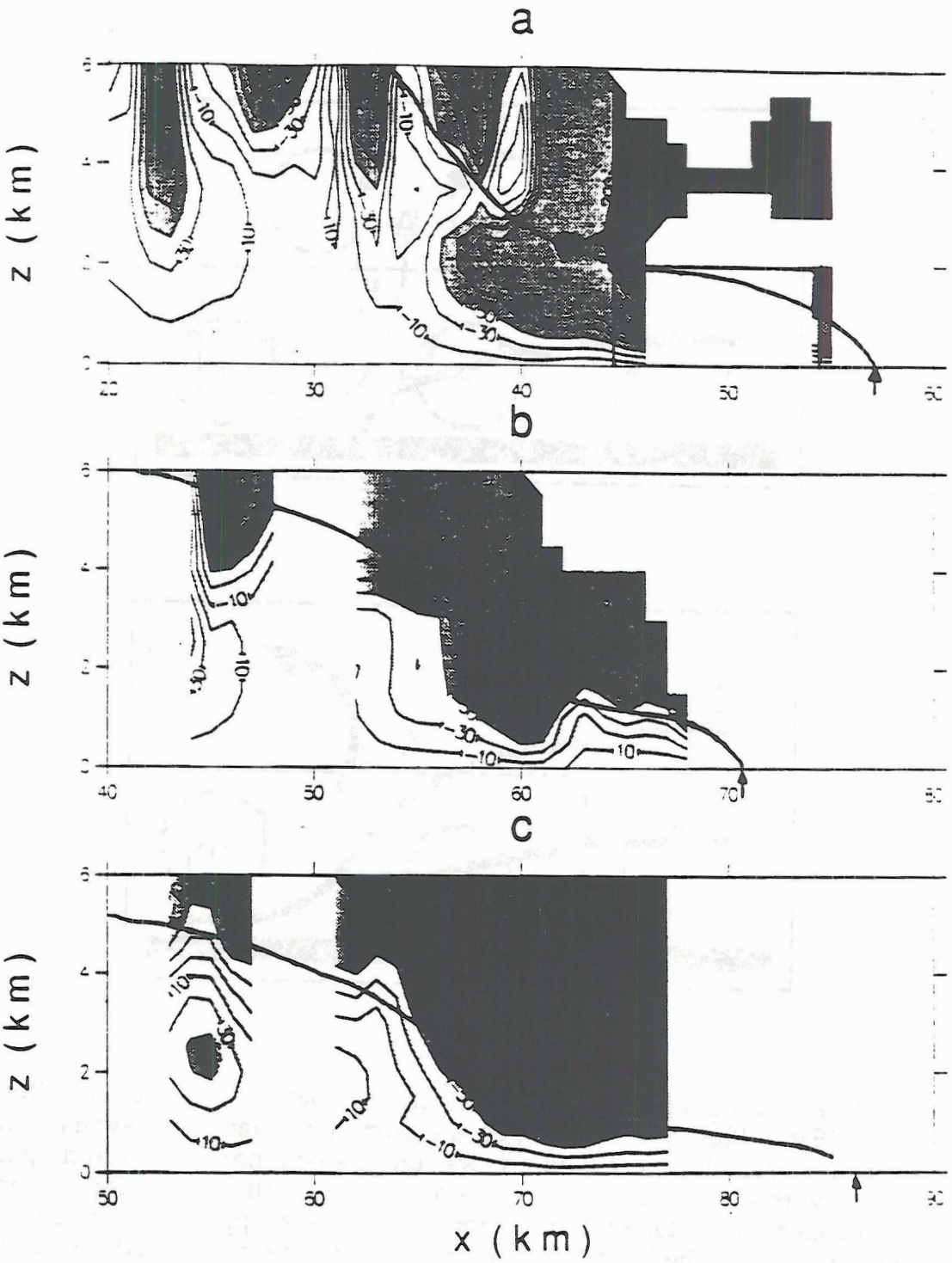

Figure 22. Left- and upper-face vorticity transport (described in text) from the 26 November 1988 DUNDEE squall line. Times are a) 1830 LT, b) 1851 LT, and c) 1913 LT. The lightest gray shading corresponds to values between 50 and -50 m^2s^{-2}, medium gray represents magnitudes between 50 and 200 m^2s^{-2}, and darkest gray greater than 200 m^2s^{-2}. The heavy curve represents the vorticity minimum. The arrow represents the gust front position. In a), the heavy box is a hypothetical integration volume (see text).

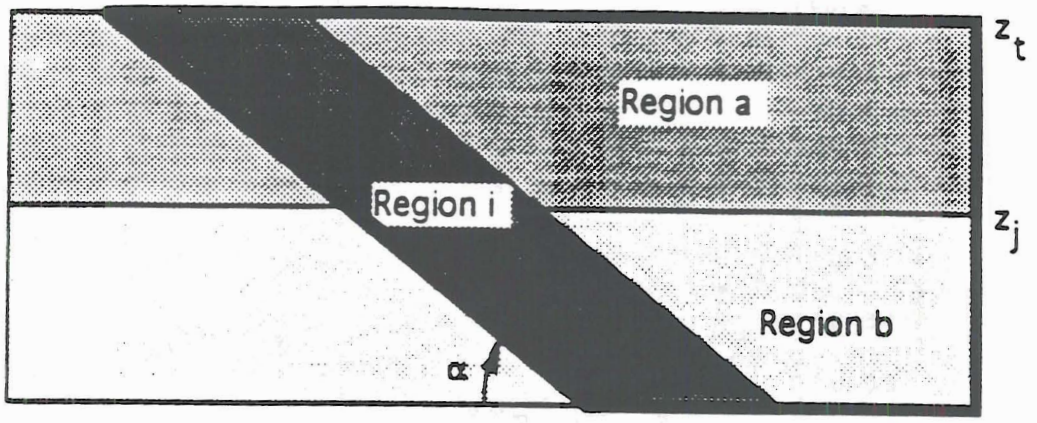

Figure 23. The three-region model. Region i is a sloping zone of constant vorticity with slope α. It is embedded in region "b" (below) characterized by constant vorticity and depth z_j, as well as region "a" (above) which is also characterized by constant vorticity and depth z_t-z_j. The bold outline denotes the region over which circulation is determined, as described in the text.

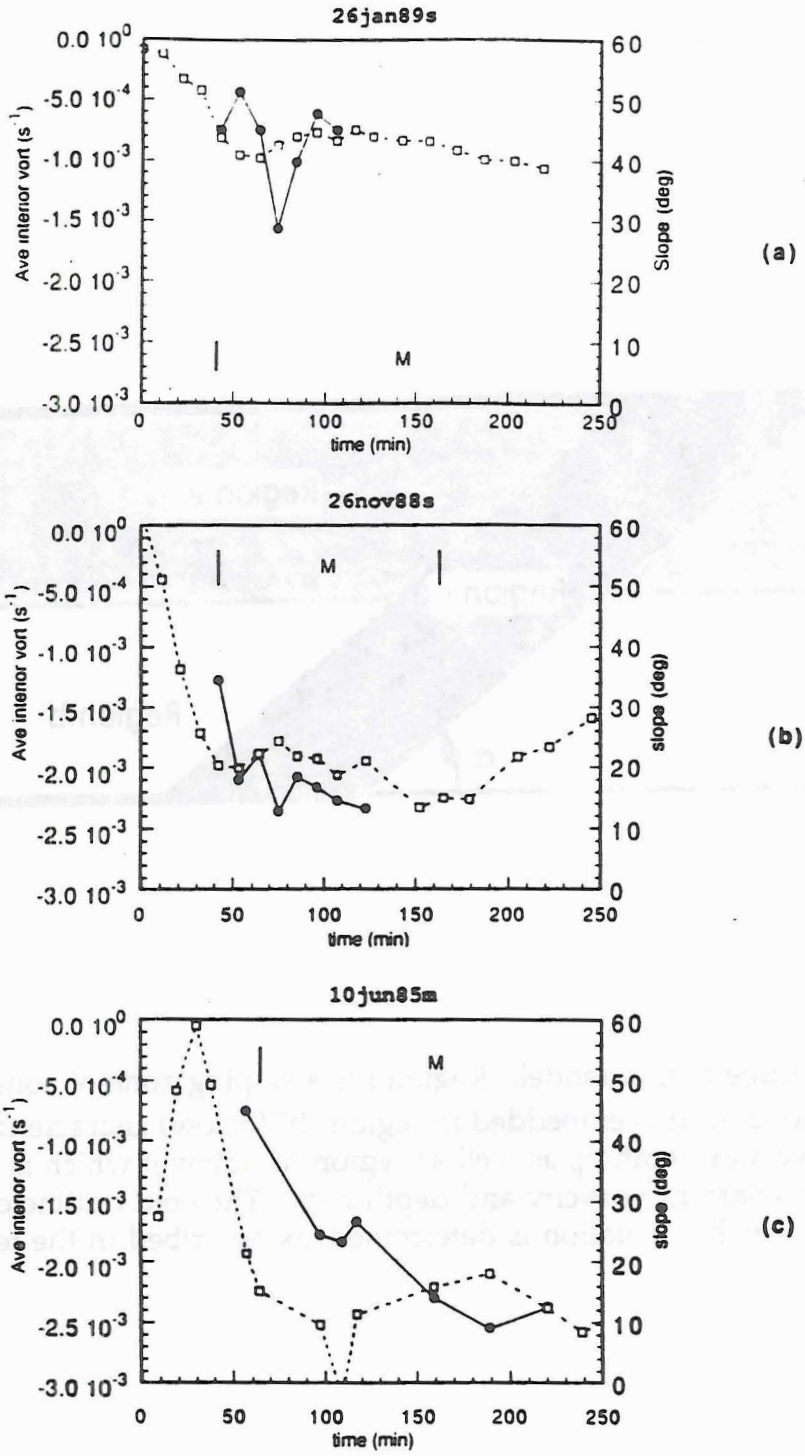

Figure 24. Observed slopes and average vorticity in the interior of six squall lines. Dashed lines with open squares are average vorticity. Solid lines with filled circles are the slope of the zone of maximum negative vorticity in degrees (scale at right). The symbol "M" represents the Mature stage, with vertical bars denoting the approximate beginning and end of that stage. a) 26 January 1989. b) 26 November 1988. c) 10 June 1985. d) 7 February 1990. e) 5 December 1989. f) 18 November 1989.

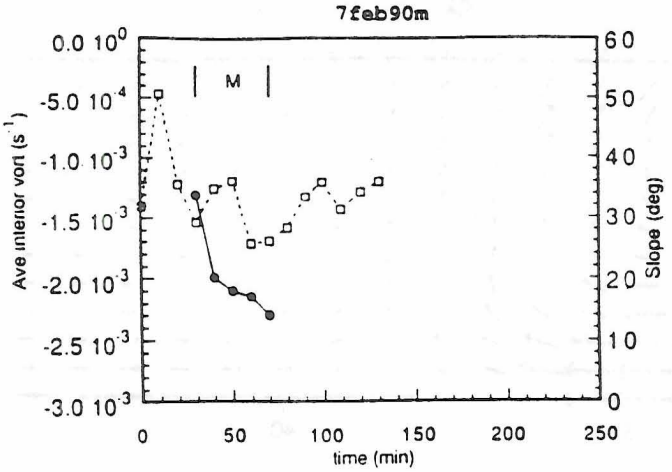

(d)

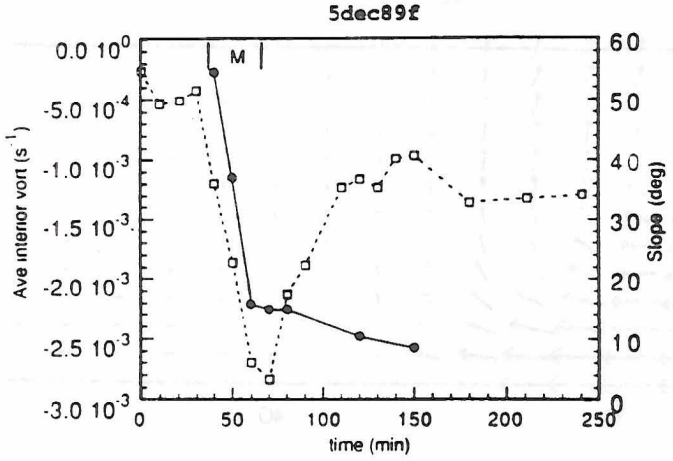

(e)

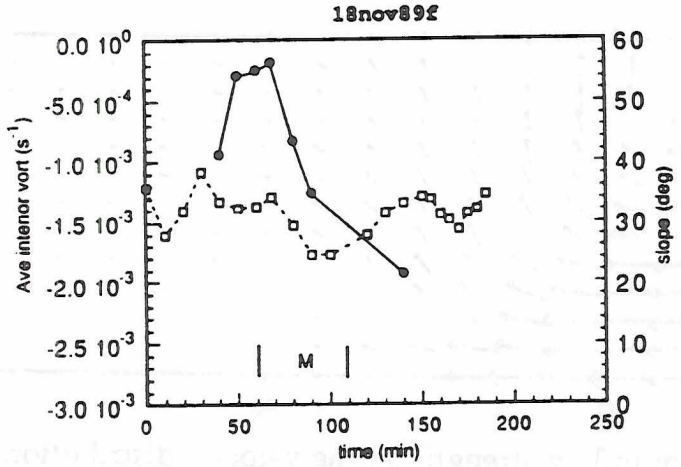

(f)

Figure 24 (continued).

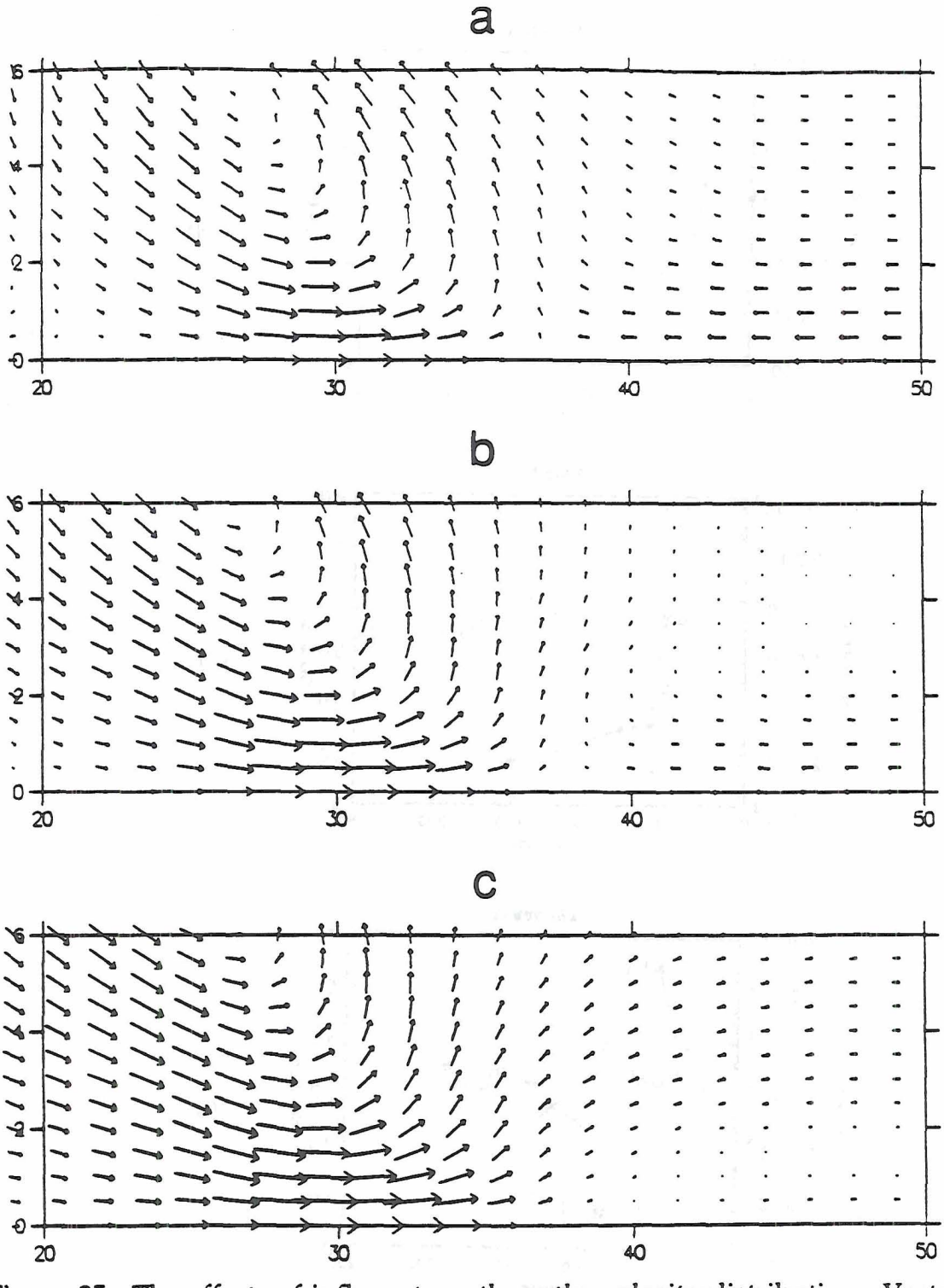

Figure 25. The effects of inflow strength on the velocity distribution. Vectors spanning one grid unit in either dimension represent 20 ms^{-1}. All plots are for lower shear of $4x10^{-3}s^{-1}$, zero upper shear, and Region i slope of 1.0 (α = 45°). Surface velocities at the right boundary (inflow strengths) are a) -18 ms^{-1}, b) -12 ms^{-1}, and c) -6 ms^{-1}.

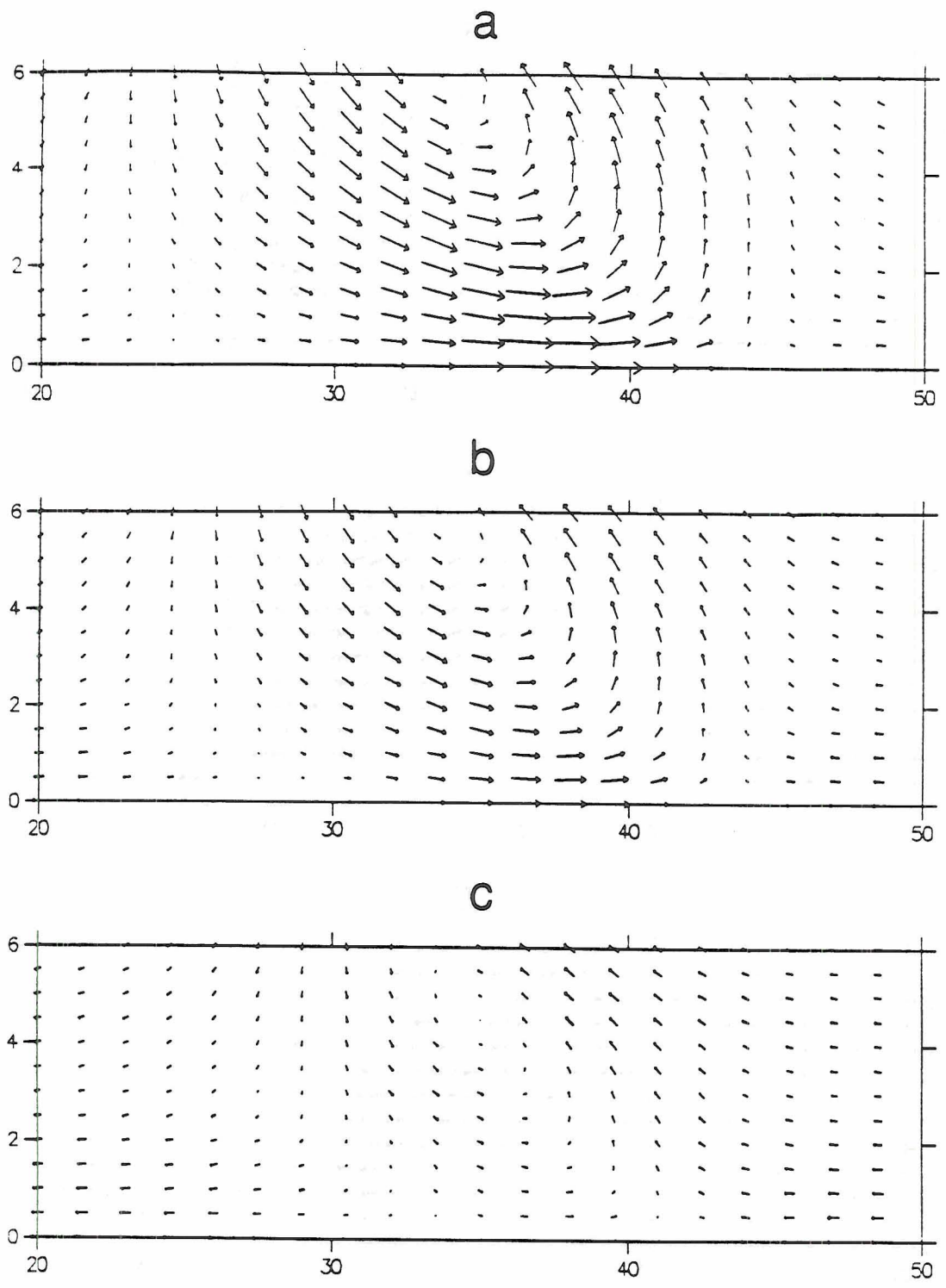

Figure 26. The effects of the strength of Region i vorticity on the velocity distribution. Vectors spanning one grid unit in either dimension represent 20 ms^{-1}. All plots are for lower shear of $2x10^{-3}s^{-1}$, zero upper shear, and inflow strength of 12 ms^{-1}. Minimum Region i vorticities are a) $-1x10^{-2}s^{-1}$, b) $-6x10^{-3}s^{-1}$, and c) $-2x10^{-3}s^{-1}$.

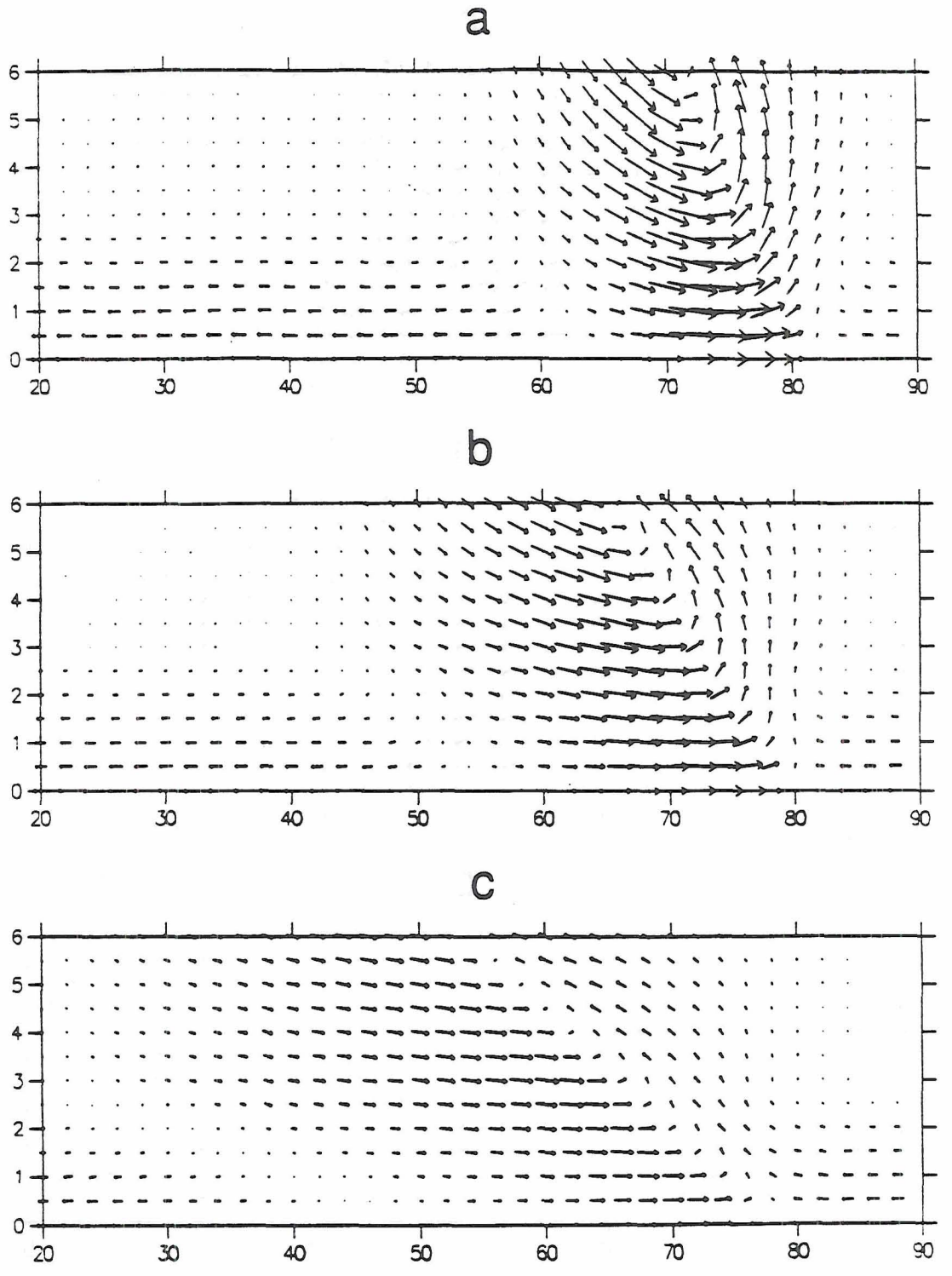

Figure 27. The effects of the slope of Region i on the velocity distribution. Vectors spanning one grid unit in either dimension represent 20 ms^{-1}. All plots are for lower shear of $2x10^{-3}s^{-1}$, zero upper shear, and inflow strength of 12 ms^{-1}. a) α=45°, b) α=27°, and c) α=14°.

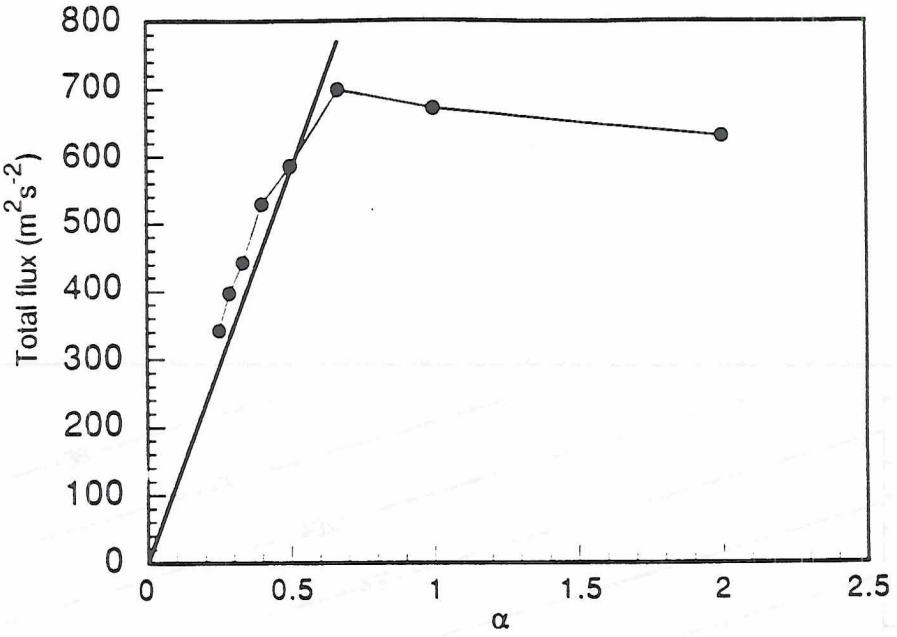

Figure 28. Total flux for conditions of zero upper shear, $4x10^{-3}s^{-1}$ lower shear, and vorticity zone strength $-1x10^{-2}s^{-1}$.

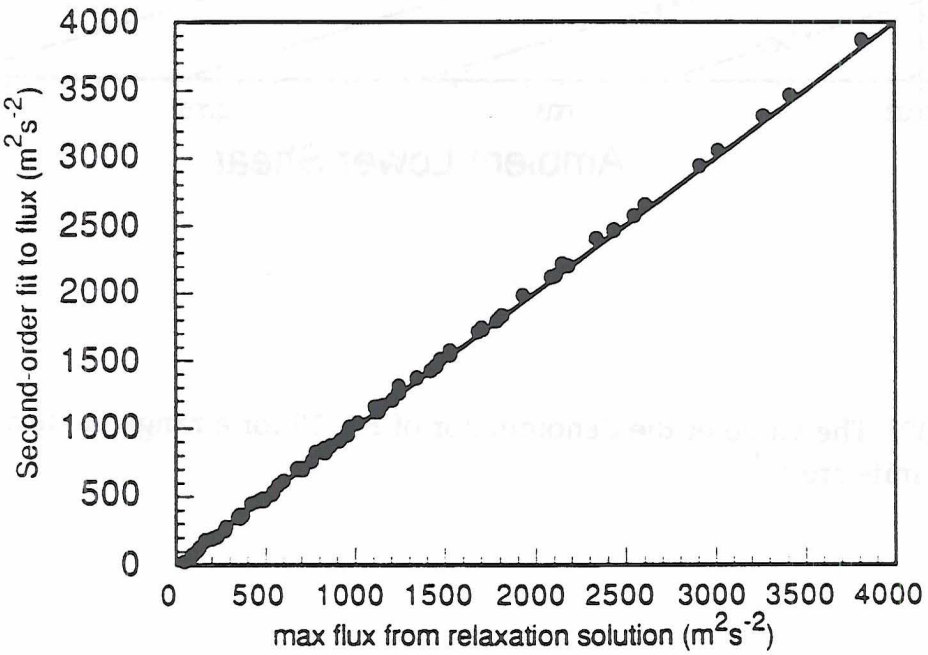

Figure 29. Total flux computed using Eq. 18 (ordinate) vs. the total flux computed using the relaxation solution. The sloping solid line represents a ratio of 1:1.

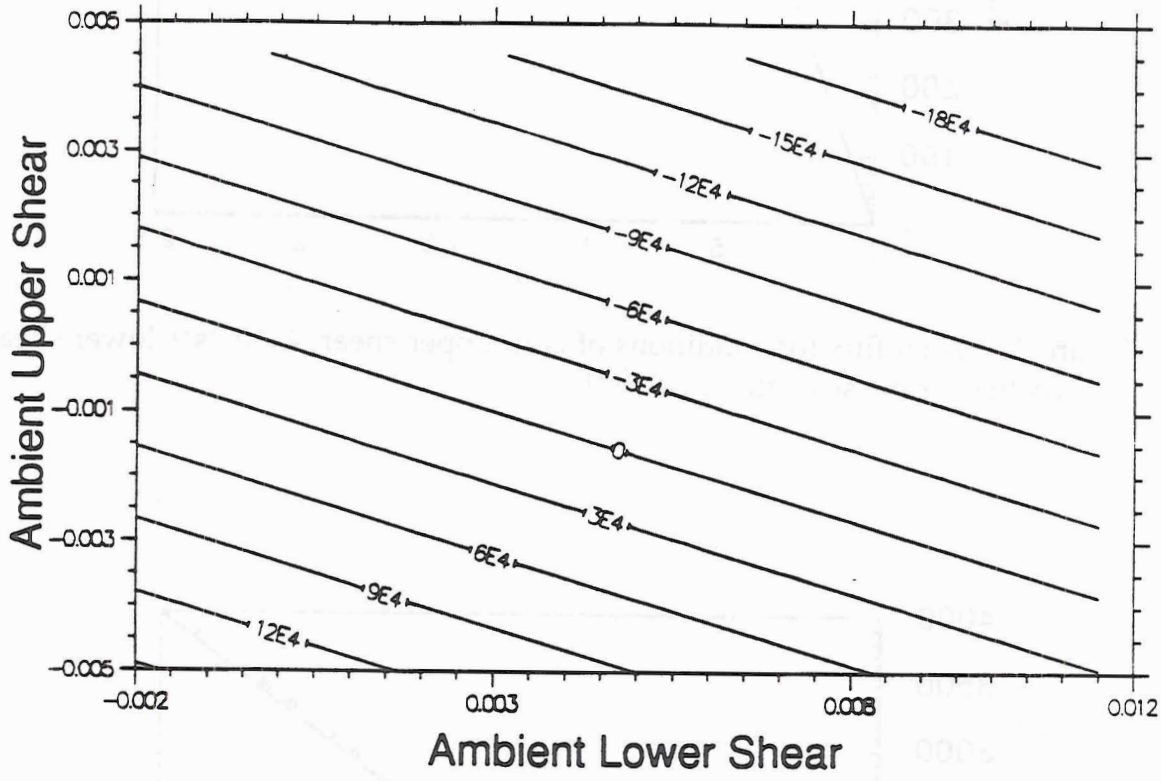

Figure 30. The value of the denominator of Eq. 18 for a range of shear values. Shears units are s^{-1}.

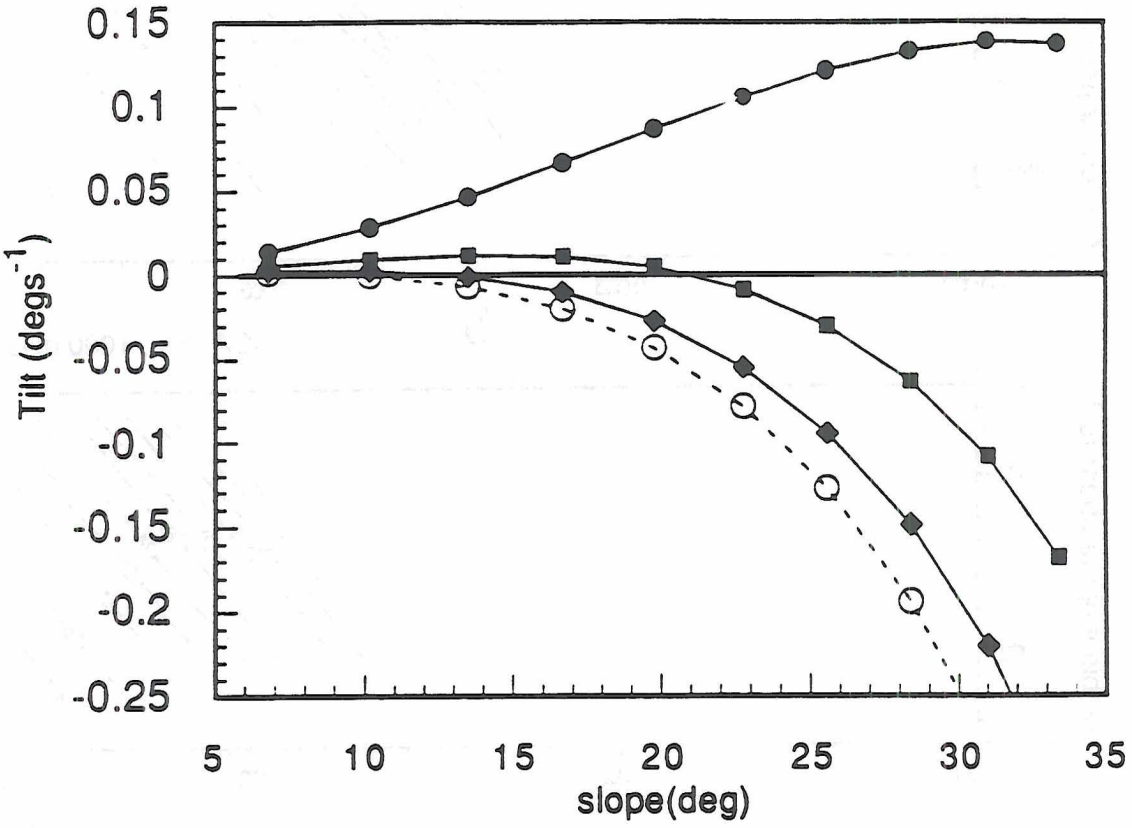

Figure 31. Examples of solutions to Eq. 18. Values on the abscissa are the slope of the Region i vorticity zone in degrees. Values on the ordinate are the tilting rate from Eq. 18, in degrees per second. See text for additional explanation.

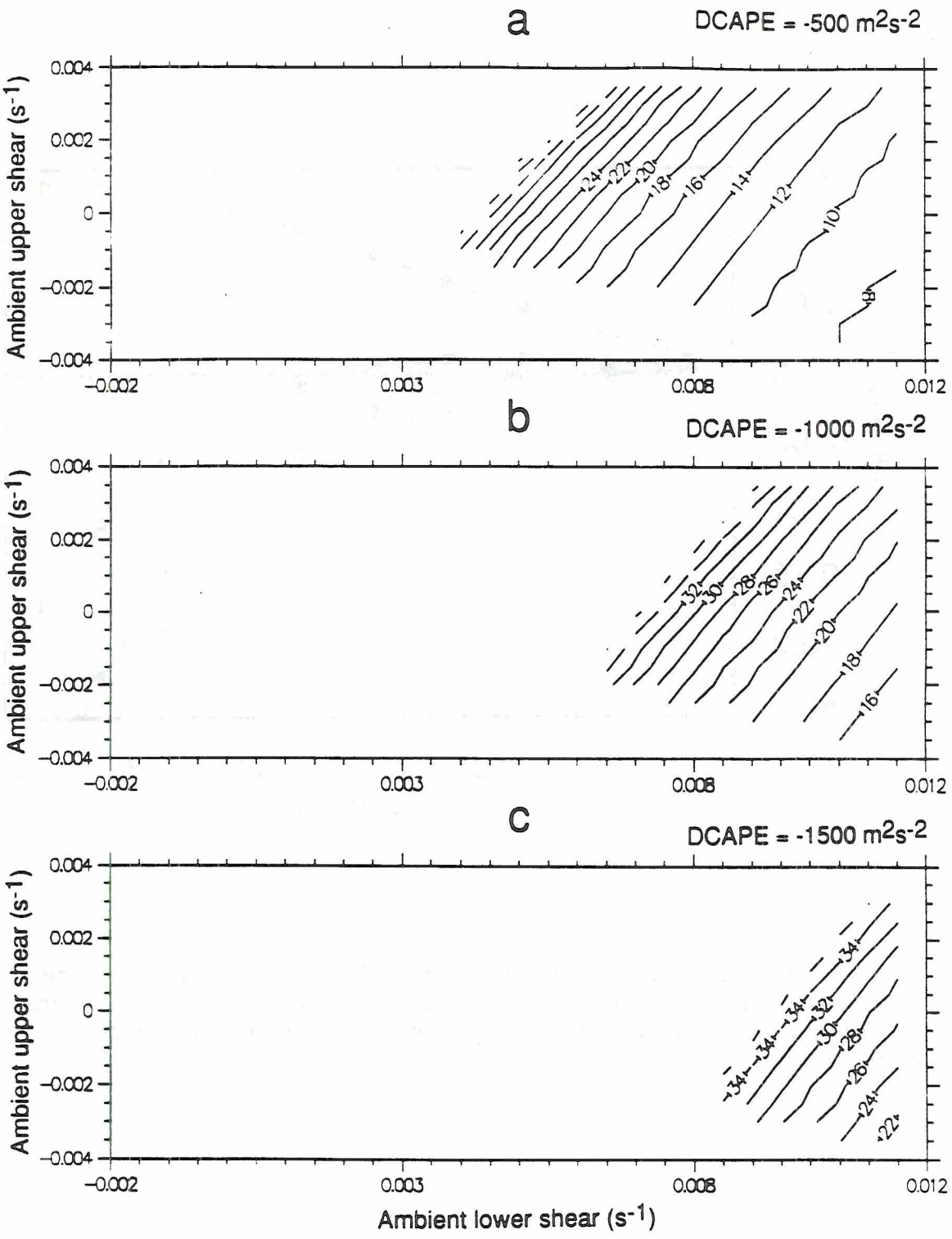

Figure 32. Equilibrium slopes (α, degrees) as a function of upper and lower shear strength, for cold pool strengths of a) -500 m^2s^{-2}, b) -1000 m^2s^{-2}, and c) -1500 m^2s^{-2}.

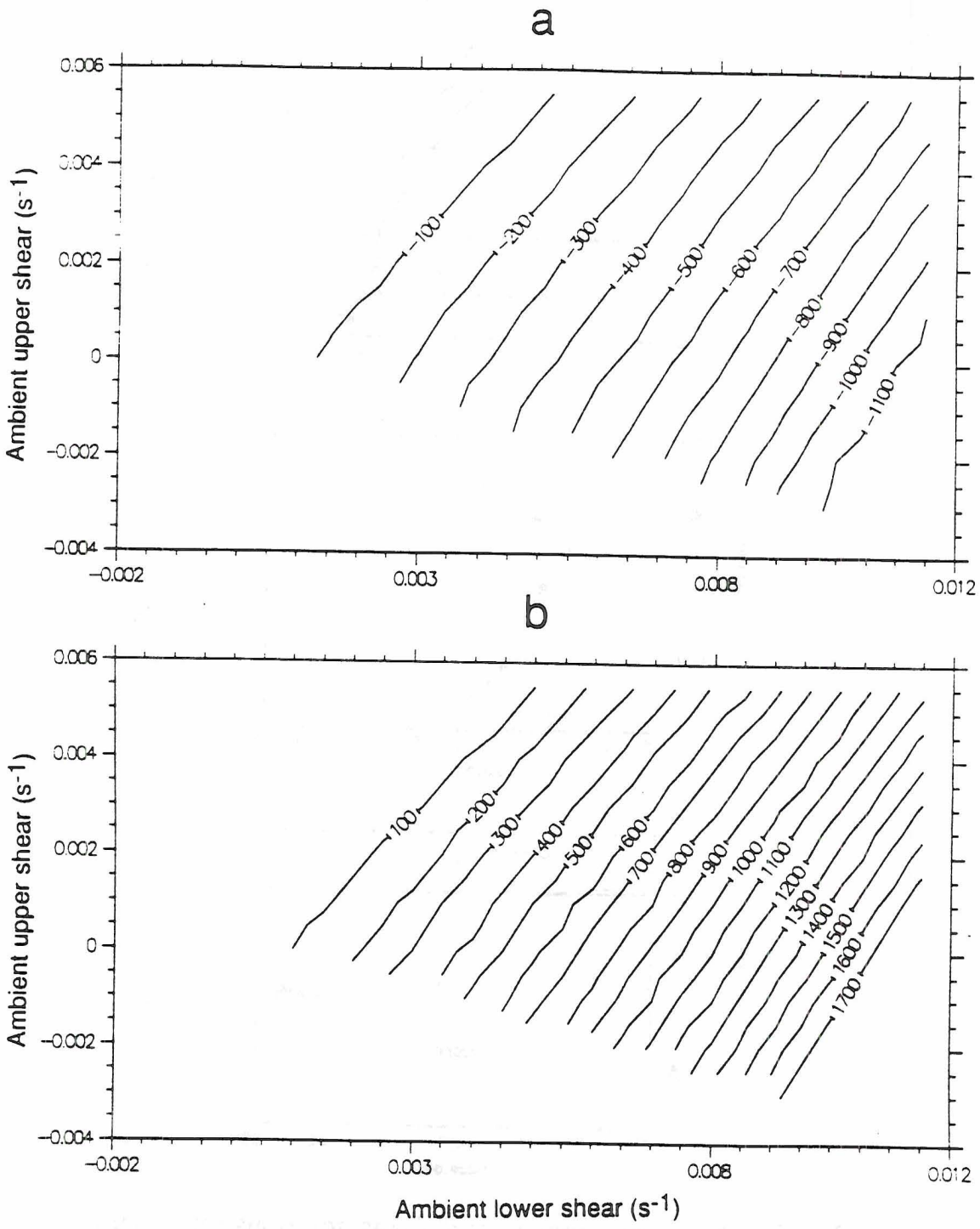

Figure 33. a) Average magnitudes of cold pool strength (m^2s^{-2}) that are associated with steady storms, as a function of upper and lower shear. b) As in a), but range of magnitudes of cold pools strengths (m^2s^{-2}) where steady storms are possible.

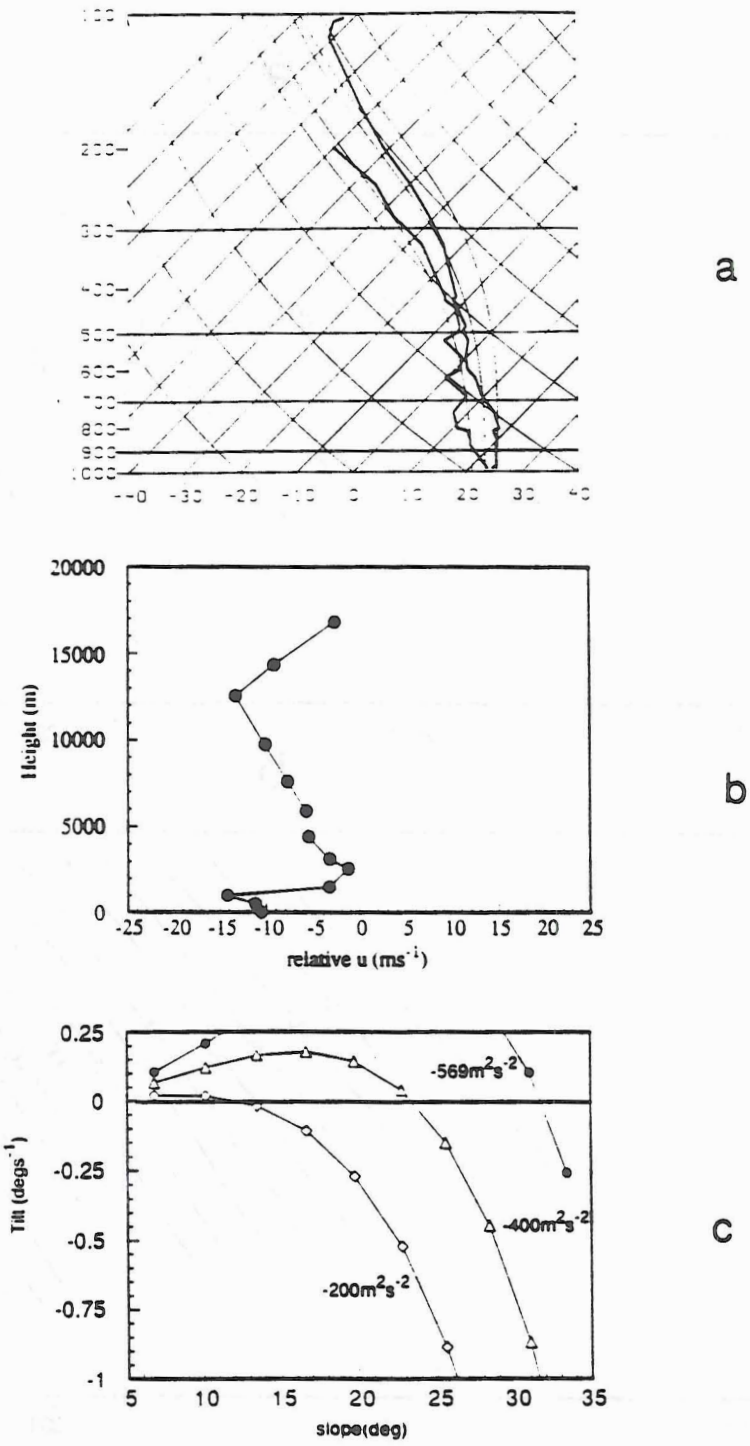

Figure 34. Pre-storm environment and tilting solutions for 26 January 1989. a) skew-T log-P diagram (temperature in degrees C) from 0000 UTC, with moist adiabats at 340, 350, and 360K; b) storm-relative line-normal environmental flow; c) tilting rate (degs^{-1}) as a function of slope α for lower and upper estimates of cold pool strength (labelled in graph).

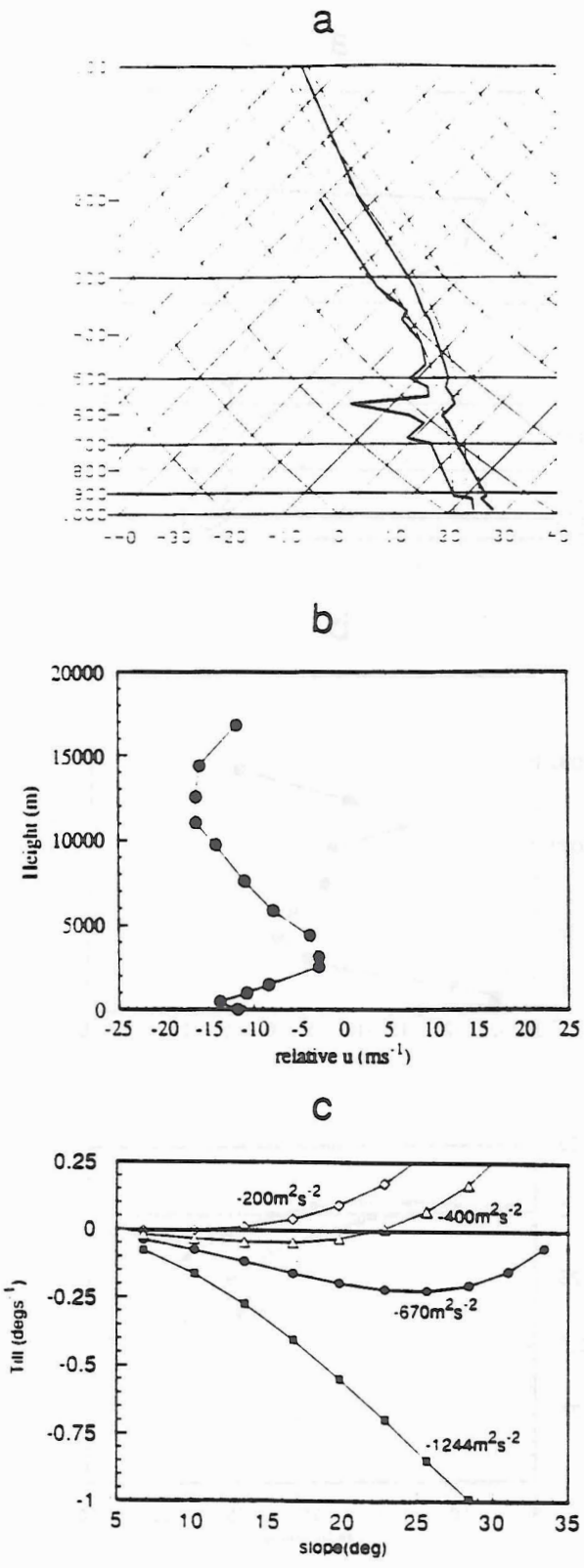

Figure 35. As in Fig. 34, but for 26 November 1988.

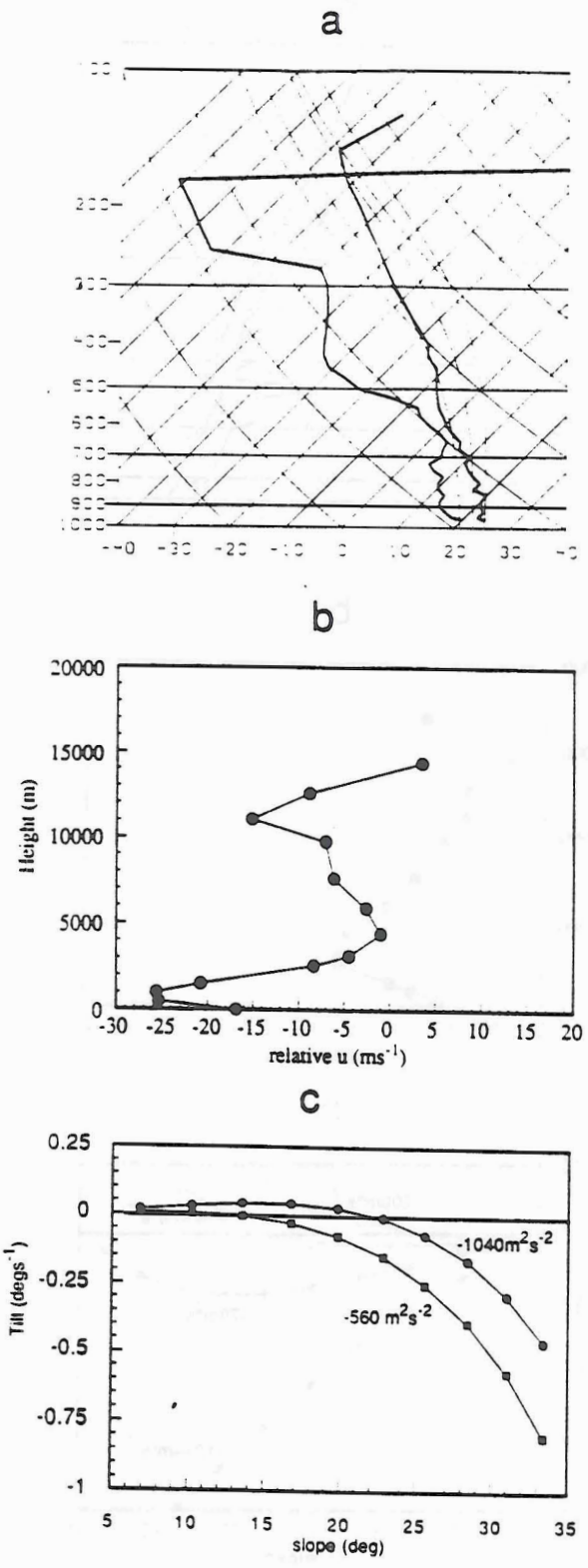

Figure 36. As in Fig. 34, but for 10 June 1985.

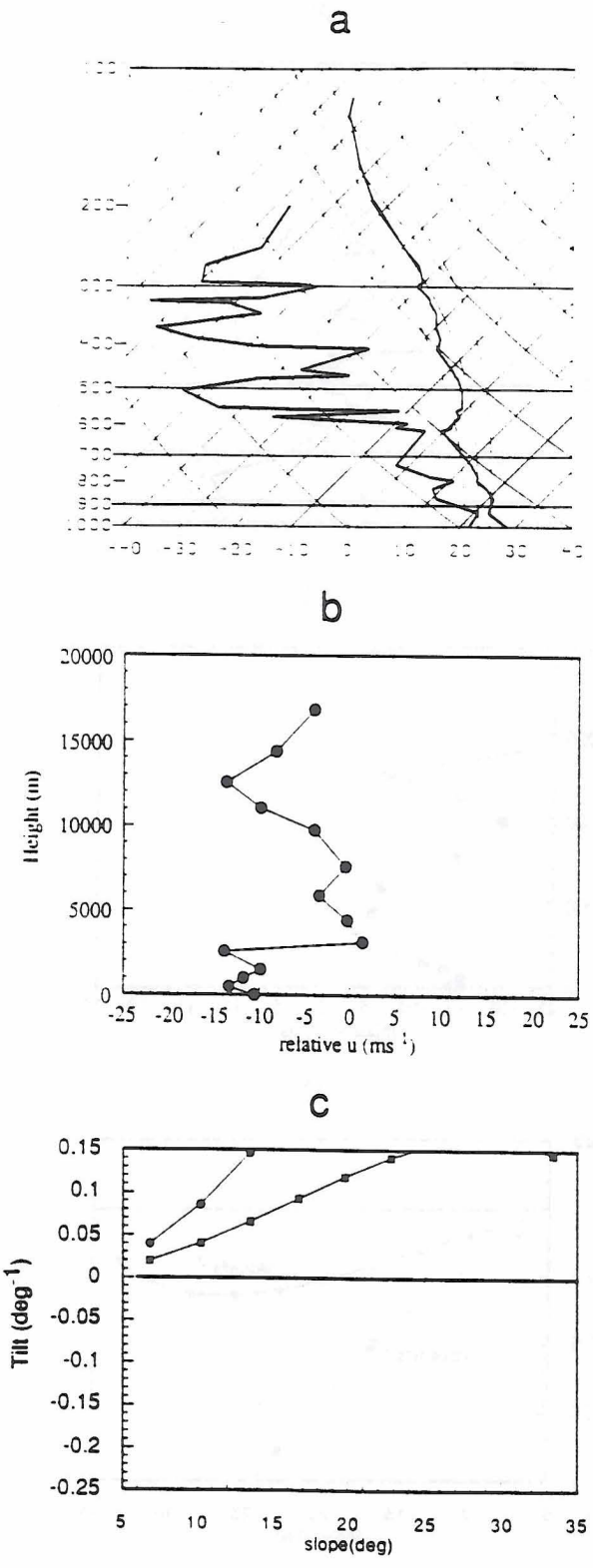

Figure 37. As in Fig. 34, but for 7 February 1990.

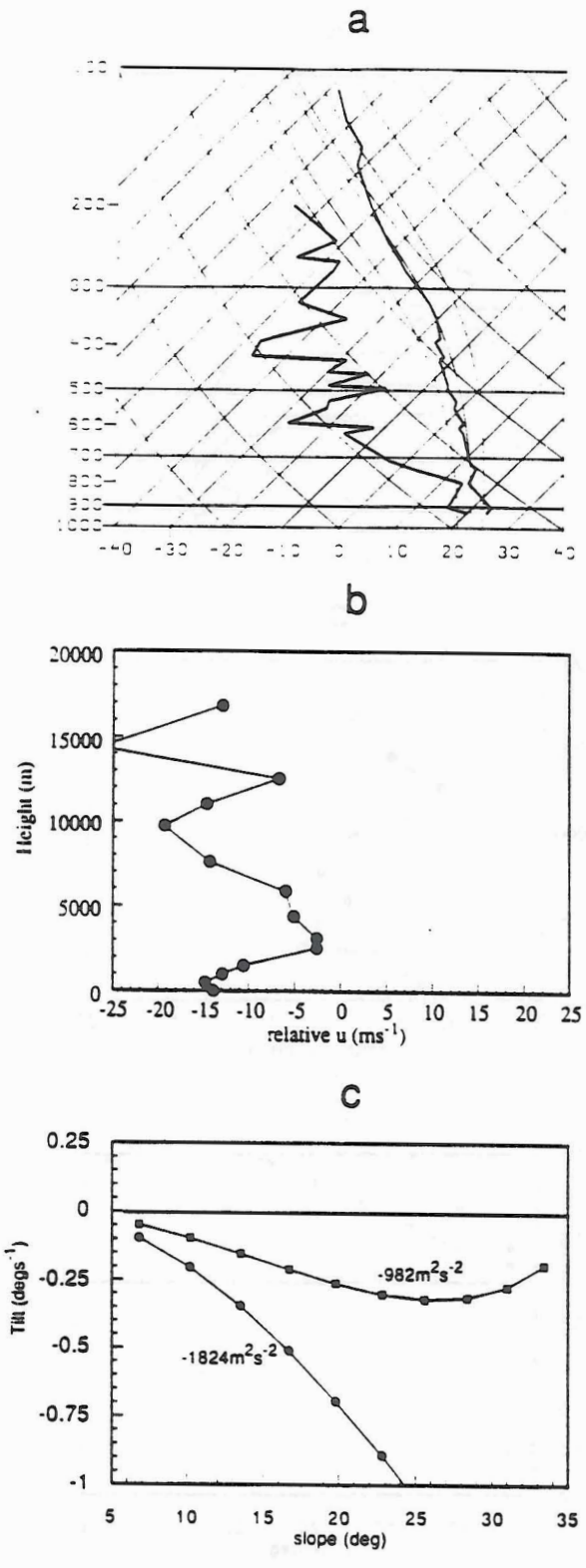

Figure 38. As in Fig. 34, but for 18 November 1989.

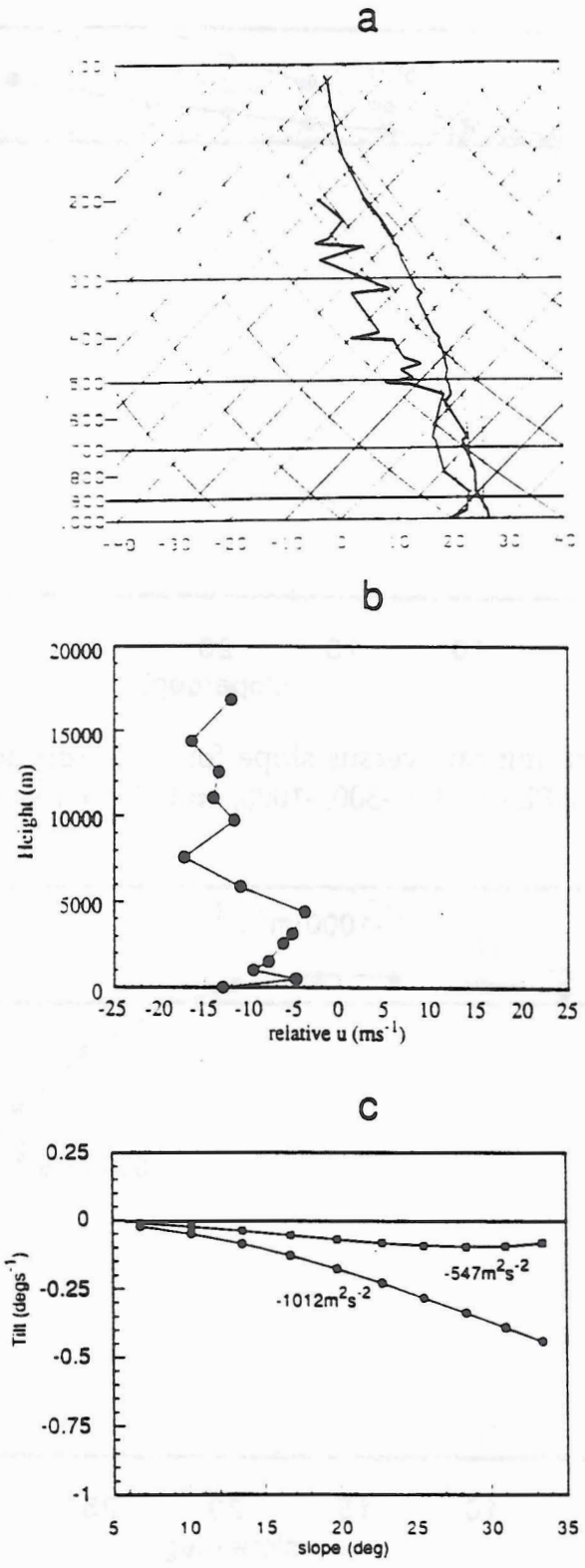

Figure 39. As in Fig. 34, but for 5 December 1989.

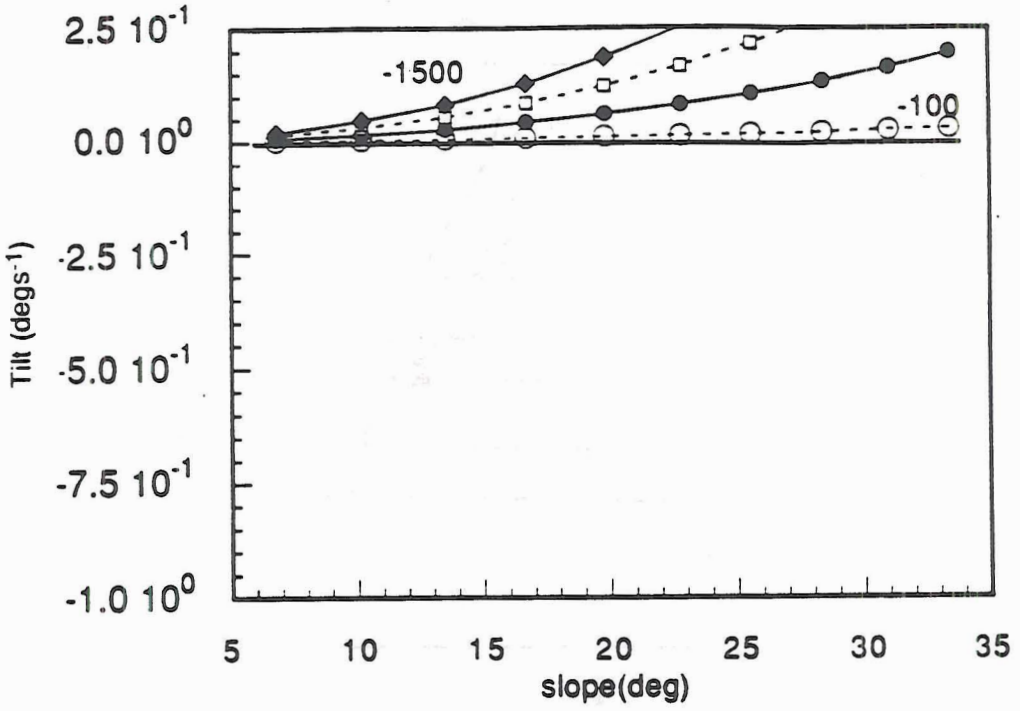

Figure 40. Graph of tilting rate versus slope for mid-latitude environments. The curves are for DCAPE of -100, -500, -1000, and -1500 m^2s^{-2}.

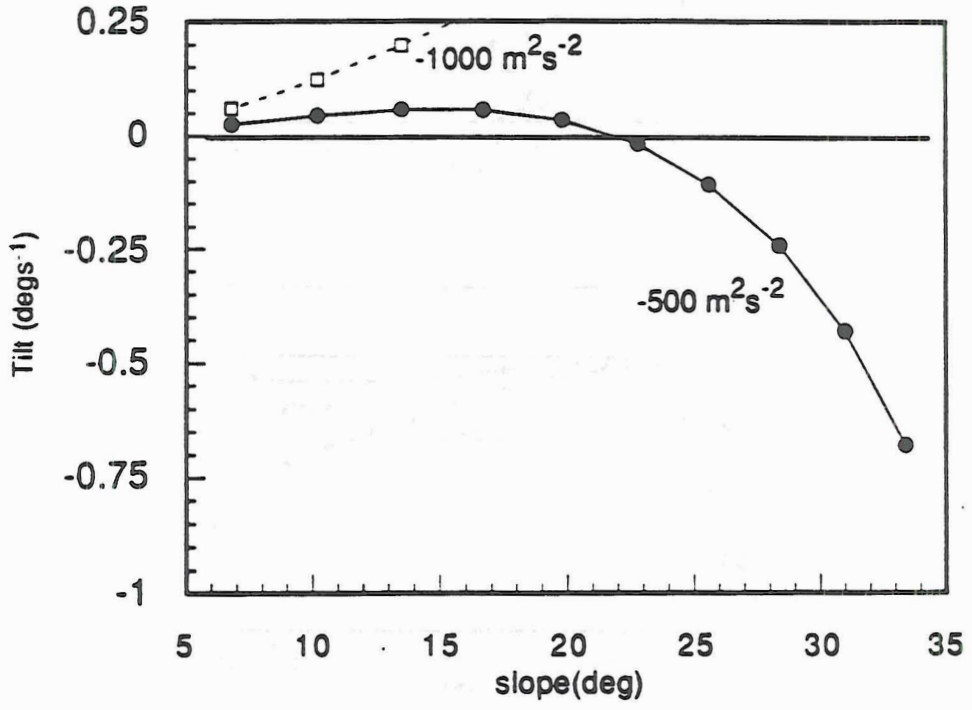

Figure 41. Graph of tilting rate ($degs^{-1}$ on ordinate) versus slope for the environmental conditions associated with the 23 June 1981 COPT 81 squall line. Cold pool strengths are indicated on the graph.

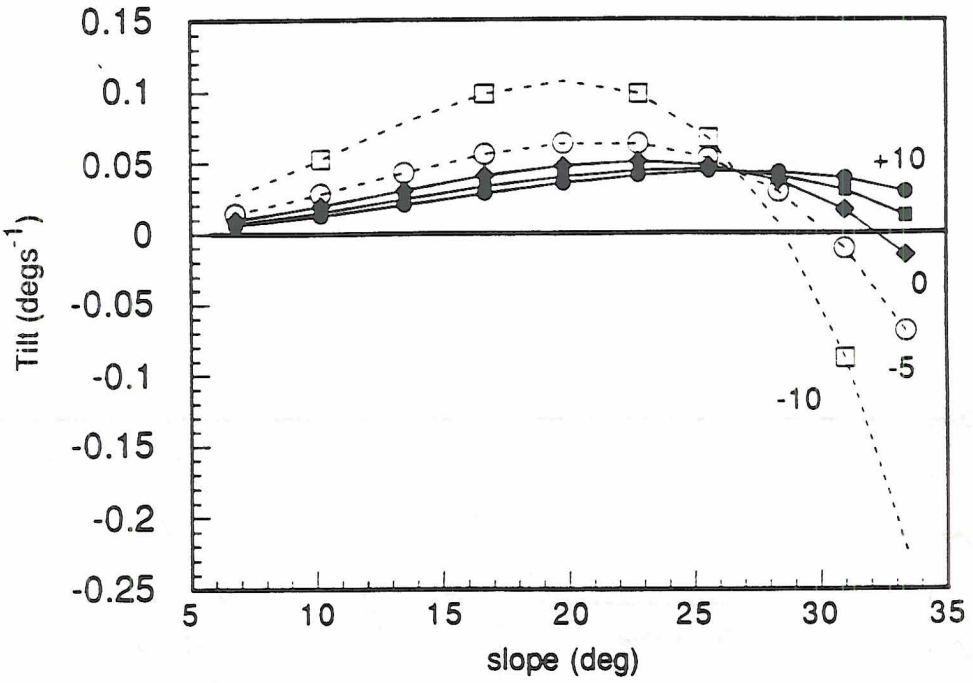

Figure 42. Graph of tilting rate versus slope for the five shear conditions examined in Thorpe et al. (1982).

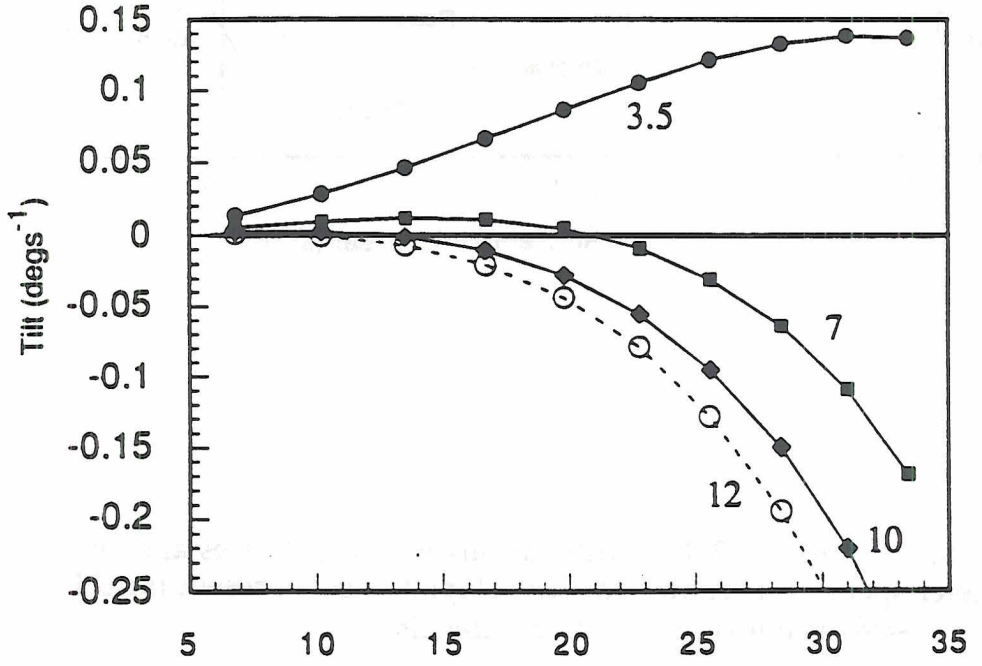

Figure 43. Graph of tilting rate versus slope for four shear configurations including the optimal shear determined by RKW, using the RKW units of ms^{-1}per2500 m.

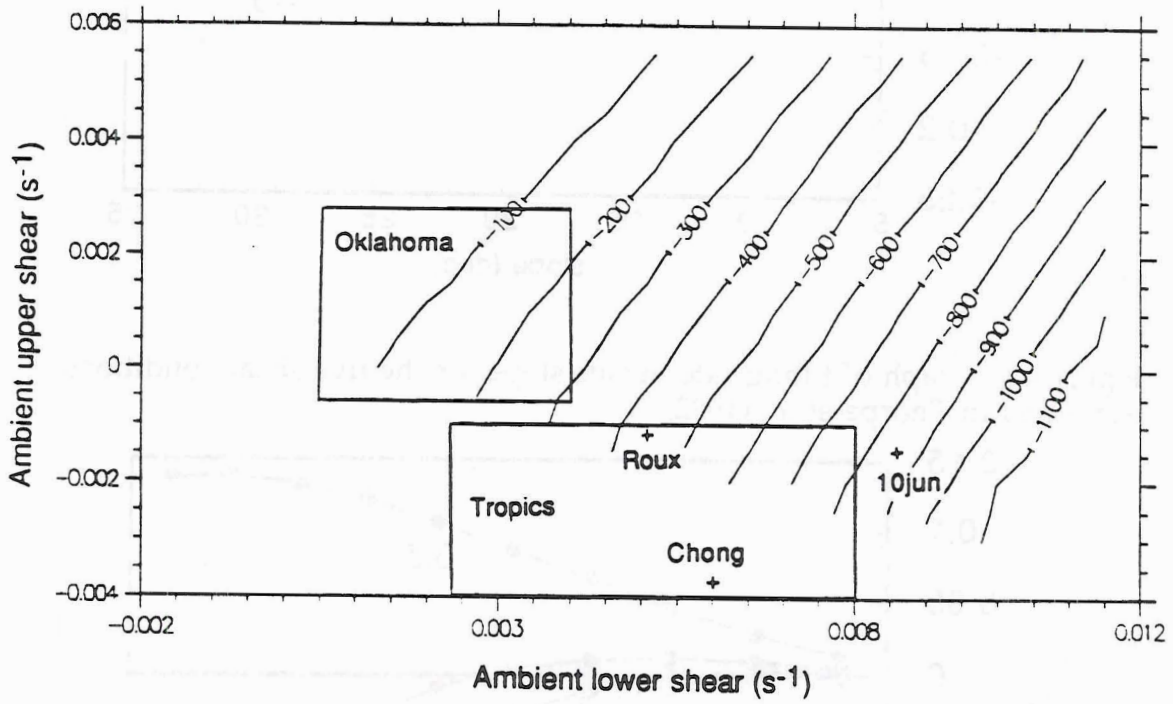

Figure 44. As in Fig. 33, but with various individual cases and climatological parameter spaces superimposed. The sloped lines represent fixed DCAPE in units of m^2s^{-2}. See text for additional details.

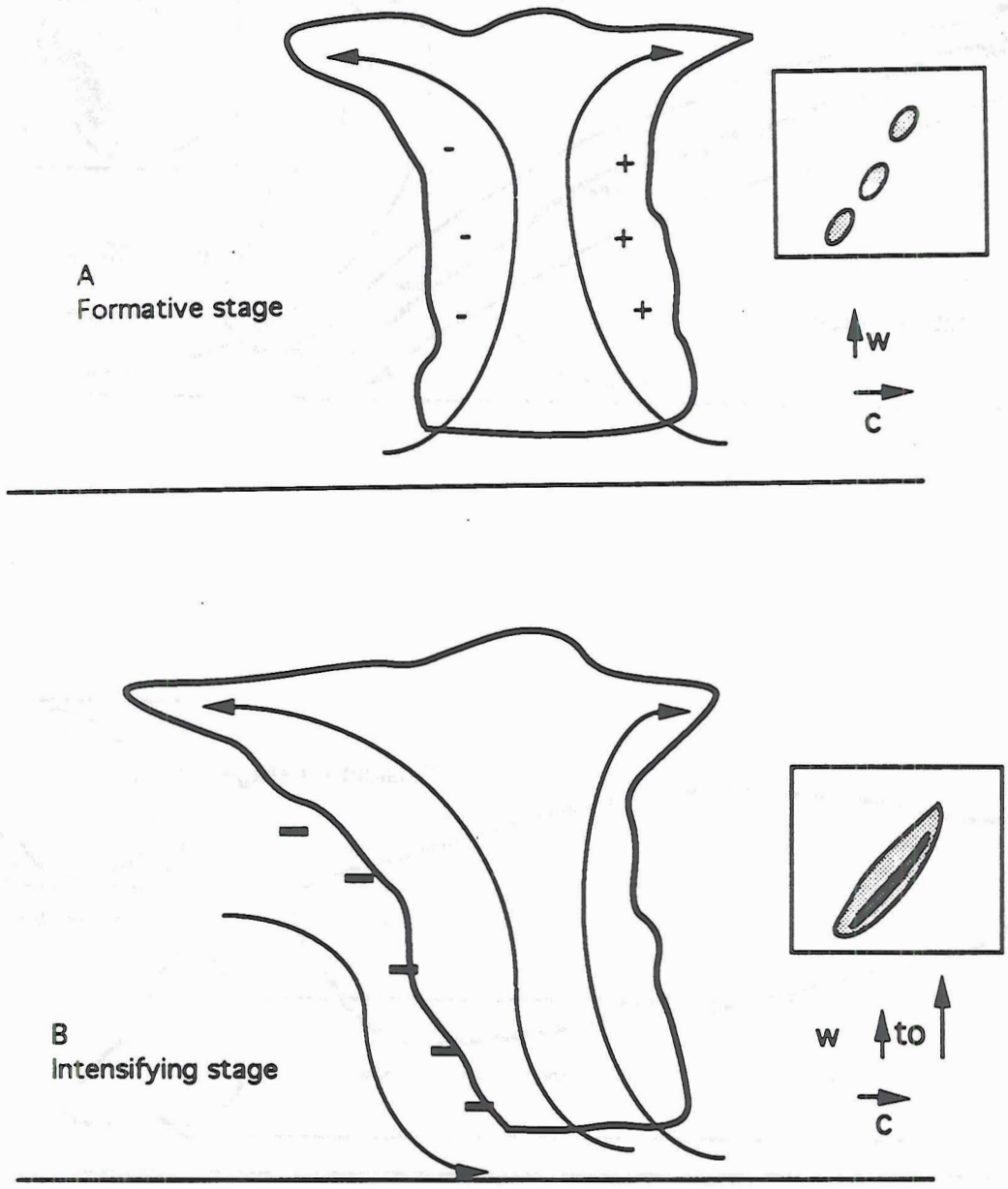

Figure 45. Conceptual model of squall line evolution. Heavy lines represent the cloud boundary and thin lines are streamlines of the line-normal flow. The sign of the vorticity is indicated with "+" and "-". The square inset represents a low-level horizontal depiction of the reflectivity. The arrow associated with the label "w" represents relative updraft magnitude in a slab average, and with "c" a relative propagation speed.

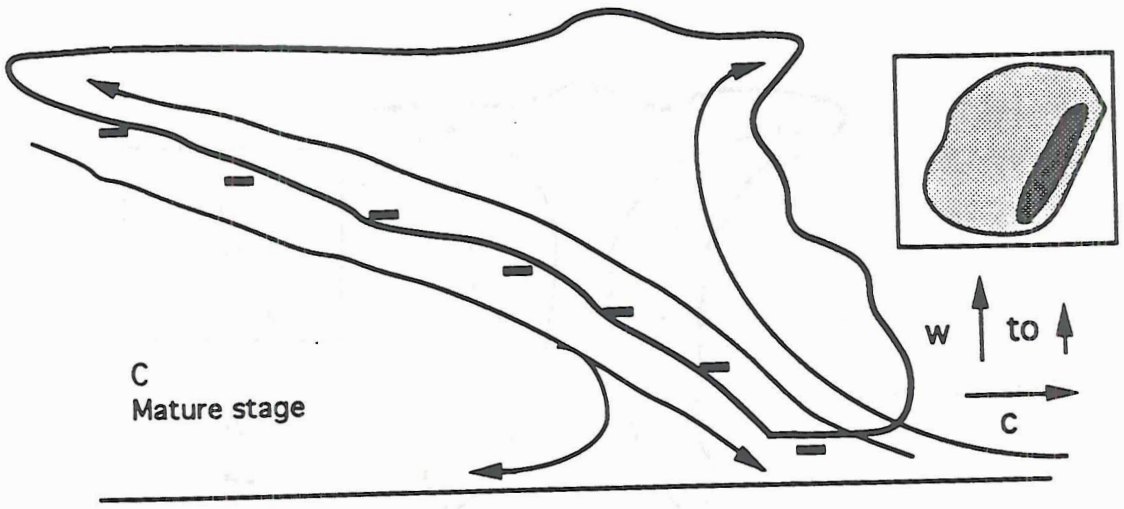

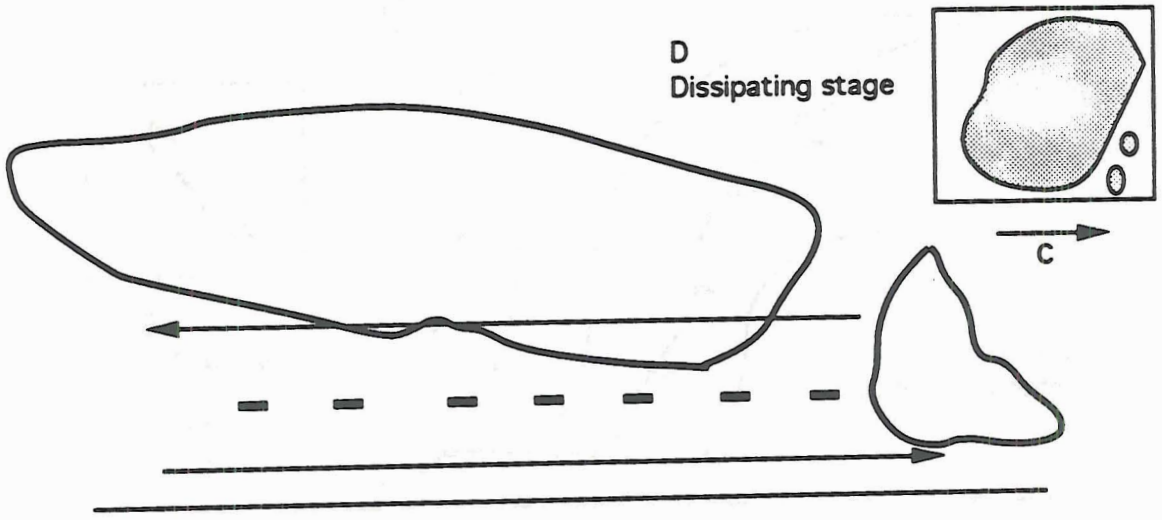

Figure 45 continued.

REFERENCES

Bluestein, H. B., and M. H. Jain, 1985: Formation of mesoscale lines of precipitation: severe squall lines in Oklahoma during the spring. *J. Atmos. Sci.*, **42**, 1711-1732.

Charba, J., 1974: Application of the gravity current model to analysis of squall-line gust fronts. *Mon. Wea. Rev.*, **102**, 140-156.

Chalon, J. P., G. Jaubert, F. Roux, and J. P. Lafore, 1988: The west African squall line observed on 23 June 1981 during COPT 81: Mesoscale structure and transports. *J. Atmos. Sci.*, **45**, 2744-2763.

Chong, M., P. Amayenc, G. Scialom, and J. Testud, 1987: A tropical squall line observed during COPT 81 experiment in West Africa. Part I: Kinematic structure inferred from dual-Doppler data. *Mon. Wea. Rev.*, **115**, 670-694.

Cotton, W. R., and R. A. Anthes, 1989: *Storm and cloud dynamics*. Academic Press, 883 pp.

Cunning, J. B., 1986: The Oklahoma-Kansas Preliminary Regional Experiment for STORM-Central. *Bull. Amer. Meteor. Soc.*, **67**, 1478-1486.

Emanuel, K. A., 1986: Some dynamical aspects of precipitating convection. *J. Atmos. Sci.*, **43**, 2183-2198.

Emanuel, K. A., 1989: Dynamical theories of tropical convection. *Aust. Met. Mag.*, **37**, 3-10.

Fovell, R. G., and Y. Ogura, 1988: Numerical simulation of a midlatitude squall line in two dimensions. *Mon. Wea. Rev.*, **45**, 3846-3879.

Hane, C. E., 1986: Extratropical squall lines and rainbands. Mesoscale Meteorology and Forecasting. P. S. Ray, Ed., American Meteorological Society, pp. 359-389.

Houze, R. A., S. A. Rutledge, M. I. Biggerstaff, and B. F. Smull, 1989: Interpretation of Doppler weather radar displays of midlatitude mesoscale convective systems. *Bull. Amer. Met. Soc.*, **70**, 608-619.

Houze, R. A., B. F. Smull, and P. Dodge, 1990: Mesoscale organization of springtime rainstorms in Oklahoma. *Mon. Wea. Rev.*, **118**, 613-654.

Hoxit, L. R., C. F. Chappell, and J. M. Fritsch, 1976: Formation of mesolows or pressure troughs in advance of cumulonimbus clouds. *Mon. Wea. Rev.*, **104**, 1419-1428.

Johns, R. H., and W. D. Hirt, 1983: The derecho-- A severe weather producing convective system. Preprints, *13th Conf. on Severe Local Storms*, Tulsa, Oklahoma, Amer. Meteor. Soc., 178-181.

Johnson, R. H., and P. J. Hamilton, 1988: The relationship of surface pressure features to precipitation and airflow structure of an intense midlatitude squall line. *Mon. Wea. Rev.*, **116**, 1444-1472.

Kessinger, C. J., P. S. Ray, and C. E. Hane, 1987: The Oklahoma squall line of 19 May 1977. Part I: A multiple Doppler analysis of convective and stratiform structure. *J. Atmos. Sci.*, **44**, 2840-2864.

Lafore, J.-P., and M. W. Moncrieff, 1989: A numerical investigation of the convective and stratiform regions of tropical squall lines. *J. Atmos. Sci.*, **46**, 521-544.

Lafore, J.-P., and M. W. Moncrieff, 1990: Reply. *J. Atmos. Sci.*, **47**, 1034-1035.

Leary, C. A., and R. A. Houze, 1979: The structure and evolution of convection in a tropical cloud cluster. J. Atmos. Sci., 36, 437-457.

Lemone, M. A., 1983: Momentum transport by a line of cumulonimbus. *J. Atmos. Sci.*, **40**, 1815-1834.

Maddox, R. A., 1980: Mesoscale convective complexes. *Bull. Amer. Meteor. Soc.*, 61, 1374-1387.

McAnelly, R. L., and W. R. Cotton, 1989: Precipitation life cycle of mesoscale convective complexes over the central United States. *Mon. Wea. Rev.*, 117, 784-808.

Ogura, Y., and M.-T. Liou, 1980: The structure of a midlatitude squall line: A case study. *J. Atmos. Sci.*, 37, 553-567.

Rotunno, R., J. B. Klemp and M. L. Weisman, 1988: A theory for strong, long-lived squall lines. *J. Atmos. Sci.*, 45, 463-485.

Rotunno, R., J. B. Klemp and M. L. Weisman, 1990: Comments on "A numerical investigation of the organization and interaction of the convective and stratiform regions of tropical squall lines." *J. Atmos. Sci.*, 47, 1031-1033.

Roux, F., 1988: The west African squall line observed on 23 June 1981 during COPT 81: Kinematics and thermodynamics of the convective region. *J. Atmos. Sci.*, 45, 406-426.

Rutledge, S. A., 1991: Middle Latitude and tropical mesoscale convective systems. *Rev. Geophys.*, Supplement (April 1991), 88-97.

Rutledge, S. A., R. A. Houze, M. I. Biggerstaff, and T. Matejka, 1988: The Oklahoma-Kansas mesoscale convective system of 10-11 June 1985: Precipitation structure and single-Doppler radar analysis. *Mon. Wea. Rev.*, 116, 1409-1430.

Rutledge, S. A., E. R. Williams, and T. D. Keenan, 1992: The Down Under Doppler and Electricity Experiment (DUNDEE): Overview and preliminary results. *Bull. Amer. Meteor. Soc.*, in press.

Schlesinger, R. E., 1975: A three-dimensional numerical model of an isolated deep convective cloud: Preliminary results. *J. Atmos. Sci.*, 32, 934-957.

Schmidt, J. M., and W. R. Cotton, 1989: A High Plains squall line associated with severe surface winds. *J. Atmos. Sci.*, 46, 281-302.

Seitter, K. L., and H.-L. Kuo, 1983: The dynamical structure of squall-line type thunderstorms. *J. Atmos. Sci.*, 40, 2831-2854.

Smull, B. F., and R. A. Houze, 1985: A midlatitude squall line with a trailing region of stratiform rain: Radar and satellite observations. *Mon. Wea. Rev.*, 113, 117-133.

Smull, B. F., and R. A. Houze, 1987: Rear inflow in squall lines with trailing stratiform precipitation. *Mon. Wea. Rev.*, 115, 2869-2889.

Smull, B. F., and R. A. Houze, 1987: Dual-Doppler radar analysis of a midlatitude squall line with a trailing region of stratiform rain. *J. Atmos. Sci.*, 44, 2128-2148.

Thorpe, A. J., M. J. Miller, and M. W. Moncrieff, 1982: Two-dimensional convection in non-constant shear: A model of mid-latitude squall lines. *Quart. J. R. Met. Soc.*, 108, 739-762.

Zhang, D.-L., and K. Gao, 1989: Numerical simulation of an intense squall line during 10-11 June 1985 PRE-STORM. Part II: Rear inflow, surface pressure perturbations and stratiform precipitation. *Mon. Wea. Rev.*, 117, 2067-2094.

Zipser, E. J., 1977: Mesoscale and convective-scale downdrafts as distinct components of squall-line structure. *Mon. Wea. Rev.*, 105, 1568-1589.